UNIVERSITA' DEGLI STUDI DI VERONA

DIPARTIMENTO DI

Neuroscienze, Biomedicina e Movimento

SCUOLA DI DOTTORATO DI

Scienze della Vita e della Salute

DOTTORATO DI RICERCA IN

Neuroscienze, Scienze Psicologiche e Psichiatriche, e Scienze del Movimento

CICLO XXXIIII

TITOLO DELLA TESI DI DOTTORATO

THE ROLE OF MENINGES AND MENINGEAL NEURAL PROGENITOR CELLS IN A PARADIGM OF ENRICHED ENVIRONMENT AND IN MULTIPLE SCLEROSIS

S.S.D. BIO/14

Coordinatore: Prof./ssa Michela Rimondini
Firma _____

Tutor: Prof./ssa Ilaria Decimo
Firma _____

Co-Tutor Dott.ssa Francesca Ciarpella
Firma _____

Dottoranda: Stefania Zorzin
Firma _____

A noi...

CONTENTS

INDEX OF FIGURES

TABLES AND LEGENDS

Experimental procedure	Mouse strain	Sex	Age at time of sacrifice	IF	WB	Rt-PCR
Enriched Environment	CD1	M	8 weeks	CTRL n=5 EE n=6	N.A.	N.A.
Enriched Environment on lineage-tracing model	GLAST-GFP	M	9-12 weeks	CTRL n=3 EE n=4	N.A.	N.A.
Enriched Environment with administration of TrkB inhibitor ANA-12	CD1	M	8 weeks	NO EE VEH n=3 EE VEH n=3 EE ANA-12 n=3 NO EE ANA-12 n=3	NO EE VEH n=3 EE VEH n=2 EE ANA-12 n=3	NO EE VEH n=4 EE VEH n=5 EE ANA-12 n=5
Fluoxetine administration	CD1	M	8 weeks	CTRL n=3 FLUOX n=3	N.A.	N.A.

TABLE 1 Table representing the number of animals used for the different experimental protocols. M= male mice, N.A. = not applicable, IF = immunofluorescence, WB = Western Blot, RT-PCR = Real Time PCR.

TOYS	DAY 1	DAY 2	DAY 3	DAY 4	DAY 5	DAY 6	DAY 7
Running wheel	X	X	X	X	X	X	X
Nesting material	X	X	X	X	X	X	X
Cardboard rolls		X			X		X
Marbles			X		X	X	
Stairs				X		X	X

TABLE 2 Scheme of the toys differentially used to perform the environmental enrichment on 7 weeks CD1 male mice. The X in the square states that the toy (raw) was present in the cage at that specific day (column). If a cell is empty, it means that the toy (row) wasn't present at that specific day (column).

Gene name	Forward sequence	Reverse Sequence
BDNF	CACATTACCTTCCTGCATCTGTTG	CTGGTGGAACATTGTGGCTTT
TUBB3	ACAATGAGGCCTCCTCTCACA	TCCATCGTTCCAGGTTCCAA
ntrk2	CACACACAGGGCTCCTTAAGG	TGGCGCAAAATGCACAGT
Slc1a3	CGCGGTGATAATGTGGTATGC	GAGGCCGACAATGACTGTCA
Gapdh	GTCCGTCGTGGATCTGA	GATGCCTGCTTCACCACCTT

TABLE 3 Table reporting the primer sequences for the RT-PCR analysis. TUBB3 is the β3-Tubulin gene, ntrk2 is the TrkB gene and Slc1a3 is the GLAST gene.

Experiment	Step	Animal group	Sex	n° animals	DPI	Score
Co-culture	/	WT C57Bl/6J pups	F, M	7	/	/
	/	WT C57Bl/6J	F, M	3	/	/
	Onset	MOG	F, M	3	10-12DPI	1
FACS	Onset-Peak	CTRL-CFA	F, M	5	12-13DPI	0
		MOG	F, M	6	12-13DPI	1-3
IF	Pre-onset	CTRL-CFA	F, M	3	5DPI	0
		MOG	F, M	3	5DPI	0
	Onset	CTRL-CFA	F, M	3	10-12DPI	0
		MOG	F, M	3	10-12DPI	1
	Peak	CTRL-CFA	F, M	3	13-15DPI	0
		MOG	F, M	3	13-15DPI	3-4
	Chronic	CTRL-CFA	F, M	3	28DPI	0
		MOG	F, M	3	28DPI	1,5-2
scRNAseq	Onset-Peak	CTRL-CFA (group 1)	F	3	16DPI	0
		CTRL-CFA (group 2)	F	3	16DPI	0
		MOG (group 1)	F	6	16DPI	1-2,5
		MOG (group 2)	F	6	16DPI	1-2,5

TABLE 4 Table reporting EAE and controls scores of the animals in different experiments. Scale: score 0, no disease; score 1, tail weakness/paralysis; score 2, paraparesis; score 3, paraplegia; score 4, paraplegia with forelimb weakness or paralysis; score 5, moribund or dead animal (Constantin et al., 1999) (Stromnes and Goverman, 2006). WT=Wild-Type, CTRL+CFA= Control with complete Freund's adjuvant, MOG= EAE Animals with MOG35-55 peptide, M= male, F= female, DPI= Day Post Immunization.

LIST OF ABREVIATIONS

5-HT = 5-hydroxytryptamine
APCs = Antigen Presenting Cells
BDNF = Brain-Derived Neutrotrophic Factors
BrdU = Bromodeoxyuridine
CFA = Freund's adjuvant
CNS = Central Nervous System
CTRL = control animal
CSF = Cerebrospinal fluid
CXCL12 = C-X-C Motif Chemokine Ligand 12
DBI = diazepam binding inhibitor
DCs = Dendritic Cells
DCX = doublecortin
DG = dentate gyrus
DPI = Day Post Immunization
EAE = Experimental Autoimmune Encephalomyelitis
EBV = Epstein-Barr virus
ECM = extracellular matrix
EE= enriched environment
FACS = Fluorescence-activated cell sorting
FGF = Fibroblast Growth Factor
FGF2 = Fibroblast Growth Factor 2
FLUOX = animal treated with fluoxetine
GABA = gamma-aminobutyric acid
GCL = Granule Cell Layer
GCs = Granule Cells
GFAP = Glial Fibrillary Acidic Protein
GFP = Green Fluorescent Protein
GL = Glomerular Layer
GLAST = Glutamate and Aspartate Transporter
GRP = Glia-Restricted Progenitor
HPA = hypothalamus-pituitary-adrenal
LP = Lumbar Punctures
MAO = Monoamine Oxidase
MAOIs = Monoamine Oxidase inhibitors
MBT = Marble Burying Test
MHCII = Major Histocompatibility Complex class II
MOG = Myelin Oligodendrocyte Glycoprotein
MRI = Magnetic Resonance Imaging
MS = Multiple Sclerosis
NEUN = NEUronal Nuclei
NG2 = Neural/Glial antigen 2
NGF = Nerve Growth Factor
NGFR = Nerve Growth Factor Receptor
NP = Neural Precursors
NRG-1 = Neuregulin-1
NSC = Neural Stem Cells
NT3 = neurotrophin-3
NT4 = neurotrophin-4
OB = Olfactory Bulb
OCD = Obsessive Compulsive Disorder
PA = Physical activity
PCPA = Para-Chlorophenyl Alanine
PDGFrβ = Platelet Derived Growth Factor receptor β
PGCs = Periglomerular Cells
PI3K = Phosphatidylinositol-3'OH-kinase
PP = Primary Progressive
PV = Parvalbumin
RG = Radial Glia
RGPs = Radial Glia Progenitors
RMS = Rostral Migratory Stream
RP = Relapsing Progressive
RR = Relapsing Remitting
SCI = Spinal Cord Injury
ScRNAseq = single-cell RNA sequencing
SER = Serotonin
SERT = Serotonin Transporter
SGZ = Sub Granular Zone
SP = Secondary Progressive
SSRI = Selective-Serotonin Reuptake Inhibitor
SVZ = Sub Ventricular Zone
TCAs = tricyclic antidepressants
TPH 2 = Tryptophan Hydroxylase
TrkA = Tropomyosin receptor kinase A
TrkB = Tropomyosin receptor kinase B
VEGF = Vascular Endothelial Growth Factor
VEH = Vehicle
VMAT 2 = Vesicular Monoamine Transporter
WT = Wild-Type
β3-Tub = Tubulin β3

SUMMARY

Leptomeninges have been indicated as a novel neurogenic niche hosting neural stem cells (NSCs) able to generate neurons which can migrate and integrate into the brain cortex (Bifari et al. 2015; Bifari et al. 2009; Bifari et al. 2017; Decimo et al. 2011; Nakagomi et al. 2011; Pino et al. 2017). Nowadays, NSC populations are characterized by dynamic behaviour in response to environmental stimuli suggesting a possible role in physiologic and pathologic conditions (Decimo et al. 2012a; Decimo et al. 2020). In literature, is known that pro neurogenic paradigms such as EE and anti-depressant treatments affect hippocampal neurogenesis. However, the effect on meninges is still unexplored (David et al. 2009; Eisinger and Zhao 2018; Kempermann 2019). Furthermore, meninges are able to promptly respond also to neural pathological states (Lin et al. 2015; Nakagomi et al. 2011; Nakagomi et al. 2012; Ninomiya et al. 2013). In fact, it has been reported that the meningeal NSCs actively reacts to CNS insults (Dang et al. 2019; Decimo et al. 2011; Ninomiya et al. 2013). However, the specific role of meningeal NSCs in autoimmune disease is still unknown. The overall aim of my thesis was to investigate how meningeal niche can respond to neurogenic stimuli contributing to brain plasticity in physiological conditions and whether and how the meningeal NSC niche can be actively involved in response to autoinflammatory pathological stimuli.

Enriched environment (EE), a particular housing condition which can offer enhanced sensory, cognitive or motor stimulation to the animal, and antidepressant treatment, are pro-neurogenic stimuli capable of increasing the number of newborn neurons in the DG of treated animals (Eisinger and Zhao 2018; Khodanovich et al. 2018). In the first part of the thesis, I characterized meningeal stem cell niche of young mice after exposure to EE and following administration of the selective serotonin reuptake inhibitor antidepressant Fluoxetine. By using immunofluorescence confocal analysis, western blot and RT-PCR we found that neural progenitors (GLAST$^+$ cells) and immature neurons (β3-tubulin$^+$ cells) were increased after the treatments and that BDNF played a pivotal role in this context, suggesting that the EE exposure was able to activate the meningeal niche. Interestingly, meningeal niche was found to be responsive also to a paradigm of Fluoxetine administration by increasing, similarly to EE exposure observations, GLAST$^+$ neural precursors and β3-Tubulin$^+$ immature neurons. These results confirm a reaction of meningeal niche to a different pro-neurogenic stimulus.

Then, we questioned about the role of meningeal niche in pathological stimuli. Exploiting the Experimental Autoimmune Encephalomyelitis (EAE) animal model, we studied the impact of the neurodegenerative Multiple Sclerosis (MS) disease on NSC meningeal population. Specifically, due to the inflammatory condition established following the development of MS disease, we focused the attention on the relationship between immune cells and NSCs and on the role of brain and spinal cord meninges as possible entry way for immune cells to the CNS parenchyma following inflammatory stimuli. By means of immunofluorescence and histological staining we found an increased number of NSCs and immune cells in meninges of brain and spinal cord animals and, in these sites, a strong presence of infiltrates, according to pathological cell recruitment of MS (Jordão et al. 2019; Wu et al. 2010). Moreover, NSCs expressing immunological marker have been found in meninges, suggesting an involvement of meninges in trophic and immune modulatory activity (Decimo et al. 2012b). Investigating in more detail the relationship between immune cells and NSCs by a genomic approach (scRNAseq) and *in vitro* techniques (co-culture and FACS analysis), we found a strong link between neutrophils and NSCs suggesting that NSCs could have immunomodulatory properties (Decimo et al. 2012a; Kokaia et al. 2012).

All together these results indicate that meninges not only harbour a neural stem cell niche but also highly and actively respond to different stimuli. Meninges may be modulated by neurogenic stimuli such as EE and Fluoxetine and may be one of crucial checkpoint at which auto-reactive T cells are licensed to enter CNS parenchyma during MS, thanks to a dynamic interplay between different cell populations that include NSCs.

Collectively, a better understanding of NSCs role in different paradigms may help to discover the mechanism that underpins the physiological and pathological processes and can help to consider meninges as a potential pharmacological target for regenerative medicine of the CNS.

CHAPTER 1 – INTRODUCTION

1.1 Meninges

1.1.1 Anatomical structure

Meninges are a system of three-layered membranes which envelop the Central nervous System (CNS) (brain and spinal cord) at each level of its organization (Decimo et al. 2012a). The three layers which compose them are called dura mater, arachnoid and pia mater (Figure 1.1).

Dura mater represents the upper layer attached to the cranial and vertebral bones and it is composed by three different layers: the endosteal layer, the meningeal layer and the border cells layer (Adeeb et al. 2012). The endosteal layer lies in tight contact with the skull and the vertebrae of the spinal cord and it contains mainly fibroblast-like cells and extracellular collagen fibers, which are responsible for the resistance typical of this layer. Below, the endosteal layer confers to the dura its flexibility, due to the high presence of fibroblast and the low content of extracellular matrix components (ECM). Last, there is the border cells layer, which is in direct contact with arachnoid layer, composed of a thin sheet of flat cells linked by desmosomes and extracellular space filled with amorphous material (Adeeb et al. 2012).

The two innermost meningeal layers, pia mater and arachnoid, are collectively called leptomeninges and are filled with cerebrospinal fluid (CSF) produced by the choroid plexus stroma (Bifari et al. 2017). Indeed, the main meningeal projection within the brain parenchyma, called the meningeal substructure, extends below the hippocampus and is continuous with the same choroid plexus stroma (Bifari et al. 2017; Decimo et al. 2012b; Mercier and Arikawa-Hirasawa 2012; Mercier and Hatton 2003) and forms the non-neural roof of the third ventricle, a structure known as choroid tissue (Decimo et al. 2020).

The arachnoid mater is in direct contact with the dura mater through its outer mesothelial layer, which is composed of few stacked flat cells separated by tight junctions. Below the mesothelial zone, the inner reticular layer is less organized and is composed of cell whose processes are linked by gap junctions and desmosomes and are surrounded by collagen fibers and small cisternae (Vandenabeele et al. 1996).

Between the arachnoid and the pia mater there is the subarachnoid space which contains the cerebrospinal fluid (CSF) that envelop the brain and the spinal cord and is crossed by arachnoid trabeculae. These structures are composed by a collagen core and are covered by leptomeningeal cells allowing the flow of CSF within the subarachnoid space (Adeeb et al. 2013).

Below the subarachnoid layer lies the pia mater which closely covers the CNS parenchyma. Pia mater can be dived into a vascular layer, composed of a network of minute blood vessels combined with collagenous fibres, and a avascular layer composed of reticular elastic fiber separated from the CNS parenchyma by the basement membrane of the glia limitans (Jones 1970). In addition, introflections of the pia and arachnoid membranes (leptomeninges) form a perivascular space (Virchow-Robin space) around every vessel of the CNS (Bifari et al. 2015) (Figure 1.1).

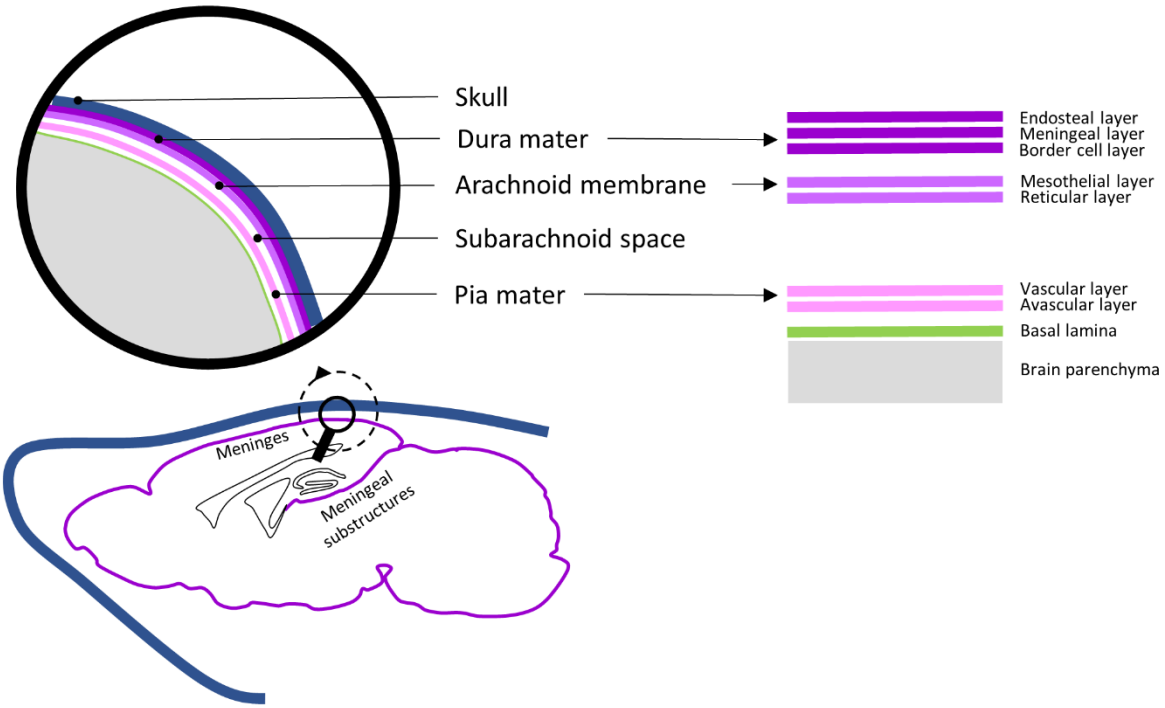

FIGURE 1.1 SCHEMATIC REPRESENTATION OF THE MENINGEAL LAYERS

This drawing depicts the localization of the meninges, covering and penetrating the CNS. The pia mater is indicated in pink and it's in close contact with the basal lamina (green) of CNS parenchyma (grey). The pia mater is divided from the arachnoid (light violet) by the subarachnoid space; the dura mater (dark violet) is the outer layer, in direct contact with the skull. Modified from Department of Neurosurgery Tokai University Hospital.

The principal function usually attributed to meninges and CSF is to protect the CNS from potential injuries and traumas (Decimo et al. 2012b; Nakagomi et al. 2011;

Nakagomi et al. 2012). However, in the past, this was wrongly considered as the only function of the meningeal layers (Decimo et al. 2012b): nowadays we know that they also anchor the CNS to the surrounding bones and that their presence is essential for CNS development (Decimo et al. 2012b).

1.1.2 Meningeal role in CNS development

Meninges originate early in development from the mesenchymal tissue that surrounds the neural tube and they are involved in the regulation of CNS development (Etchevers et al. 2001). Specifically, meninges are necessary for , the genesis of the cerebral cortex (Radakovits et al. 2009), cerebellum (Sievers et al. 1986) and hippocampus (Hartmann et al. 1992). The primordial of meninges, “meninx primitive”, is initially composed of mesenchymal neural crest cells and an early vascular net of endothelial cells and *in vivo* and *in vitro* studies have underlined its importance for the survival and the subsequent growth of neural progenitors (Decimo et al. 2020).

The meninges, due to their distribution and connection with the vascular system, supply brain structures with various growth/trophic factors, which are essential for the development and function of the brain's neural progenitors and differentiating cells. The meninges in fact, exert direct effects on Radial Glia (RG) cells by secreting high levels of retinoic acid. This process leads the RG cells to neurogenic divisions, thus regulating the generation of cortical neurons and the development of the anterior hindbrain (Siegenthaler et al. 2009). Furthermore, they also contribute to the proper development of the spinal cord, as they are able to serve axonal guide molecules for motor and sensory neurons (Suter et al. 2017), and the correct formation of the dentate gyrus (Hartmann et al. 1992).

The meninges also play a role in the development of the corpus callosum and in the migration of oligodendrocyte precursor cells (OPCs) into the developing cerebral cortex by secreting signalling factors like BMP-4 and BMP-7 and proteins of the TGFβ family (Choe et al. 2014; Choe et al. 2012).

The meninges are also implicated in the development of the lymphatic network and in the modulation of immune cells as they are a source of VEGF-C, essential for these processes (Song et al. 2020).

1.1.3 Meninges and CNS homeostasis

Recently, have been established a more complex consideration of meningeal functions as modulator of CNS homeostasis and disease. Indeed, the role of meninges in CNS also involves production and interaction with different components of the extracellular matrix (ECM). Meningeal cells have in fact been shown to synthetizes collagen and non-collagen proteins including fibronectin, laminin and tenascin (Decimo et al. 2012b; Mercier 2016; Sarrazin et al. 2011). These ECM components are localized at the surface of the brain and around the blood vessels inside the brain and can aggregate into organized structures, called fractones, that have been shown to be next to stem cells in different brain areas such as in the subventricular zone. The presence of those structures in meninges, confer to them the potential to modulate stem cell homeostasis and cortical function (Bifari et al. 2015; Decimo et al. 2020).

Furthermore, meninges are an important source of several trophic factors such as FGF-2, insulin-like growth factor-II, chemokine 12, retinoic acid, growth factors and cytokines, including those promoting stem cell proliferation and differentiation (Belmadani et al. 2015; Bifari et al. 2015; Borrell and Marín 2006; Decimo et al. 2012a; Reiss et al. 2002; Stumm and Höllt 2007).

Interestingly, cells of the meninges have been shown to be highly responsive to principal mitogens such as EGF, FGF-2, and BDNF (Day-Lollini et al. 1997). Heparan sulfate proteoglycans enrichments have been found in regions associated to neural stem cell proliferation (Kerever et al. 2007; Mercier and Arikawa-Hirasawa 2012).

Altogether the data indicate that meninges are an important structure that modulates brain function during embryogenesis and adult life.

1.2 Meningeal neural stem cell niche

1.2.1 Meningeal neurogenesis in physiological condition

Different groups demonstrated that NSCs, which can differentiate into neural lineage cells, could be induced in brain meninges (leptomeninges) (Belmadani et al. 2015; Bifari et al. 2017; Dang et al. 2019). In fact, all the features, finding and characterization of meningeal membranes beforementioned, has given consistency to the concept of meninges as putative NSC niche (Decimo et al. 2012a).

Meninges can be considered a NSC niche for three main reasons (Bifari et al. 2017). In the first place, meninges host subsets of non-parenchymal multipotent cells (Bifari et al. 2017; Decimo et al. 2011; Decimo et al. 2020). Secondly, non-parenchymal PDGFrβ$^+$ progenitors (which are perivascular cells) can differentiate into neurons without needing proliferation *in vitro* (Karow et al. 2012), while meningeal cells can produce neurons *in vivo,* both, in physiological conditions and after transplantation in the post-natal brain (Bifari et al. 2009; Bifari et al. 2017; Decimo et al. 2020). Thirdly, it has been proved (Decimo et al. 2012b; Scadden 2006) that the meningeal niche is a tissue microenvironment able to host and maintain neural progenitors for the whole life of the organism. All these three features are present in other well-established neurogenic niches, like the SVZ, giving consistency to the theory that meninges could be considered a NSC niche.

This hypothesis has been furtherly confirmed by several studies (Bifari et al. 2015; Bifari et al. 2009; Decimo et al. 2011) which showed the presence of nestin-positive cells in brain meninges of embryonic and adult rodent: nestin, an intermediate filament of neuroepithelial derivation, has been linked with stemness properties in many tissues (neural and non-neural) (Lendahl et al. 1990; Wiese et al. 2004). The cells extracted from meningeal biopsies were able to grow as neurospheres and to differentiate *in vitro* and *in vivo* into neurons or mature MBP$^+$ oligodendrocytes, proving their stemness properties (Dolci et al. 2017). As cells expressing nestin have been identified in human encephalic and spinal cord meninges (Decimo et al. 2012b), this increases the probability that the observation of meningeal stemness in rodents could be extended to humans as well.

The neurogenic potential of meninges has been furtherly proved in a recent study (Bifari et al. 2017), in which it was proved the existence of a pool of embryonic RG-like meningeal cells able to migrate and differentiate into functional neurons in the neonatal brain cortex (Figure 1.2). In this study, both gene and protein expression analysis revealed glutamate/aspartate transporter (GLAST) expressing cells in meninges (Bifari et al. 2017). Other RG specific markers have been found in meningeal cells. As in the ventricular zone of the developing cortex (Götz et al. 1998), also in perinatal mouse and in adult meninges, were found cells expressing RG-like PAX6 gene (Bifari et al. 2017) and PAX6 protein (Zeisel et al. 2015). Similarly, SOX2, the HMG-Box

transcription factor, expressed in the neural tube during development and in postnatal RG cells (Zappone et al. 2000), were found in embryonic, early postnatal and rarely also in adult brain meninges (Bifari et al. 2015; Nakagomi et al. 2011; Qin et al. 2008). These findings are extremely relevant as they indicate that (1) quiescent/embryonically born neural progenitors could participate in early postnatal differentiation into cortical neurons, (2) the concept of brain plasticity could be broaden than how it's currently intended and (3) neural precursors do not only reside in brain parenchyma, as it's currently postulated, but, instead can also come from meninges, highlighting meningeal tissue as an important source of neurogenic cells.

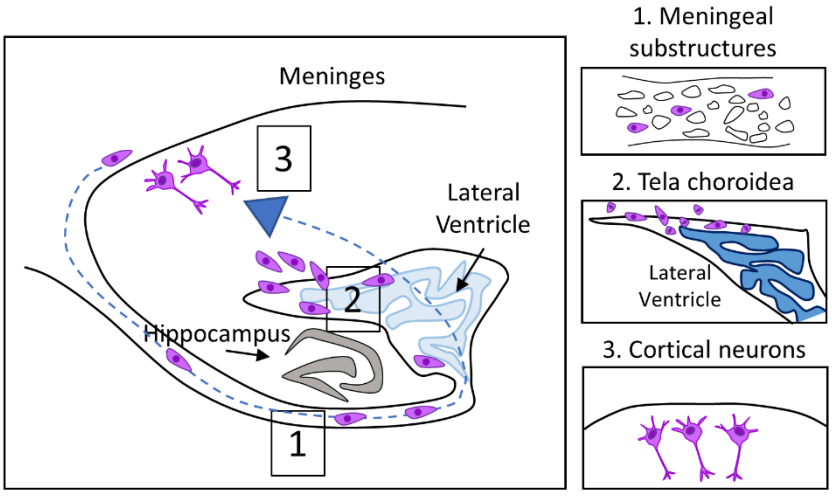

FIGURE 1.2 SCHEME OF PROPOSED MODEL OF MENINGEAL CELL MIGRATION AND DIFFERENTIATION
Meningeal neurogenic cells (violet) (box 1) migrate to the cortex via the tela choroidea (box 2, the thin layer covering the ventriculus) and differentiate to neurons (box 3). These meningeal neurogenic cells are distinct from the neurogenic ventricular radial-glia. Large dashed blue arrow shows the path of migration of meningeal neurogenic cells to the cortex. Adapted from (Bifari et al 2017).

1.2.1.1 Neurogenic stimuli

The generation of newborn neurons was known to be restricted only to embryonic developmental stage however, neurogenesis has been proven to occurs also in adulthood in specific brain regions: the SVZ and the SGZ of the hippocampus and, recently, in meninges. Adult neurogenesis in mammals can be modulated by several stimuli, including exposure to enriched environment (EE) (Benarroch 2013; Venna et al. 2014) and antidepressant treatments (David et al. 2009; Micheli et al. 2018; Samuels and Hen 2011; Wang et al. 2008).

EE is a combination of housing condition and social stimulation which can offer enhanced sensory, cognitive or motor stimulation to the animal (Zhou et al. 2017). It has been shown to induce hippocampal neurogenesis, and its therapeutic effect has been used to ameliorate brain injury outcomes (Forbes et al. 2020).

Similarly, fluoxetine (FLUOX), a selective serotonin reuptake inhibitor (SSRI) antidepressant (Ferguson 2001; Samuels and Hen 2011), as well as other SSRI antidepressants like imipramine, also increase hippocampal neurogenesis (David et al. 2009; Duman and Monteggia 2006; Samuels and Hen 2011).

Several molecular pathways can link EE with its own neurogenic effect but the most known pathway involve the brain-derived neurotrophic factor (BDNF): EE exposure is able to increase the concentration of these pro-neurogenic molecules in the brain of the treated animals and, thus, this lead to a significant increase in the DG neurogenesis (Benarroch 2013; Eisinger and Zhao 2018).

BDNF is a member of the neurotrophin family and it plays a fundamental role in neuronal development, synapse formation and synaptic plasticity (Bjorkholm and Monteggia 2016). It is widely expressed throughout the CNS: it is synthesized in the neuronal/glial cell bodies and then transferred to the terminals, where it is released to perform its functions (Bjorkholm and Monteggia 2016).

BDNF is a ligand for several receptors such as: the tropomycin receptor kinase B (TrkB) (Klein et al. 1991) and the neurotrophin receptor p75 (also called NGFR, nerve growth factor receptor). However, while the BDNF-TrkB bond has a high affinity, the interaction between BDNF and p75 is a low affinity interaction (Formaggio et al. 2010; Meeker and Williams 2015). TrkB receptors are expressed both at pre- and post-synaptic level and, when bound by BDNF, they regulate postsynaptic neural responses and neurotransmitter release (Madara and Levine 2008).

The link between BDNF and TrkB can regulate different intracellular pathways (Eisinger and Zhao 2018; Park and Poo 2013). The first pathway involves phospholipase C-γ (PLC-γ), which in turn can activate protein kinase C (PKC). The second is based on mitogen activated protein kinase (MAP), which leads to the activation of Ras and causes the production of further downstream effectors. Finally, the third pathway involves phosphatidylinositol-3'OH-kinase (PI3K) which can activate the AKT-mTOR signalling pathway (Park and Poo 2013).

Given the crucial role of BDNF signalling in EE-induced neurogenesis and the evidence of TrkB expression in meningeal NSC (Bifari et al. 2017; Pino et al. 2017), the meningeal niche could potentially be responsive to stimuli like EE and antidepressant.

1.2.2 Meningeal neuronal stem cell niche in pathology

The meningeal niche not only acts as a reservoir of new neurons, but actively responds to CNS insults such as stroke, physical injury, epilepsy, spinal cord injury, and neurodegenerative disease (Decimo et al. 2011; Decimo et al. 2020; Nakagomi et al. 2011; Nakagomi et al. 2012). According to this, NSC niche is activated following disease, and precursor cells migrate and participate to the parenchymal reaction (Decimo and others 2012a; Morrison and Spradling 2008). In pathological condition, NSC niche activation can be induced by different signals such as abnormal neurotransmitter release, invasion by inflammatory molecules, chemokines, and immune cells, that results in the proliferation of niche cells, change of the molecular signature and nature of neural progenitors and remodelling in ECM composition (Decimo et al. 2020). Different approaches such as lineage tracing and *in vivo* labelling as well as histological, *ex vivo* and *in vitro* have been used to describe disease-induced activation of meningeal NSC niche.

Nakagomi et al. reported that under pathological conditions, new neural progenitors are generated in adult brain in non-conventional neurogenic regions such as leptomeninges (Nakagomi et al. 2015). In fact, in the post-stroke meninges and in the perivascular space of the infiltrating pial vessels, were found cells expressing markers of Nestin, PDGFrβ and SOX2. In addition, through *in vivo* labelling techniques, an increase in DCX^+ cell in meninges has been shown following ischemia, which migrates to the post-stroke cortex (Nakagomi et al. 2011). Following spinal cord injury, meningeal NSCs increase their self-renewal and proliferative properties, start to express DCX marker and migrate to the neural parenchyma where they contribute to the neural parenchymal reaction (Decimo et al. 2011). Furthermore, some DCX^+ cells were also found to express the phagocytic marker CD68 which is fundamental in the progression of neurodegenerative disease (Unger et al. 2018).

The function of these DCX^+ cells is not yet known, but they seem to be strongly related to the inflammatory process.

A strong reaction of meninges was also found in other disease models, as the case of the activation of Nestin^{+} cells with an anti-epileptogenic role in an animal model of epilepsy that ignites the amygdala (Ninomiya et al. 2013). During disease these meningeal NSCs have a neurogenic potential capable of generating oligodendrocytes. Indeed, following transient ablation of OPCs in the adult brain, a strong activation of NSCs residing in cortical meninges was observed (Dang et al. 2019).

Overall, under physiological conditions, *in vivo* data suggest that the neural precursors residing in meninges are able to promptly respond to pathological states. Accumulated disease-induced meningeal neural precursors migrate into the neural parenchyma and contribute to neural regeneration of the CNS. Furthermore, the *in vivo* neurogenic and oligodendrogenic differentiation potential of meningeal NSCs has been demonstrated both in healthy and disease conditions (Dang et al. 2019).

Overall, the meninges are a source of adult, somatic, endogenous NSCs that could be modulated *in vivo* and *in vitro*. A better understanding of the molecular signals activating endogenous meningeal NSCs and inducing their expansion, migration, and neural differentiation potential, will set the stage for potential relevant new approaches for regenerative medicine of the CNS. Drugs acting by modulating the meningeal endogenous neural progenitors may provide new and effective therapies for CNS disorders. For this reason, they represent a promising pharmacological target for regenerative medicine and novel therapies for CNS disorders, such as multiple sclerosis.

1.2.2.2 Meninges in MS

1.2.2.2.1 Pathogenesis of MS

Multiple Sclerosis (MS) is a chronic inflammatory neurodegenerative disease of the CNS, characterized by inflammatory infiltrates, demyelinating plaques, and axonal damage (Glatigny and Bettelli 2018) that occur in white and grey matter of the brain and spinal cord (Dendrou et al. 2015). MS is the most common progressive neurological disease affecting young adults (Figure 1.3) (Dobson and Giovannoni 2019) with 2.2 million cases of MS worldwide, corresponding to a prevalence of 30.1 cases per 100.000 population (data of 2019). The prevalence of MS varies considerably

between countries: highest rate in high-income countries (North America and Europe) and lowest rates in Eastern Asia and sub-Saharan Africa (Howard et al. 2016).

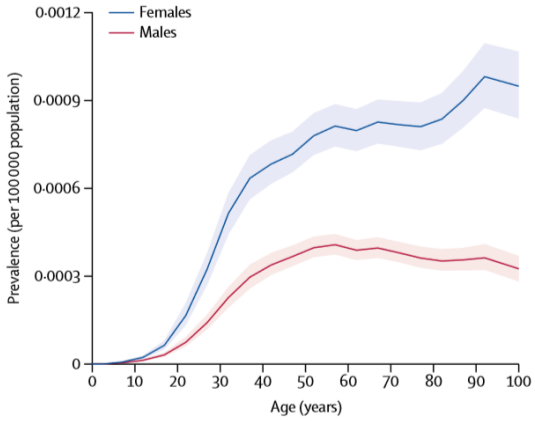

FIGURE 1.3 AGE-STANDARDISED PREVALENCE OF MULTIPLE SCLEROSIS IN 2016, BY AGE AND SEX (Adapted from Wallin et al. 2019)

Nowadays the trigger(s) of MS remains elusive. Its pathogenesis can be explained by multifactorial model incorporating interaction between genetic, epigenetic, and infectious, nutritional, climatic, or other environmental influences, including sunlight exposure, smoking and Epstein-Barr virus (EBV) infection (Baranzini and Oksenberg 2017; Belbasis et al. 2015). Consequentially optic neuritis, diplopia, sensory loss, limb weakness, gait ataxia, loss of bladder control, and cognitive dysfunction are the common neurological manifestation of MS. MS leads to chronic progressive disability in most cases, resulting in a significant socio-economic impact. Currently, drugs available are partly effective, but whether they alter the long-term course of MS remains unclear (Palace et al. 2015).

Pathogenesis of MS is characterized by the loss of immune homeostasis and self-tolerance. This condition led to infiltration of activated peripheral mononuclear cells in brain and spinal cord, causing an unregulated pathologic inflammatory response toward structural components of the CNS. The damaged tissue in CNS is caused by a complex and dynamic interplay between different cell types resulting in multifocal lesions known as MS plaques. Lesions have been classified into 'active' plaque, occurring in the acute phase of MS, and 'inactive' plaque, generally associated to chronic phase of MS. Acute active MS plaques are characterized by heavy lymphocyte infiltration (mainly $CD8^+$ T cells and $CD20^+$ B cells, with fewer $CD4^+$ T cells), activated

microglia (particularly at the lesion edge and containing myelin debris), macrophages (containing myelin debris) and large, reactive (sometimes multinucleated) astrocytes (Frischer et al. 2015; Reich et al. 2018). In contrast, inactive plaques are sharply circumscribed, hypocellular and have well-defined demyelination, reduced axonal density, reactive astrocyte gliosis, variable microglial activation and a lower density of lymphocytes than active lesions (Prineas and Lee 2019). MS plaques are mostly associated to inflammation and whether the inflammatory process is arrested at early stage, plaques are partly remyelinated (shadow plaques) highlighting the importance of early diagnosis of MS. Most often, lesions are observed in highly myelinated white matter regions which are principally composed by nerve axons and myelinating oligodendrocytes. Hence, white matter plaques are considered as hallmark of MS, and they can be easily detected thought magnetic resonance imaging (MRI). Furthermore, it has been observed that cortical grey matter, which comprises less myelinated nerve cells and dendrites, glial cells, and many capillaries, also greatly contributes to disease pathogenesis (Horakova et al. 2012; Reich et al. 2018).

Nowadays, an exact diagnosis of MS relies on medical history and neurological examination using imaging techniques such as MRI, lumbar punctures (LP) for cerebrospinal fluid (CSF) analysis, evoked potentials, and blood sample analysis (Ghasemi et al. 2017).

In 1996 spectrum of clinical subtypes of MS have been defined reflecting important consideration not only for prognosis but also for treatment decision. This standardized description, revised in 2013 (Lublin et al. 2014), divides MS course into: primary progressive (PP), secondary progressive (SP), relapsing-remitting (RR) and relapsing-progressive (RP). From MS international federation, in approximately 85% of patients the initial form of the disease is RR-MS which is characterized by alternating periods of symptomatic phases—relapses, from which the recovery can be complete or partial, and asymptomatic phases free of new neurological symptoms—remissions (Figure 1.4A). Nonetheless, years after disease onset, many RR-MS patients progress to SP-MS, in which the functional recovery disappears and neurological dysfunction increase (Figure 1.4B). Moreover, 10-15% of people with MS are diagnosed with PP-MS which lacks distinct relapses but showing a slow onset and steadily worsening symptoms (Figure 1.4C) (Klineova and Lublin 2018). On the other hand, the last

common type of MS is PR-MS (about 5%) in which individuals show a steady neurologic decline with a clear manifestation of relapses and unfortunately the disease continues to progress without remission (Figure 1.4D).

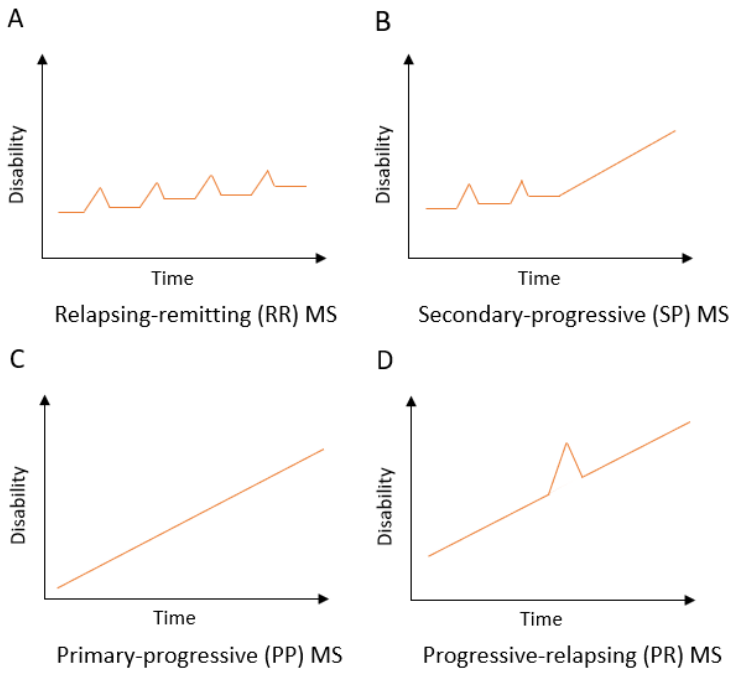

FIGURE 1.4 DIFFERENT CLINICAL COURSES OF MS
Adapted from Lublin & Reingold SC. Neurology, 1996

Currently, the most widely accepted hypothesis regarding MS pathogenesis relies on an auto-reactive leukocytes involvement in disease development (Lemus et al. 2018; Nakahara et al. 2012). From genetic and pathological studies (Gay et al. 1997; International Multiple Sclerosis Genetics et al. 2011), inflammation in MS is due to the selective recruitment of cells from specific target antigens that are present only in the CNS (probably autoantigens). The pathogenic immune response to CNS autoantigens could be initiated in two mechanisms: intrinsic model and extrinsic model of the CNS (Hemmer et al. 2015). The intrinsic model suggests that in the CNS take place the initial event leading to the release of CNS antigens at the periphery. According to this, there is the activation of myelin naïve antigen T cells in the peripheral lymph nodes (CNS draining cervical lymph nodes) by cross-reactive myelin epitopes or myelin-exposing dendritic cells that bring to the onset of disease. When myelin-reactive T cells drain into the CNS for immune surveillance, they are reactivated by cells expressing myelin

epitopes. Subsequently, myelin-reactive T cells infiltrate the CNS parenchyma resulting in inflammation and stimulation of the blood brain barrier (BBB). Following BBB stimulation, myelin-reactive T cells are assumed to be allowed to enter the CNS parenchyma leading to tissue damage (Hemmer et al. 2015).

On the other side, the extrinsic model suggests that the initial event takes place outside CNS leading to an aberrant immune response toward CNS.

In general, the pathogenesis of MS is mediated primarily by T cells. The key role of T cells, particularly $CD4^+$ T cells, in MS has been confirmed in experimental autoimmune encephalomyelitis (EAE), which is the main animal model of MS. Studies on MS and EAE have largely focused on $CD4^+$ T cells. However, many other lymphocyte subsets have been implicated in disease pathogenesis (Rahmanzadeh et al. 2018; Rangachari et al. 2017). Among those subsets include lymphocytes belonging to the adaptive immune system, to the innate immune system, and innate-like B and T lymphocytes that exhibit properties of both innate and adaptive immunity (Van Kaer et al. 2019). Several of these cell types infiltrate the CNS of MS patients and they have been implicated in the efficacy of disease-modifying treatments, contributing to the pathogenesis of EAE (Van Kaer et al. 2019).

As regards treatments, MS still lack an efficient cure. Therapies can be divided in treatments for MS attacks, treatments to modify the MS progression and treatment for MS signs and symptoms. Nevertheless, none of them leads to whole remission from disease and patients need treatments all lifelong (Nafee T. et al. 2018). In this context, research aiming to find out new treatments for the cure of MS is of fundamental importance.

1.2.2.2.2 Molecular mechanism of MS

The MS pathogenic events are mediated by T cells through several mechanisms such as direct cytokine-induce damage and other in indirect mechanisms such as activation of different cell types like B cells, neutrophils and macrophages (Kurschus 2015).

In EAE mouse model, the induction of the disease is initiated through injection of autoantigen-containing CFA emulsion causing strong T cells responses and consequent CNS myelin destruction (Figure 1.5). After immunization with myelin antigens, antigen-presenting cells (APCs) are activated in the lymph nodes by the M.

tuberculosis component of CFA causing the endocytosis of autoantigen present within CFA emulsion. Most of injected antigen will be loaded on major histocompatibility class (MHC) class II presentation pathway to naïve T cells. Different types of $CD4^+$ T helper cells have been described to play a role during EAE pathogenesis such as T helper type 1 (Th1), T helper 17 (Th17), gamma delta T (γδ T) and T regulatory (Treg) (Fletcher et al. 2010; Rostami and Ciric 2013). Furthermore, few studies demonstrated that also $CD8^+$ T cells contributed to EAE pathogenesis showing that $CD8^+$ T cells have a regulatory function in EAE (Feizi et al. 2021; Wagner et al. 2020; Weiss et al. 2008). Myelin-specific activated T cells enter the bloodstream and subsequently the CNS (Figure 1.5). However, the exact mechanism on how T cells reach and infiltrate the CNS remains hypothetical (Schläger et al. 2016). During EAE, around day 8 or 9 after immunization, infiltration of T cells into the CNS occurs. Infiltrating T cells are mainly Th17 cells that express IL-17. It has been described (Hu et al. 2010) that IL-17 is able to induce the secretion of metalloproteases (such as MMP1, MMP3, MMP9, MMP12 and MMP13), cytokines such as macrophages granulocyte-colony stimulating factor (GF- CSF), IL-6 and chemokines (CCL2, CCL7, CCL20, CXCL1, CXCL2, CXCL5) by local tissue cells (Russi et al. 2018). These molecules act as chemoattractors for additional T cells and myeloid cells in the developing CNS lesion. Furthermore, the integrity of the BBB is compromised by IL-17 through the induction of reactive oxygen species (ROS) in endothelial cells. Through permeabilized BBB, other immune cells including neutrophils, B cells and monocytes/macrophages migrate to the CNS. In particular, neutrophils enter the CNS early in disease and may play an important role in the destruction of the BBB and in the maturation of local APCs in the CNS. However, the actual role of neutrophils in the CNS has not yet been elucidated (Russi et al. 2018).

Generally, resident or immigrant APCs in the CNS encounter the related myelin antigen which leads to the reactivation and differentiation of autoreactive T cells which in turn activate nearby immune or neural cells and attract additional inflammatory cells to the CNS through the production of cytokines (Constantinescu et al. 2011; Glatigny and Bettelli 2018). Activated macrophages secrete matrix metalloproteases (MMP2 and MMP9) causing destruction of the parenchymal basement membrane formed by astrocytes in the BBB which allows leukocytes to leave the perivascular space and infiltrate the CNS parenchyma (Agrawal et al. 2006).

Furthermore, elements of humoral immune response and soluble mediators also contribute to pathology through complement activation, direct cytotoxicity (Hemmer et al. 2006). Plasma cells produce antibodies that can bind and activate complement or induce antibody-dependent cytotoxicity and antibody production can be enhanced by Th2 cells that are capable of producing IL-4 (Constantinescu et al. 2011). The consequence of all the pathological mechanisms already described is that myelin is destroyed and generally lacks the potential for regeneration, after several damage peaks with consequent clinical signs of EAE.

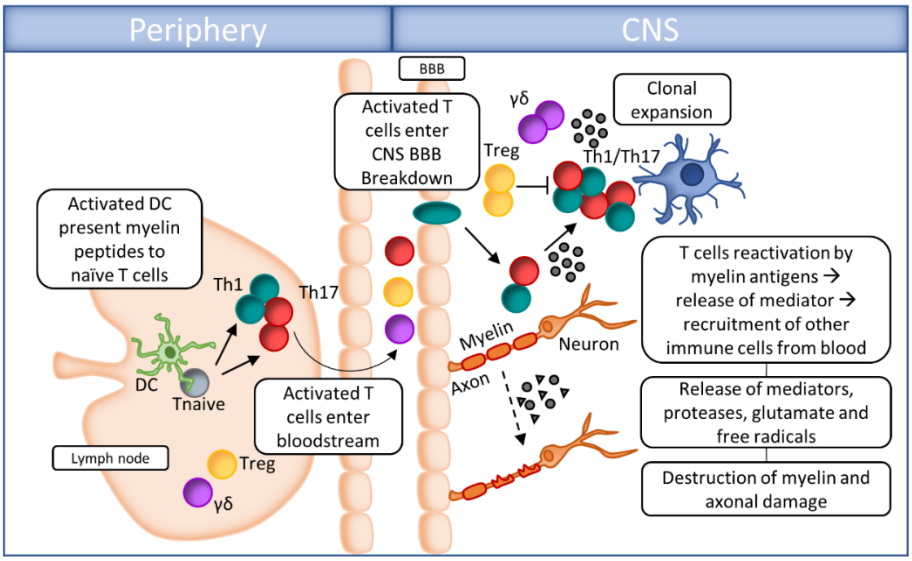

FIGURE 1.5 MIGRATION AND EFFECTOR FUNCTION OF T CELLS IN THE CNS DURING EAE
(Adapted from Fletcher et al. 2010)

1.2.2.2.3 Meningeal role in MS

It has been shown that leukocytes circulating under physiological conditions infiltrate the brain and play an indispensable and trophic role in maintaining healthy brain function (Deczkowska et al. 2016). In relapsing and remitting MS (RRMS) and related EAE animal model, leukocyte support is lost and their accumulation and aberrant activation lead to autoimmune disease (Grigoriadis and van Pesch 2015).

Leptomeninges represent a checkpoint for activated T cells to enter the CNS parenchyma and subsequently become able to reach areas of antigen availability and tissue damage (Schläger et al. 2016). Reactive brain T cells extravasate into the

leptomeningeal vessels. Subsequently, they move by crawling or rolling along the leptomeningeal structures in close contact with the perivascular leptomeningeal macrophages (Bartholomaus et al. 2009; Schlager et al. 2016). Through intravital microscopy studies, the importance of the interaction of reactive brain T cells with resident meningeal stromal cells and macrophages was demonstrated (Bartholomaus et al. 2009; Schläger et al. 2016). As a result of these interactions, effector T cells produce proinflammatory mediators and cause tissue invasion with consequent inflammatory infiltrations (Bartholomaus et al. 2009; Schlager et al. 2016). Extravascular reactive brain T cells are strongly activated in the leptomeninges and upregulate proinflammatory cytokines (interferon (INF)-g, interleukin (IL)17, tumor necrosis factor (TNF)-a, IL2), protease (matrix metalloproteinase (MMP)9, 14), chemokines/chemokine receptors (CCR5, CXCR3, CXCR4) and surface activation markers (OX40 antigen, IL2 receptor, VLA-4 and LFA-1 integrins) (Grigoriadis and van Pesch 2015). Within the leptomeninges, therefore, a strong up-regulation of chemokines (CCL5, CXCL9-11 and CXCL12), of integrin ligands (fibronectin and ICAM-1) is generated (Schläger et al. 2016) which in turn leads to further attachment of T cells and migration into the CNS parenchyma (Schläger et al. 2016).

Meningeal leukocyte infiltrates consist of T cells, B cells, plasma cells, monocytes and macrophages. In the meninges during acute disease as well as during relapses, infiltrates of T cells are observed when neither BBB permeability nor significant increases in the number of peripherally derived immune cells in the CNS are observed. In the meninges, already a few days after the onset of the disease, the development of the organization of the tertiary lymphoid tissue has been described. Meningeal antigen-presenting phagocytic cells have been shown to interact productively with myelin-specific T cells in the subarachnoid space (Pikor et al. 2015). Furthermore, lymphoid-like stromal cells, specific network of extracellular matrix and expression of homeostatic cytokines and chemokines have been described in meningeal infiltrates during MS (Pikor et al. 2015). The extension of the meningeal lymphoid tissue is associated with subpial cortical damage and disease progression (Magliozzi et al. 2007).

1.2.2.2.4 Animal model for MS

Over the years different animal models have been commonly used to investigate the immunopathological mechanisms behind the MS. Animal modeling has been critical for addressing MS pathogenesis and a single animal model cannot capture the entire spectrum of heterogeneity of human MS (Procaccini et al. 2015). Different animal models of MS are available such as Experimental Autoimmune Encephalomyelitis (EAE), the virus-induced forms (mainly Theiler's Murine Encephalomyelitis Virus, TMEV) and toxic-induced models of demyelination. In these animal models the disease initiation is artificial raising the question whether them could really represent a suitable model for MS. Indeed, the time-frame of disease onset is different between humans and mice disease: in humans, disease remains undetected for years before disease onset, whereas in animal model disease onset can be detected within weeks after the induction of disease. However, the use of MS animal models has many advantages in terms of convenient source of tissue from CNS, as a testing tool to study disease development and for a novel therapeutic approach.

As before mentioned, the most-studied MS model is EAE which supports the autoimmunity hypothesis of disease development (Procaccini et al. 2015). In EAE animal model the autoimmunity to CNS components is induced through immunization with self-antigens derived from myelin protein. In order to enhance the immune response and to induce the typical oscillation of MS symptoms, Freund's adjuvant (CFA) which contains high amount of heat-inactivated Mycobacterium tuberculosis was added (Munoz et al. 1984). Experiments were performed in different animal species such as guinea pigs and monkeys, but the murine animals resulted the best model to investigate the most common types of MS (RR-MS and chronic progressive phase). The onset of MS in EAE model normally initiates after about 10 days of injection and it is characterized by ascending paralysis firstly beginning at the tail, followed by limb and forelimb paralysis which can be assessed by using a 5-points scale (Brocke et al. 1994). EAE may be induced in different genetic backgrounds (SJL/J, C57BL/6). In particular, C57BL/6 mice develop a chronic progressive course of disease. The induction of disease is given by administration of autoantigens: myelin oligodendrocytes glycoprotein (MOG35-55) which is a very minor component (0.01%-

0.05% of membrane protein) expressed on the outer surface of CNS myelin. Injection of MOG35-55 is able to induce directly CNS autoimmunity reflecting the development of chronic form of disease without remission. Furthermore, it has been shown (Berard et al. 2010) that depending on the dose of MOG35-55/adjuvant injected a chronic (high dose) or RR disease course (low dose) can be obtained (Figure 1.6) suggesting the key role of MOG35-55 for disease development.

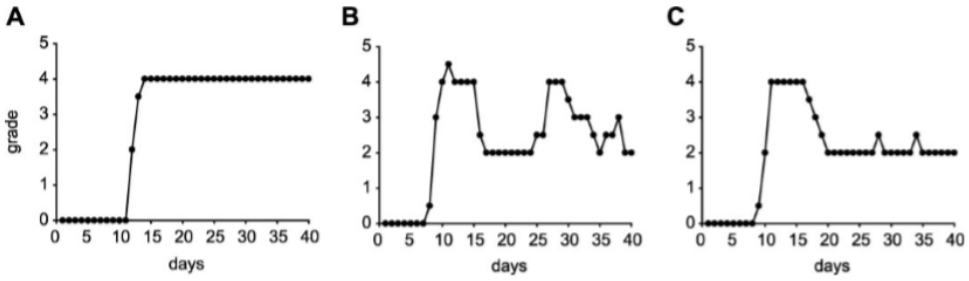

FIGURE 1.6 CLINICAL COURSE OF CHRONIC AND RR-EAE IN C57BL/6
Graphs showing examples of single representative mice with chronic-EAE (A), and the multiphasic (B) and monophasic (C) forms of RR-EAE. Adapted from Berard et al. 2010.

EAE model do not reflect the MS in pattern of tissue damage. For example, one of the hallmarks of MS disease are sharply demarcated white matter lesions with marked vesicular disruption of the myelin sheaths. Whereas typical EAE is characterized by only limited myelin damage without vesicular change. These difference between EAE and MS give rise to growing evidence suggesting a significant role for other cells in disease pathogenesis like B cells (Comi et al. 2021). Both antibody-dependent and antibody-independent mechanisms are thought to underlie B cell–mediated CNS injury in MS. B cell functions implicated in pathogenesis included antigen presentation to T cells and driving auto proliferation of brain-homing T cells, production of soluble toxic factors contributing to oligodendrocyte and neuronal injury, production of proinflammatory cytokines and chemokines and contribution to the formation of ectopic lymphoid aggregates in the meninges. These B cell actions may contribute to both MS relapses and disease progression (Comi et al. 2021).

Those drawbacks were solved with the development of a new disease model that exactly recapitulated the pathology of human MS (Comi et al. 2021; Hauser 2020). Benefits of therapies were present almost immediately, indicating a direct effect on B

cells rather than on antibody products of plasma cells, likely due to interference with antigen presentation or cytokine secretion by disease-associated B cells.

The proof of principle studies led to pivotal trials, global approvals by regulatory agencies, and major changes in the treatment of MS. Both translational and clinical research has now been recast, focused on B cells as mediators of both aspects of MS: inflammation and neurodegeneration (Comi et al. 2021; Hauser 2020).

AIMS

Meninges are an essential structure with trophic, immune and neurogenic properties. In physiological conditions they have several roles such as the production and releasing of several trophic factors important for neural cell migration and survival, the regulation of cerebrospinal fluid dynamics, and they allow numerous immune interactions affecting neural parenchymal functions (Barber et al. 2018; Borrell and Marín 2006; Choe et al. 2012; Davare et al. 2014; Decimo et al. 2020; Louveau et al. 2017). Recently, meninges emerged as important player in development and neurogenesis (Chau et al. 2015; Lehtinen et al. 2011; Suter et al. 2017), necessary for the development of the whole forebrain and for the survival and the subsequent growth of neural progenitors (Bifari et al. 2015; Bifari et al. 2009; Catala 1998; Dang et al. 2019; Etchevers et al. 2001).

Meninges are a neural stem cell (NSC) niche (Bifari et al. 2015; Bifari et al. 2009; Bifari et al. 2017; Decimo et al. 2012a; Decimo et al. 2012b). A subset of non-parenchymal multipotent cells expressing GLAST, PDGFrβ, Nestin and Vimentin neural stem cell marker (Bifari et al. 2017; Decimo et al. 2011; Decimo et al. 2020) resides in meninges and can differentiate into neurons *in vitro* and *in vivo*.

Similarly to traditional neural stem cells niche, meninges are featured of the active presence of signalling molecules, growth factors and ECM components as well as of the capability to host and maintain neuronal progenitor cells throughout the organism's lifetime (Decimo et al. 2012b; Scadden 2006) However, little is known about the responsiveness of meningeal niche to neurogenic stimuli. Alike the hippocampal niche (Eisinger and Zhao 2018; Kempermann 2019; Young et al. 1999), also meninges seem to be able to sense signals from outside and inside the brain and to modulate the properties of NSCs accordingly (Decimo et al. 2012a; Kerever et al. 2007; Mercier and Arikawa-Hirasawa 2012) but how meningeal NSCs respond to neurogenic stimuli such as EE tasks (Kempermann et al. 1997) or drugs (Zhou et al. 2016) (e.g., fluoxetine) and their potential role in CNS plasticity has never been assessed.

In pathological condition, meningeal NSCs are able to promptly respond also to neural pathological states (Lin et al. 2015; Nakagomi et al. 2011; Nakagomi et al. 2012; Ninomiya et al. 2013). It has been reported that the meningeal niche actively reacts to CNS insults as in stroke, physical injury, epilepsy, spinal cord injury and neurodegenerative disease (Dang et al. 2019; Decimo et al. 2011; Kumar et al. 2014; Nakagomi et al. 2011; Nakagomi et al. 2012). In

those pathological scenari, meningeal NSCs respond increasing their self-renewal and proliferative properties, differentiating and migrating to the neural parenchyma to contribute to the neural regeneration of the CNS (Dang et al. 2019; Decimo et al. 2011; Ninomiya et al. 2013). Importantly, in autoinflammatory diseases meninges have been proposed as an important checkpoint at which immune cells are licensed to infiltrate into CNS parenchyma and reach areas of antigen availability and tissue damage (Schläger et al. 2016; Yasuda et al. 2019). However, the specific role of meningeal NSC in autoimmune disease like MS is still unknown. Our preliminary data indicate that the immune system induces changes in the leptomeningeal niche and modifies the phenotype of the NSCs. *Ex vivo* analysis on SCID immunodeficient mice, revealed that the decrease in meningeal NSC number is correlated with the absence of adaptive immune system. These data suggest that meningeal NPCs are necessary to balance and maintain the immunological homeostasis in meninges, but more analyses are needed to understand and clarify the fundamental relationship between these two populations.

In this context the following outstanding questions remain unanswered:

How does meningeal NSC niche react to neurogenic and pharmacological stimuli?

Which is the molecular mechanism behind meninges response?

Does meningeal NSC interact with immune cell in vivo?

How does the meningeal niche is altered during autoimmune disease like MS?

Which are the cellular and molecular mechanisms that regulate the interaction between meningeal NSCs and brain reactive T cells in MS?

Working Hypothesis

During the course of my studies, I explored the hypothesis that meningeal niche can respond to neurogenic stimuli contributing to brain plasticity in physiological conditions. Moreover, I investigated whether and how the meningeal neural stem cells niche can be actively involved in response to autoinflammatory pathological stimuli such as in multiple sclerosis (MS) disease. Specifically, I studied the relationship between the meningeal NSCs and the immune cells to elucidate the role of this interaction in the MS pathogenesis and to identify a potential new pharmacological target for treatments of MS.

In order to pursuit this hypothesis, I focused on the following aims (Scheme 1):

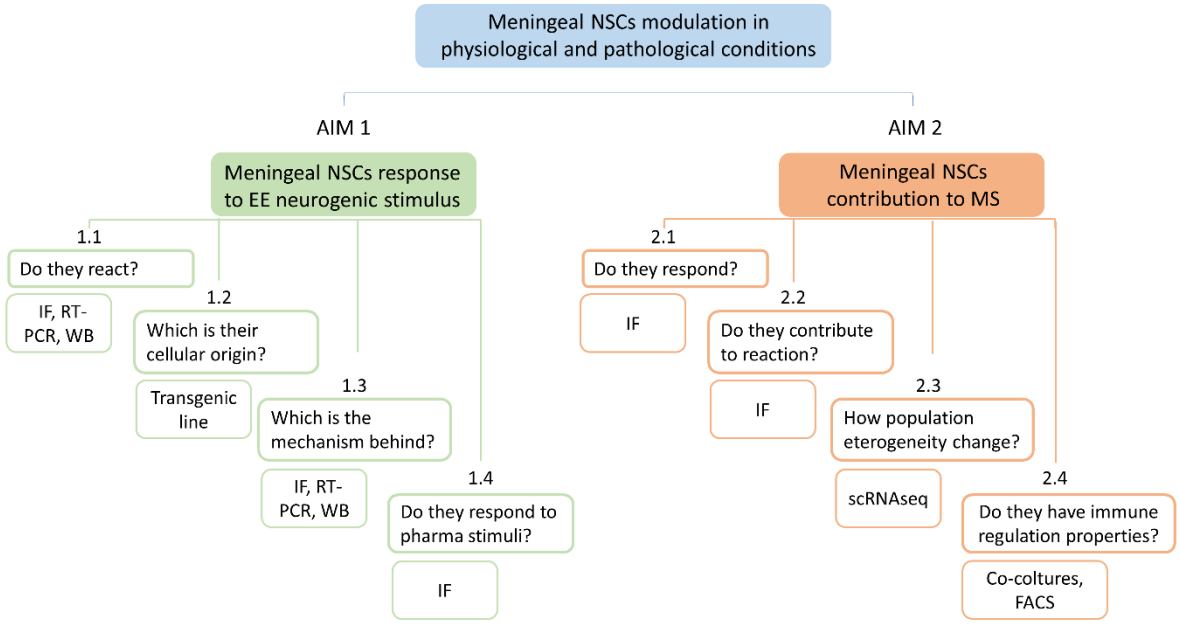

SCHEME 1 - SCHEME DESCRIBING THE MAIN AIMS OF MY THESIS

The experimental plan summarizes the objectives of this project. In a general context of meningeal NSC niche characterization of physiological and pathological conditions (Blue) we focused our attention on the response of meningeal NSC niche to neurogenic stimuli like EE (Green) and the reaction of the niche to a neurodegenerative and autoimmune disease like MS (Orange). NSCs=Neural stem cells, EE=Enriched Environment, MS=Multiple Sclerosis, IF=Immunofluorescence, RT-PCR=Real Time PCR, WB= Western Blot, scRNAseq= Single Cell RNA sequencing, FACS=Fluorescent Activated Cell Sorting

AIM 1: Characterization of meningeal NSC niche response to neurogenic stimuli

Aim 1.1 Meningeal response to EE stimulations

We aimed to investigate whether, in physiological condition, meningeal NSC niche can respond to neurogenic stimuli. We exposed young mice to EE and observed the changes in meningeal NSC population by complementary analyses including immunofluorescence confocal microscopy, RT-PCR and Western blot. Given the evidence of EE effects on hippocampus, this tissue was firstly examinate as control.

Aim 1.2 Lineage tracing of meningeal cells

To elucidate the identity of cells involved in meningeal response to EE, we performed lineage tracing experiments taking advantage on the use of the transgenic mouse line GLAST-YFP which allows to visualize and follow the fate and contribution of the radial glial cell population.

GLAST YFP mice were exposed to EE and meninges were analysed through immunofluorescence confocal microscopy.

Aim 1.3 Molecular mechanism and pharmacological validation

In order to investigate the molecular mechanism responsible for meningeal reaction to EE exposure, I studied the BDNF-TrkB interaction. Taking advantage of ANA-12, a TrkB non-competitive inhibitor that abolished the EE-induced meningeal niche changes, I performed immunofluorescence confocal microscopy, RT-PCR and Western blot analysis of meningeal samples from different groups: animals exposed to EE and injected with ANA-12 inhibitor, animals exposed to EE and injected with the vehicle, single-housed animals without EE, receiving vehicle injections.

Aim 1.4 Response to pharmacological neurogenic stimuli

Finally, to confirm the responsiveness of meningeal niche to a pharmacological neurogenic stimulus, I exploited a paradigm of Fluoxetine administration and I performed immunofluorescence confocal microscopy on brain meninges of CD1 mice treated with Fluoxetine.

AIM 2: Meningeal niche in a murine model of Multiple sclerosis

Aim 2.1 Meningeal niche Response to EAE

It has been described that neural precursor cells present in meninges are able to react following injury and disease (Decimo et al. 2011; Decimo et al. 2020; Nakagomi et al. 2011; Nakagomi et al. 2012). We specifically aimed to investigate meningeal NSC niche in a model of multiple sclerosis (MS) disease. To this end, I established an animal model of experimental autoimmune encephalomyelitis (EAE), and I characterized the meningeal NSCs by combining several approaches. Once the mice have been immunized with myelin-oligodendrocytes glycoprotein (MOG)35-55 peptide, analysis were performed at different stages of the pathology: at the pre-onset stage (5 days post immunization (DPI)), at onset stage (12 DPI), at peak stage (15DPI) and during the chronic phase of disease (28 DPI). In order to investigate meningeal NSC niche response in MS, I performed immunofluorescence and confocal microscopy analysis on brain and spinal cord meninges.

Aim 2.2 Meningeal cell contribution to parenchymal reaction

Once established that meningeal cells react in the defined pathological scenario, I focused on the investigation of meningeal cells contribution to parenchymal reaction. By using high resolution immunofluorescence confocal microscopy analysis, I checked for specific point of

cell infiltrations in brain and spinal cord parenchyma during the different stages of the pathology.

Aim 2.3 Meningeal cell population heterogeneity in EAE

In this section I characterised meningeal cell population heterogeneity in EAE model. To investigate the composition of the entire meningeal cell population (immune and stromal cells) during EAE, I performed single cell RNA sequencing (scRNAseq) on meningeal tissue derived from control and EAE mice. Data analysis was done in collaboration with the Dr. Lucas Schirmer research group.

Aim 2.4 Immune-regulation properties of meningeal NSCs

In order to understand the immune-regulation properties of meningeal NSCs in EAE model, I combined different approaches including *in vitro* co-culture of NSCs and T cells, FACS analyses and immunofluorescence confocal microscopy.

CHAPTER 2 – MATERIAL AND METHODS

2.1 Animals

Animal housing and all experimental procedures were approved by the Istituto Superiore della Sanita` (I.S.S., National Institute of Health), Italy and the Animal Ethics Committee (C.I.R.S.A.L., Centro Interdipartimentale di Servizio alla Ricerca Sperimentale) of the University of Verona, Italy (authorization number: 237/2016-PR; date of approval: 3rd March 2016; protocol number: 56DC9.13). Unless otherwise stated, animals were kept in a non-reversed light cycle, temperature between 20-24°C, humidity between 45-60% and food and water were provided ad libitum.

2.1.1 Animals for enriched environment

For Enriched environment experiments, wild-type (WT) CD1 mice and GLAST-GFP transgenic mice (Mori et al. 2006; Nakamura et al. 2006) were used as reported in Table 1. WT CD1 mice were purchased from Charles River Laboratory Italia (Calco, Italy), while GLAST-GFP transgenic mice were obtained by intercrossing GLAST-CreERT2 mice (Mori et al. 2006) with the CAG-CAT-EGFP reporter line (Nakamura et al. 2006).

2.1.1.1 Exposure to EE

Seven-week-old CD1 male mice (n=6) were housed together in a single rat cage for 1 week. A running wheel and nesting material were always present in the cage, while other toys (stairs, cardboard rolls and marbles) were added alternatively to the cage, to preserve novelty, according to what is shown in Table 2. Animals were sacrificed after 7 days of EE exposure. Seven-week-old CD1 male mice (n=5) single-housed in a normal cage for 1 week were used as control animals, as previously described (Lopez and Laber 2015). Animals were sacrificed 7 days after the start of the experiment.

2.1.1.2 GLAST-GFP exposure to EE

GLAST-CreERT2 mice (Mori et al. 2006) were intercrossed with the CAG-CAT-EGFP reporter line (Nakamura et al. 2006) (GLAST-GFP) that allow to label by GFP all the GLAST^{+} cells and their progeny following tamoxifen administration, creating the GLAST-GFP strain. Seven to ten weeks old male GLAST-GFP mice (n=7) were induced using 3 daily Tamoxifen (T5648-1G, Sigma-Aldrich, St. Louis) gavage before the start of the EE protocol. Tamoxifen was dissolved into sunflower seed oil at a 30mg/ml concentration and the mice received 3.5 mg of Tamoxifen for 35 g of body weight.

Animals were left 2 days alone to recover from the handling and then were either subjected to EE (n=4) or control treatment (n=3) as previously described. Observing that the gavage procedure stressed the animals in a significant way, we decided to prolong the EE exposure from 1 to 2 weeks in order to give them the time to recover.

2.1.1.3 Exposure to EE and TrkB inhibitor ANA-12

Seven-week-old CD1 male mice (n=12) were injected intraperitoneally with i) 10 µl/g of TrkB inhibitor ANA-12 (Cazorla et al. 2011) dissolved in sunflower seed oil supplemented with 1% DMSO at 0.1 mg/ml concentration, three consecutive days before the start of the experiment and at the third day of the experiment or ii) vehicle (sunflower seed oil + 1% DMSO). This administration protocol was adapted from Moy et al 2019 (Moy et al. 2019).

After the injections, mice were divided into four experimental groups: EE ANA-12 (animals exposed to EE and injected with the inhibitor; n = 11), EE VEH (animals exposed to EE and injected with the vehicle; n = 10), NO EE VEH (single-housed animals receiving just vehicle injections; n = 10), NO EE ANA-12 (single-housed animals receiving the inhibitor; n = 3).

2.1.2 Animals for Fluoxetine experiment

Four-week-old CD1 male mice (n=8) were treated orally with fluoxetine (Fluoxetine Hydrochloride, LRAA9180, Sigma-Aldrich, St. Louis) for 4 consecutive weeks.

2.1.2.1 Fluoxetine administration

The drug was dissolved into the water (0.16 mg/ml concentration) contained in the dispenser normally present in mice cages, and mice were able to freely access the water containing the drug. As fluoxetine is light-sensitive, a tinfoil sheet was used to cover the water dispenser, in order to avoid any kind of light-induced change on the drug. The drug-containing water was changed by the operator two times per week and the dispenser was weighted to evaluate the average water consumption for every animal. On the basis of this evaluation, on average, animals took 29 mg/kg/day of fluoxetine via oral administration. The control group consisted of age matched CD1 male mice (n=4) which normal water was administered to.

All the animals used in the experiment were administrated the Marble Burying Test (MBT), while only n=3 per experimental group were used for subsequent immunofluorescence analysis.

2.1.2.2 Marble test administration

Behavioral marble test was performed at the end of the 3rd week of fluoxetine treatment to preliminarily assess the efficacy of the treatment (Baek et al. 2015). Animals (n = 12, n=4 CTRL and n=8 FLUOX) were individually placed into a new cage containing 15 equally spaced marbles placed over approximately 5 cm of saw dust and they were allowed to acclimate for 2 minutes. Then, their behaviour was video-recorded for 30 minutes. The number of buried marbles (criterium of at least ¾ of its surface under the saw dust) was blindly assessed. All the behavioral testing was performed during the light phase, between 12:00 and 16:00 p.m..

2.1.3 Animals for EAE

For EAE experiments, wild-type C57BL6/J 8-10 weeks-old female and male mice (n= 56) were purchased from Charles River Laboratory Italia (Calco, Italy). As regards EAE animals we induced n=33 mice through MOG peptide injections (see 2.1.3.1 section), controls animals (n=23), instead, received subcutaneous injections of CFA supplemented with 0.8 mg of Mycobacterium tuberculosis. Mice also received intravenous injections of 50ng of PTX (Pertussis Toxin), via lateral vain in mice tail, on day 0 and 2.

2.1.3.1 EAE induction

As regards EAE animals, wild-type C57BL6/J 8-10 weeks-old female and male mice (n=33) were immunized with subcutaneous injections of emulsion containing 300µg of MOG35-55 peptide emulsified in CFA supplemented with 0.8 mg of Mycobacterium tuberculosis. Mice also received intravenous injections of 50ng of PTX (Pertussis Toxin), via lateral vain in mice tail, on day 0 and 2.

Animals were followed daily up to a period of 28 days post-immunization (DPI) and scored for EAE according to the following scale: score 0, normal neurological exam; score 1, tail weakness/paralysis; score 2, paraparesis; score 3, paraplegia; score 4, involvement of forelimbs paraparesis; score 5, moribund or dead animal.

Animal were sacrificed at different time point of the disease: pre-onset (5 DPI), onset (12DPI), peak (15DPI) and chronic (28 DPI).

2.2 Ex vivo analysis

2.2.1 Tissue preparation and immunofluorescence

At the end of the experimental procedures, all animals were anesthetized by intraperitoneal injection of Zoletil (50 mg/kg) and Xylazine (7 mg/kg). Once the pedal reflex was lost, animals were sacrificed by intracardiac perfusion of PBS with 4% paraformaldehyde (PFA)/4% sucrose (pH 7.4) solution. Brains were extracted, fixed in 4% PFA solution and transferred into 10% and subsequently 30% sucrose solution. By cryostat cutting, 35 µm thick medio lateral sagittal brain sections were obtained and processed by immunofluorescence as previously described (Formaggio et al. 2010). Immunostaining on cryosections was performed after 30 minutes incubation in blocking solution (PBS 1X with 0.25% Triton X-100, 2% BSA). If required by the specific antibody combination, mouse serum (1:100) was added during incubation in blocking solution. Sections were then incubated with primary antibodies in blocking solution overnight at 4°C. After rinsing 6 times for 5 minutes in blocking solution, appropriate secondary antibodies were applied for 4 hours at room temperature. After final washing steps in blocking solution and then in PBS, nuclear staining with 4',6-Diamidino-2-Phenylindole Dihydrochloride (DAPI, Molecular Probes-Thermo Fisher Scientific) or TO-PRO™-3 Iodide (TO-PRO-3, Molecular Probes-Thermo Fisher Scientific) was performed, and slides were mounted using 1,4-Diazabicyclo [2.2.2] octane (DABCO, Sigma-Aldrich). Staining for the nuclear marker of proliferation Ki67 required a different blocking solution (PBS 1X with 0.5% Triton X-100, 2% BSA).

For immunofluorescence staining using GFP and TrkB antibodies, as they are both produced in the same host, we developed the following protocol using a conjugated primary antibody and a non-conjugated primary antibody.

Cryosectioned sagittal sections were obtained as previously described. Immunostaining was performed after 30 minutes incubation in blocking solution (PBS 1X with 0.25% Triton X-100, 2% BSA). Sections were then incubated with the non-conjugated rabbit primary antibody in blocking solution overnight at 4°C. After rinsing 6 times for 5 minutes in blocking solution, the appropriate secondary antibody was applied for 4 hours at room temperature. Following additional rinsing in blocking solution 6 times for 5 minutes, the GFP-conjugated antibody was added to the

sections, which were incubated overnight at 4°C. Final washing steps, nuclear staining and mounting procedure were performed as previously described.

2.2.2 Antibodies for immunofluorescence staining

The following primary antibodies were used: anti-GLAST (anti-EAAT1; rabbit, 1:200, Abcam, AB416), anti-GLAST (guinea pig; 1:200; Frontier Institute, AB2571717), anti-PDGFrβ (goat, 1:200, R&D, AF1042), anti-DCX (goat, 1:200, Santa Cruz, SC-8066), anti-DCX (rabbit, 1:400, Cell Signaling, 4604S), anti-β3 tubulin (mouse, 1:400, Promega, G7121), anti-laminin (rabbit, 1:400, Sigma-Aldrich, L9393), anti-laminin-Alexa Fluor 488 (1:500, Invitrogen, PA5-22901), anti-laminin DyLight 550 (1:500, Invitrogen, PA5-22903), anti-MHCII (rat, 1:200, Invitrogen, 14-5321-82), anti-CD68 (rat, 1:200, Invitrogen, 14-0681-82), Ly6G (mouse, 1:200, BioXCell, BE0075-1), anti-CD163 (mouse, 1:200,- GeneTex, GTX54358), anti-CD3 (rabbit, ABCAM, AB5690), anti-MBP (rabbit, 1:200,DAKO, A0623), anti-TrkB (anti-tyrosin kinase receptor B, 1:200, rabbit, Santa Cruz, SC-12), anti-Ki67 (rabbit, 1:200, Abcam, AB16667), anti-GFP-Alexa Fluor 488 (rabbit, 1:500, Invitrogen, A21311), anti-iba1 (rabbit,1:200, WAKO, 019-19741), anti-GFAP (goat, 1:400, Abcam, AB53554).

The following secondary antibodies were used: donkey anti-rabbit Alexa Fluor 488 (1:500, Molecular Probes-Thermo Fisher Scientific), donkey anti-rabbit Alexa Fluor 647 (1:500, Molecular Probes-Thermo Fisher Scientific), donkey anti-goat Alexa Fluor 546 (1:500, Life Technologies-Thermo Fisher Scientific), goat anti-mouse CY3 (1:500, Jackson ImmunoResearch), donkey anti-mouse 488 (1:500, Molecular Probes, A-21202), donkey anti-rat CY3 (1:500, Jackson ImmunoResearch), donkey anti-rat 488 (1:500, Molecular Probes, A21208), donkey anti-guinea pig CY3 (Jackson ImmunoResearch). For nuclear staining, TO-PRO™-3 (1:3000, Molecular Probes-Thermo Fisher Scientific) and DAPI (1:2000, Molecular Probes-Thermo Fisher Scientific) were used.

2.2.3 Immunofluorescence image acquisition, analysis and quantification

Immunofluorescence imaging of brain section was performed using an Eclipse Ti Nikon microscope (Nikon, Tokyo, Japan) and a Zeiss L710 confocal microscope (Carl Zeiss, Munich, Germany). Acquisition parameter settings (pinhole, gain, offset, laser intensity) were kept fixed for each channel in different sessions of observation at the

fluorescence and confocal microscope. For confocal microscopy, single-plane images were acquired to realize all the quantifications.

As regards EE and EAE experiment, quantification of different markers and nuclei was done by counting positive cells above the basal lamina (identified by laminin reactivity) in at least 15 brain slices for each experimental group (n ≥ 3 animals analysed), analysing at least 5 slices from each animal.

At least two images representing 200µm of meningeal tissue each were taken from each slice. A total of 2mm of meninges was analysed for each animal at least.

For spinal cord meninges, quantification of different markers and nuclei was done by counting positive cells in meninges analysing at least 18 slices from each animal for each experimental group (n ≥ 3 animals analysed).

Evaluation of the DG area in EE and Fluoxetine experiment was realized designing a user-defined region of interest (R.O.I.) using the Fiji-Image J software (Schindelin et al. 2012). The R.O.I. were delineated taking into consideration the nuclei composing the DG.

2.2.4 Haematoxylin and eosin protocol for EAE animals

Haematoxylin and eosin (Abcam, ab245880) staining was performed on transversal brain and spinal cord slice to identify cells infiltrations. The slices were immersed inside PBS 1X for one minute to be rehydrated, then they were immersed for 3 minutes in haematoxylin solution concentrated 1:4. After washing in water, the slices were immersed for 1 second in the eosin solution concentrated 1:2 in ethanol and then washed again with water. At the end slices passed through consecutive immersion of 30 second in ethanol solution at increase concentrations of 50%, 70% and 95%. After, slices were immersed for 15 minutes in Xilene solution and were mounted with Micromount (DiaPath).

2.3 Protein extraction from mouse meninges and immunoblot analysis

A subset of mice (n=8) used for EE experiments were processed for immunoblot analysis. At the end of the experimental procedures, mice (NO EE VEH n=3, EE VEH n=2, EE ANA-12 n=3) were anesthetized by intraperitoneal injection of Zoletil (50 mg/kg) and Xylazine (7 mg/kg) and sacrificed via decapitation. Brain was quickly extracted, meninges and hippocampi were harvested using tweezers under an optical

microscope and washed with HBSS solution (sterile water, HBSS 10X, HEPES 0.3 M, 1% Pen/Strep) and then with PBS1X. Proteins were extracted via mechanical homogenization (GentleMACSTM M tubes, Miltenyi Biotec) in NP-40 buffer (150 mM NaCl, 1.0% NP-40, 50 mM Tris pH 8.0) in the presence of protease and phosphatase inhibitors. Samples were incubated on ice for 30 min and centrifuged at 10,000 x g for 15 min at 4°C. The supernatants were collected and concentrated with centrifugal filters (Amicon Ultra 10KDa) according to the manufacturer's instructions. Protein concentration was determined with the Bicinchoninic Acid (BCA) protein assay Kit (Thermo Scientific). Aliquots (25 µg each) were run through a 4–15% SDS–polyacrylamide gel electrophoresis (PAGE), and electro blotted onto a PVDF membrane (Trans-Blot Turbo Transfer System, Bio-Rad Laboratories). The membranes were then blocked (EveryBlot Blocking Buffer, Bio-Rad Laboratories), probed with the primary antibodies overnight at +4°C. The following primary antibodies were used: anti-DCX (Cell Signalling, cat.no. 4604, 1:500), anti TRK-B (Genetex, cat.no. GTX133722, 1:500), anti β3-tubulin (Promega, cat.no. G7121, 1:500), anti p75 (Promega, cat.no. G3231, 1:1000). Subsequently, an incubation with anti-Mouse or anti-Rabbit HRP-conjugated secondary antibodies (Promega) for 2 h at room temperature was performed. Chemiluminescence-based immunostaining (Clarity Western ECL Substrate, Bio-Rad Laboratories) was performed. Images were acquired with the Chemidoc MP Imaging System (Bio-Rad Laboratories). Quantitative analyses were performed using Image Lab™ software, version 6.0.1 for Windows (Bio-Rad Laboratories) and normalising to the total protein content of each lane.

2.4 RNA extraction from mouse brain meninges and real time (RT)-PCR analysis

After the experimental procedures, a subset of mice (n=14) used for EE experiments were destined for further Rt-PCR analysis (NO EE VEH n=4, EE VEH n=5, EE ANA-12 n=5), anesthetized by intraperitoneal injection of Zoletil (50 mg/kg) and Xylazine (7 mg/kg) and sacrificed via decapitation. After collecting the heads, skin and skulls were removed to access the brain, which was then extracted. Meninges were harvested using tweezers under an optical microscope and collected into HBSS solution (sterile water, HBSS 10X, HEPES 0.3 M, 1% Pen/Strep). After centrifugation at 300g per 1 minute, HBSS was substituted with PBS1X and centrifuged at 300g per 1 minute. Total

RNA was extracted from fresh mouse meningeal tissue (NO EE VEH n=4, EE VEH n=5, EE ANA-12 n=5) using the RNeasy Plus Micro Kit (Qiagen, Cat No. 74034) according to the manufacturer's protocol and RNA abundance was evaluated using the NanoDrop™ One/OneC Microvolume UV-Vis Spectrophotometer (ThermoFisher Scientific). Reverse transcription was carried out using Superscript VILO Master Mix (Invitrogen, Thermo-Fisher Scientific, Waltham, USA). Expression level of the ntrk2, BDNF, Slc1a3 and TUBB3 (for primer sequences see Table 3) genes was quantified by Sybr Green-based Real time PCR (7900HT Real-time PCR System, Applied Biosystem) according to the ΔΔCt method (Livak and Schmittgen 2001) and by using Gaphd reference gene for data normalization.

2.5 *In vitro* analysis for EAE experiments

2.5.1 Meningeal cell extraction and dissociation from adult mouse brain

Meningeal cells were isolated from meningeal brain tissue of n=29 wild-type C57BL6/J 8-10 weeks-old mice. Briefly, animals were anesthetised and sacrificed by decapitation, brain immediately removed from the skull and collected into HBSS solution (sterile water, HBSS 10X, HEPES 0.3 M, 1% Pen/Strep). Meninges were harvested using tweezers under a microscope and collected into a GentleMACS violet tube previously prepared with 2338 µl of PBS, 12,5 µl of enzyme A, 100 µl of enzyme D and 50 µl of enzyme R according to Multi Tissue Dissociator protocol (Multi tissue Dissociator KIT; Miltenyi Biotech). The Gentlemacs tubes were brings to the GentleMACS™ Dissociator (Miltenyi Biotec) to run the tissue dissociator program 37_Multi_F.

After centrifugation at 500 g per 2 minutes, supernatant was discard, 3 ml of Percoll 30% (Sigma Aldrich, GE17-0891-01) in PBS 1X was added to the pellet to resuspend it. The suspension was transferred in a 50 ml falcon and filtered using a cell strainer. Another 2 ml of Percoll 30% in PBS1X were used to wash the remaining tissue still left in the violet tube. The cellular suspension is then transferred very slowly in a 15 ml falcon filled with Percoll 70% in PBS1X. The 15 ml falcon was centrifuged at 2500 g for 20 minutes at 4°C. After centrifugation were visible three phases, the top one white containing cells debris was removed and the middle one red phase containing the cells is harvested and transferred in a 50 ml falcon containing 30 ml of PBS1X ice cold. After

centrifugation at 1000 g for 10 minutes, supernatant was removed, the pellet resuspended in 5 ml of PEB (PBS 1X, BSA 0.5%, EDTA 2Mm) and transferred in a 15 ml falcon. The falcon was centrifuge at 300 g for 10 minutes, the supernatant was removed, and cells were cultivated and/or destinated for further experiments.

These meningeal adult cells were used for the following experiment: Single cell RNA sequencing (see section 2.5.1.1) and for FACS experiment (see section 2.5.1.2).

2.5.1.1 Single cell RNA sequencing (scRNAseq)

Single cell RNA sequencing (scRNAseq) was performed on adult meningeal cells isolated from EAE and control mice, as previously described (see section 2.5.1). Two different control groups (C57BL/6J mice injected with CFA; n = 3 mice each group) and two different EAE groups (C57BL/6J immunised MOG mice at onset and peak of disease; n = 6 mice each group) were used to isolate cells. Once meningeal cells were extracted, dissociated and counted, cells were diluted in order to have 800 cells/µl in PBS 1X containing 0,04% BSA.

The scRNAseq was performed by the Technological Platform Center of Verona University using the 10X Genomics Chromium Single Cell 3' Technology and the Chromium Next GEM Single Cell 3' Reagent Kits v3.1.Inc (10x Genomics).

As a result of the quality control performed on the total amount of extracted cells from the brain meninges, we applied a quality control at 10% of mitochondrial DNA (mtDNA). This metric can identify whether there is a large amount of mitochondrial contamination from dead or dying cells and discard it from the analysis. All scRNAseq analysis was performed in collaboration with Professor Lucas Schirmer, Department of Neurology, Medical Faculty Mannheim, Heidelberg University.

2.5.1.2 Fluorescence activated cell sorting (FACS) analysis

FACS analysis was performed on adult meningeal cells isolated from EAE (n = 6) and control (n = 5) mice, as previously described (see section 2.5.1).

Once meningeal cells were extracted, dissociated, and counted the cells were divided in different tubes in order to have 300.000 cells/tube. For each condition (CTRL+CFA and MOG) cells were incubated for 15 minutes with the primary antibody for the biotinylated PDGFrβ. After the period of incubation was added 1 ml of PBS and the cells centrifugated at 300 g for 5 minutes. After centrifugation the supernatant was removed, and cells were resuspended in 1 ml of PBS 1X. Then, each tube for condition

was incubated for 15 minutes with the secondary antibody, the Streptavidin-PE and the antibody already conjugated MHCII-FITC. Cells were washed with 1 ml of PBS 1X, centrifuged at 300 g for 5 minutes, the supernatant was removed, and cells resuspended in 300 µl of PEB. Fluorescence-activated cells sorting (FACS) analysis was performed with BD-LSR-Fortessa X20 Configuration (BDBioscience). Data were analysed using FlowJo software.

Antibodies used for FACS experiment: anti-PDGFrβ-biotinylated (goat, 1:50, R&D, BAF1042), Streptavidin-PE (1:100, Invitrogen, 12-4317-87) and anti-MHCII-FITC (rat, 1:100, Invitrogen, 11-5322-82).

2.5.2 Meningeal cell extraction and dissociation from pup mouse brain

NSCs were dissociated from P0 pups' meninges (n=7). Animals were sacrificed by decapitation. Head was collected into HBSS solution (sterile water, HBSS 10X, HEPES 0.3 M, 1% Pen/Strep). Meninges were harvested using tweezers under microscope and collected into HBSS solution. After centrifugation at 300g per 1 minute, HBSS was substituted with PBS1X and centrifugated at 300g per 1 minute. Collagenase 0.2% and CaCl2 2mM were added to meninges samples and dissociation was performed using the gentleMACS™ Dissociator (Miltenyi Biotec). After incubation per 10 minutes at 37°C, Trypsin 1X and DNase were added and then sample was incubated at 37°C per 10 minutes. After centrifugation at 300g per 2 minutes, supernatant was discarded, and sample was resuspended in PEB (PBS1X, 0.5% BSA, 2mM EDTA). Cells obtained were destinated for further experiments.

These meningeal cells from pups were used for the following experiment: cell sorting (see section 2.5.2.1) and co-culture experiment (see section 2.5.2.1.1).

2.5.2.1 PDGFrβ cell sorting

The already dissociated cells from pup brain meninges where then sorted with the aim to isolate PDGFrβ^{+} cells as previously described (Bifari et al. 2009; Decimo et al. 2011). Firstly, sample was centrifugated at 600g per 10 minutes and supernatant was discarded. We used biotinylated-anti-goat-PDGFrβ antibody (1:50, R&D, BAF 1042) in 100µL of PBS1X and performed 15 minutes of incubation at 4° temperature. Following, we added 1mL of PEB (PBS1X, 0.5% BSA, 2mM EDTA) and subsequent centrifugation at 300 g per 10 minutes discarding supernatant. Then, we resuspended sample in 90µL of PEB and 20µL of Streptavidin beads (Streptavidin MicroBeads Miltenyi, 130-048-

101) that are able to bind biotinylated-anti-goat-PDGFrβ antibody. Resuspended sample was kept at 4° temperature per 15 minutes. After incubation, 1mL of PEB was added and centrifugated at 300g per 10 minutes. Sample was resuspended in 500µL of PEB. Loading LS column with sample allowed the retention of PDGFrβ$^+$ cells thanks to its ability of stringent depletion of unwanted cells. PDGFrβ$^+$ cells were then washed out from LS column with DMEM. At the end, already sorted cells were cultured in growing medium (Dulbecco modified Eagle medium (DMEM) containing 2% B27 supplement (GIBCO), 1% N2 supplement (GIBCO), 1% antibiotic-antimycotic (GIBCO) plus 20ng/mL epidermal growth factor (EGF) and 20 ng/mL basic fibroblast growth factor (bFGF)).

2.5.2.1.1 Co-culture

With the aim to evaluate NSCs-immune cells interaction, in vitro experiment was performed between PDGFrβ$^+$ cells (see section 2.5.2.1) and T cells. PDGFrβ$^+$ cells, deriving from meninges of P0 mice C57BL/6J (see section 2.5.2). Two conditions were studied through independent experiments: immune-activation effects of PDGFrβ$^+$ cells on naïve T cells, deriving from C57BL/6J mice lymph nodes and spleen, and immune-activation effects of PDGFrβ$^+$ cells on resting T cells, deriving from EAE mice lymph node and spleen. Resting state of T cells were obtained after 7-10 days after their extraction in order to achieve the lowest proliferation state. In both experiments, PDGFrβ$^+$ cells were stained with CellTracker™ Blue CMAC (7-amino-4-chloromethylcoumarin) (ThermoFisher, C2110) dye and plated on poly-D lysine (Sigma, P6407) at fixed concentration of 50.000 cells/well. On the other hand, T cells were added in suspension at different concertation ratios (1:1, 1:10, 1:100). Co-culture was performed for 48h and then analysed through FACS analysis.

2.6 Statistics

Data are expressed as mean ± SEM. Statistical differences were calculated by two tailed Student's t-test or ordinary One-Way ANOVA test using GraphPadPrism (GraphPad Inc., La Jolla, CA). $p \leq 0.05$ was considered statistically significant.

CHAPTER 3 – RESULTS

In this work, we explored the hypothesis that meningeal niche i) can respond to neurogenic stimuli contributing to brain plasticity in physiological conditions and ii) can be actively involved in response to autoinflammatory pathological stimuli. To corroborate those idea, we performed *in vivo* and *in vitro* experiments by using animal models (mice) subjected to i) enriched environment or ii) experimental autoimmune encephalomyelitis (EAE), resembling the multiple sclerosis (MS) disease.

3.1 AIM 1: Characterization of meningeal NSC niche response to neurogenic stimuli

3.1.1 EE exposure induces meningeal niche remodeling

To assess the first hypothesis, we decided to expose seven-week-old CD1 male mice to EE represented by larger cages enriched with various toys and group-housed animals for 1 week. EE is a pro-neurogenic stimulus, able to induce neurogenesis in traditional neurogenic niches, including hippocampus. The presence of newborn neurons in the DG of animals treated with EE is considered a gold standard to evaluate the effectiveness of the beforementioned treatment. Therefore, to assess the effectiveness of the EE treatment on the meningeal niche, we evaluated the presence of cells expressing the proliferation marker Ki67 or the newborn immature neuron marker DCX in sagittal mice brain sections at retrosplenial cortical level by immunofluorescence and confocal analysis (Figure 3.1A-C). To validate the EE treatment, analysis was firstly performed on hippocampal region (Eisinger and Zhao 2018; Kempermann 2019; Young et al. 1999) (Figure 3.1D-G). The number of $Ki67^+$ and DCX^+ cells in DG of treated mice was significantly higher compared to control mice (number of $Ki67^+$ cells per mm2 of DG area: CTRL: 11.06 ± 3.513, n=5; EE: 29.31 ± 5.876, n=6; p=0.0325; number of DCX^+ cells per mm^2 of DG: CTRL: 463 ± 44.57, n=5; EE: 706.5 ± 62.84, n=6; p=0.0142) (Figure 3.1E,G). These results confirmed that EE was able to induce neurogenesis at the hippocampal level, as already stated in literature (Eisinger and Zhao 2018; Kempermann 2019; Young et al. 1999).

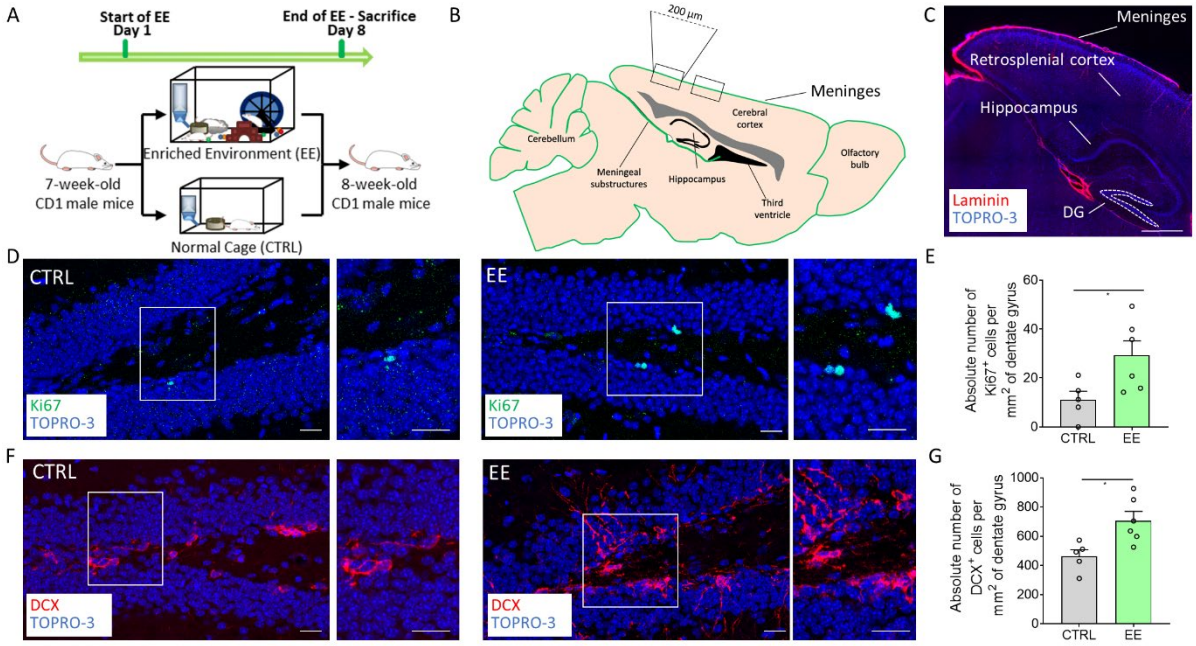

FIGURE 3.1 – HIPPOCAMPAL NICHE IS RESPONSIVE TO ENRICHED ENVIRONMENT EXPOSURE

(A) Schematic representation of the experimental design used for EE exposure. (B) Scheme depicting the sagittal section of mouse brain highlighting the specific regions where brain external meninges were analyzed. (C) Sagittal brain section of CD1 mice, with laminin (red) identifying brain meninges. White dashed lines delineate the dentate gyrus (DG) area used for quantification. (D) Sagittal brain section of CD1 mice showing hippocampal Ki67$^+$ (green) cells in non-treated (CTRL) and treated (EE) animals. A white box highlights a DG zone reported as a magnification on the right panel. (E) Graph showing the number of Ki67$^+$ cells per mm2 of the DG in CTRL and EE animals. (F) Sagittal brain sections of CD1 mice showing hippocampal DCX$^+$ (red) cells in CTRL and EE mice. A white box highlights a DG zone reported as a magnification on the right panel. (G) Graph showing the number of DCX$^+$ cells per mm2 of the DG in CTRL and EE animals. Data are presented as mean ± SEM; * = p value ≤ 0.05, ** = p value ≤ 0.01, *** = p value ≤ 0.001, **** = p value ≤ 0.0001. In pictures C, D and F nuclei are in blue (TOPRO-3 nuclear staining). Picture C is a single plane confocal image. Pictures D and F are maximum intensity projections of z-stack confocal images. Scale bars represent 500µm (C) and 20µm in the magnified pictures (D, F).

After defining the effectiveness of the treatment on the hippocampus, we proceeded to characterize the potential effects that EE could have on meningeal NSC niche. To this aim, we first analysed the number of cell nuclei identified by the nuclear marker TOPRO-3 and the expression of Ki67 in 2 mm (5 brain sections, 2 segments of 200 µm each section for each animal) of cross-sectioned brain retrosplenial meninges (Figure 3.2A-C). As shown by figure 3.2B and C, the number of meningeal cells and proliferation index is almost identical between the control and the treated animals. This suggested that, at least regarding cell proliferation, the exposure to EE doesn't affect the meningeal layers.

Meningeal NSCs is known to be characterized by radial glia-like cells expressing GLAST and immature neurons expressing β3-Tubulin (Decimo et al. 2020). Therefore, we focused on the

distribution and analysis of those cell populations (Figure 3.2D-G). We found a significant increase of GLAST$^+$ cells and of β3-Tubulin$^+$ cells in treated mice compared to the control group (number of GLAST$^+$ cells per 2 mm of cross-sectioned meninges: CTRL: 10.2 ± 0.9028, n=5; EE: 13.5 ± 0.8756, n=6 ; p=0.0284; number of β3-Tubulin+ cells per 2 mm of cross-sectioned meninges: CTRL: 8.8 ± 0.6042, n=5; EE: 15.58 ± 1.158, n=6; p=0.0009) (Figure 3.2 F,G). These data indicated that the exposure to EE conditions was able to increase meningeal NSC population, suggesting that meningeal niche respond to the neurogenic stimulus.

As reported in literature, EE-mediated neurogenesis is carried out via molecular mediators including the BDNF/TrkB signaling pathway (Eisinger and Zhao 2018; Samuels and Hen 2011). Therefore, we investigated if the EE treatment could have an effect on meningeal cells expressing the TrkB receptor of BDNFs. To achieve this goal, we first confirmed the expression of TrkB and β3-Tubulin in meningeal cells via Western Blot Analysis (Figure 3.2H) comparing meningeal samples with hippocampal ones as positive controls. We then proceeded to analyse retrosplenial meningeal tissue through immunofluorescence and confocal analysis of mice exposed to EE. We found a significant increase of TrkB$^+$ retrosplenial meningeal cell population in response to EE exposure (number of TrkB$^+$ cells per 2 mm of cross-sectioned meninges: CTRL: 2 ± 0.5477, n=5; EE: 6.833 ± 0.4773, n=6; p<0,0001) (Figure 3.2I-K). By investigating the phenotype of TrkB$^+$ cells, we detected a rare population of immature neurons co-expressing β3-Tubulin and the BDNF receptor TrkB in both control and treated animals. While this double positive population was extremely sporadic in the control animals, it was significantly increased in EE exposed mice (number of β3-Tubulin$^+$/TrkB$^+$ cells per 2 mm of cross-sectioned meninges: CTRL: 1.2 ± 0.3742, n=5; EE: 4.333 ± 0.4216, n=6; p=0.0004) treated groups (Figure 3.2I-K).

The meningeal niche is endowed with fractones, small laminin-based structures, extracellular matrix (ECM) components able to bind and concentrate growth factors and exerting a trophic role for NSC niche (Mercier 2016), and immune cells fundamental to maintain neurogenesis (Ziv et al. 2006). In order to investigate possible changing in meningeal brain homeostasis following EE exposure, we evaluated the distribution of the fractones and the number of macrophages, identified by laminin$^+$ puncta (Bifari et al. 2015) and CD68 marker, respectively (Figure 3.2L-O). We found a statistically significant increase in the number of meningeal fractones and CD68$^+$ cells in EE compared to CTRL animals (number of fractones per 2 mm of cross-sectioned meninges: CTRL: 56.2 ± 8.599, n=5; EE: 90.25 ± 4.393, n=6; p=0.0048; number

of CD68⁺ cells per 2 mm of cross-sectioned meninges: CTRL: 5.432 ± 0.4638, n=5; EE:10.34 ± 1.878, n=6; p= 0.0456; Figure 3.2M,O). These data indicated that EE induced changes in meningeal ECM and macrophages suggesting a trophic activation of the meningeal niche.

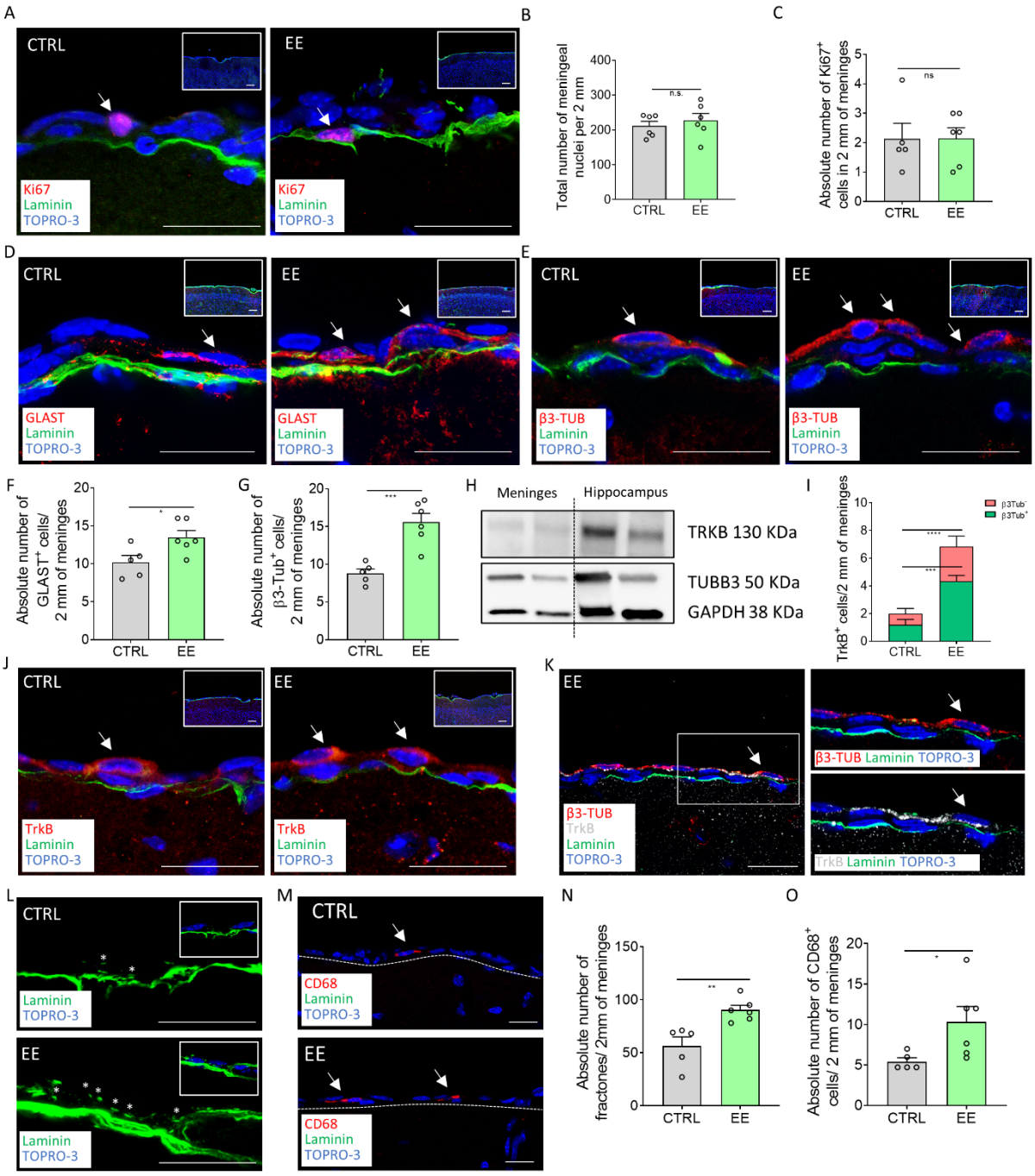

FIGURE 3.2 – MENINGEAL NICHE IS RESPONSIVE TO ENRICHED ENVIRONMENT EXPOSURE

(A) Sagittal brain sections of CD1 mice showing Ki67⁺ (red) cells above meningeal basal lamina (green) in CTRL and EE mice. An insert illustrates a panoramic image where the single-cell level image was taken. (B) Graph showing the number of nuclei in 2mm of retrosplenial brain meninges of CTRL and EE animals. (C) Graph showing the number of Ki67⁺ cells in 2mm of retrosplenial brain meninges of CTRL and EE animals. (D) Sagittal brain

sections of CD1 mice showing GLAST$^+$ (red) cells above meningeal basal lamina (green) in CTRL and EE mice. An insert illustrates a panoramic image where the single-cell level image was taken. (E) Sagittal brain sections of CD1 mice showing β3-Tubulin$^+$ (red) cells above meningeal basal lamina (green) in CTRL and EE mice. An insert illustrates a panoramic image where the single-cell level image was taken. (F) Graph showing the number of GLAST$^+$ cells in 2mm of retrosplenial brain meninges of CTRL and EE animals. (G) Graph showing the number of β3-Tubulin+ cells in 2mm of retrosplenial brain meninges of CTRL and EE animals. (H) Representative western blotting analysis of mouse brain protein extracts which shows the presence of TrkB and β3-Tubulin proteins both in mouse meningeal samples and in hippocampal samples. (I) Graph showing TrkB$^+$/β3-Tubulin$^+$ and Trkb$^+$/β3-Tubunlin$^-$ cells in 2mm of retrosplenial brain meninges of CTRL and EE animals. (J) Sagittal brain sections of CD1 mice showing TrkB$^+$ (red) cells above meningeal basal lamina (green) in CTRL and EE mice. An insert illustrates a panoramic image where the single-cell level image was taken. (K) Sagittal brain section of CD1 mice exposed to EE showing a cell double positive for β3-Tubulin (red) and TrkB (white) above meningeal basal lamina (green). A white box highlights a double positive cell reported as a magnification on the right panel. (L) Sagittal brain sections of CD1 mice showing fractones (*) identified via laminin (green) staining in retrosplenial brain meninges of CTRL and EE mice. An insert illustrates laminin staining (fractones) below meningeal nuclei (TOPRO-3). (M) Sagittal brain sections of CD1 mice showing CD68$^+$ (red) cells in brain meninges of CTRL and EE mice. Meninges are delineated using white dashes. (N) Graph showing the number of fractones in 2mm of retrosplenial brain meninges of CTRL and EE animals. (O) Graph showing the number of CD68$^+$ cells in 2mm of retrosplenial brain meninges of CTRL and EE animals. Data are presented as mean ± SEM; * = p value ≤ 0.05, ** = p value ≤ 0.01, *** = p value ≤ 0.001, **** = p value ≤ 0.0001. In pictures A, D, E, J, K, L and M nuclei are in blue (TOPRO-3 nuclear staining). Picture M is a single plane confocal image. Pictures A, D, E, J, K and L are maximum intensity projections of z-stack confocal images. Scale bars represent 20µm in the magnified pictures (A, D, E, J, K, L, M) and 100 µm in the panoramic anchor images (A, D, E, J). White arrows indicate positive cells while asterisks indicate fractones.

Taken together, these results indicate that the meningeal niche responds to the EE pro-neurogenic stimulus by increasing the subsets of meningeal NSCs and immature neuron populations, fractones and macrophages.

3.1.2 EE-induced NSCs in meninges derive from GLAST$^+$ radial glia progenitors

In order to identify the origin of the immature neurons which we found to react to EE stimulus increasing their number, we took advantage of an inducible transgenic mouse model for radial-glia cells. GLAST-CreERT2 mice (Mori et al. 2006) intercrossed with the CAG-CAT-EGFP reporter line (Nakamura et al. 2006) (GLAST-GFP) allowed to label by GFP all the GLAST$^+$ cells and their progeny following tamoxifen administration. After three days of tamoxifen induction via oral gavage, we subjected the mice to 15 days of EE and then we analysed the brain and the retrosplenial meninges of control and treated mice (Figure 3.3A, B) (Mori et al. 2006).

At first, we confirmed the effectiveness of the EE protocol in GLAST-GFP mice by assessing the increased number of DCX cells in the DG of treated mice (Figure 3.3C, D) (number of DCX$^+$ per mm2 of DG area, CTRL: 386.4 ± 36.7, n=3; EE: 751.8 ± 56.24, n=4; p= 0.0042). The time of the exposure to EE was increased to 15 days as we couldn't observe hippocampal neurogenic

response in GLAST-GFP mice after only 7 days, possibly due to gavage administration of tamoxifen (Figure 3.3C) (Balcombe et al. 2004; Brown et al. 2000).

We then analyzed through immunofluorescence and confocal analysis the distribution and fate of GFP^+ GLAST-derived progenitors. As expected, we found GFP^+ cells in cortex, DG, striatum and meninges both in EE-treated and control mice, suggesting that the recombination took place in the correct way as already stated in literature (Figure 3.3E-F) (Mori et al. 2006). We observed a statistical increase of GFP^+ cells in meninges after exposure to EE (number of GFP^+ cells per 2 mm of cross-sectioned meninges: CTRL: 6.167 ± 1.244, n=3; EE: 10.62 ± 0.9157, n=4; p=0.0315) (Figure 3.3G). Since there was no change in meningeal retrosplenial cortex cell number, the total increase in GFP^+ cells may arise from migrating progenitors coming from other brain regions.

With the aim to assess the lineage of immature neurons that reacted to EE exposure, we performed immunofluorescence for β3-Tubulin and GFP markers to detect a possible co-expression. Interestingly, we found the presence of a double positive GFP^+/ β3-$Tubulin^+$ cell population in EE treated mice meninges (Figure 3.3H-J). On the contrary, double positive cells were almost absent in control mice, potentially suggesting that part of immature neurons differentiated from GLAST-derived cells following EE treatment (number of GFP^+/ β3-$Tubulin^+$ cells per 2 mm of cross-sectioned meninges: CTRL: 0.3333 ± 0.3333, n=3; EE: 1.893 ± 0.3362, n=4; p= 0.0237; Figure 3.3G, J). Furthermore, as confirmation of the data obtained in CD1 mice, we observed, following EE exposure, an overall increase of β3-$Tubulin^+$ immature neurons in meninges (Figure 3.3J) (number of β3-$Tubulin^+$ cells per 2 mm of cross-sectioned meninges: CTRL: 13.17 ± 0.6009, n=3; EE: 19.33 ± 1.113, n=4; p= 0,0072).

Moreover, we detected an higher number of $TrkB^+$/GFP^+ cells in meninges of EE animals compared to controls (Figure 3.3K-L) (number of GFP^+/$TrkB^+$ cells per 2 mm of cross-sectioned meninges: CTRL: 0.3333 ± 0.1667, n=3; EE: 2.72 ± 0.5725, n=4; p= 0.0182; number of $TrkB^+$ cells per 2 mm of cross-sectioned meninges: CTRL: 2.167 ± 0.1667, n=3; EE: 7 ± 1.186, n=4; p=0.0187) (Figure 3.3G, M) suggesting they were partially derived from $GLAST^+$ radial glia lineage.

Altogether, these data indicated that, following EE exposure, the increased β3-$Tubulin^+$ immature neurons and $TrkB^+$ cells in meninges partially originated from radial glia $GLAST^+$ cells.

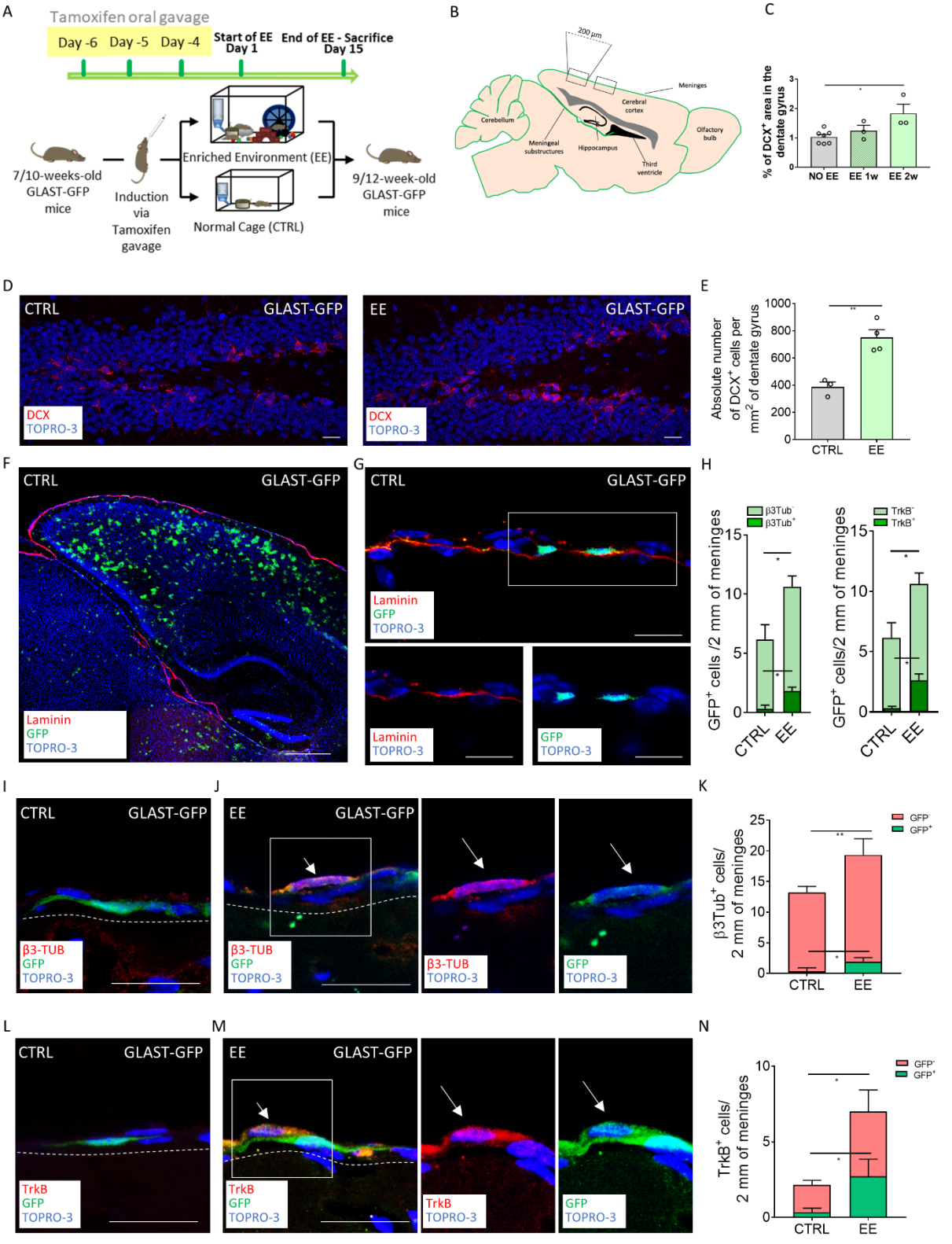

FIGURE 3.3 – LINEAGE-TRACING CONFIRMS RADIAL GLIAL ORIGIN OF THE EE-INDUCED IMMATURE NEURONS

(A) Schematic representation of the experimental design used for EE exposure on GLAST-GFP mice. (B) Scheme depicting the sagittal section of mouse brain highlighting the specific regions where brain external meninges were analyzed. (C) graph reporting the percentage of DCX$^+$ area in the DG of GLAST-GFP animals subjected to either 1 (EE 1w) or 2 weeks (EE 2w) of EE exposure. (D) Sagittal brain section of GLAST-GFP mice showing hippocampal DCX$^+$ (red) cells in CTRL and EE mice. (E) Graph showing the number of DCX$^+$ cells per mm2 of the

dentate gyri (DG) in CTRL and EE animals. (F) Sagittal brain section of GLAST-GFP CTRL mice, with laminin (red) identifying brain meninges and GFP (green) identifying the transgene expression. (G) Sagittal brain section of GLAST-GFP mice showing GFP^+ (green) cells above meningeal basal lamina identified via laminin (red) staining. A white box highlights GFP positive cells reported as split channels on the below panel. (H) Graphs showing $GFP^+/\beta3\text{-Tubulin}^+$ and $GFP^+/\beta3\text{-Tubulin}^-$ cells (left) and $GFP^+/TrkB^+$ and $GFP^+/TrkB^-$ cells (right). (I) Sagittal brain section of GLAST-GFP CTRL mice showing a cell only positive for GFP (green). White dashes delineate meninges. (J) Sagittal brain section of GLAST-GFP mice showing a cell positive for both β3-Tubulin (red) and GFP (green) in EE mice. A white box highlights a double positive cell reported as split channels on the right. White dashes delineate meninges. (K) Graph showing the $\beta3\text{-Tubulin}^+/GFP^+$ and $\beta3\text{-Tubulin}^+/GFP^-$ cells in 2mm of retrosplenial brain meninges of CTRL and EE animals. (L) Sagittal brain section of GLAST-GFP CTRL mice showing a cell only positive for GFP (green). White dashes delineate meninges. (M) Sagittal brain section of GLAST-GFP mice showing a cell positive for both TrkB (red) and GFP (green) in EE mice. A white box highlights a double positive cell reported as split channels on the right. White dashes delineate meninges. (N) Graph showing the $TrkB^+/GFP^+$ and $TrkB^+/GFP^-$ cells in 2mm of retrosplenial brain meninges of CTRL and EE animals. Data are presented as mean ± SEM; * = p value ≤ 0.05, ** = p value ≤ 0.01. In pictures D, F, G, I, J, L and M nuclei are in blue (TOPRO-3 nuclear staining). Pictures F and G are single plane confocal images. Pictures D, I, J, L and M are maximum intensity projections of z-stack confocal images. Scale bars represent 20µm in D, G, I, J, L, M and 500µm in F. White arrows indicate positive cells.

3.1.3 TrkB/BDNF signaling modulate meningeal niche response to enriched environment exposure

Our results indicated that TrkB, the main receptor of BDNF, was expressed in meninges and, following EE, it increased in association with β3-Tubulin meningeal immature neurons (Figure 3.2I-K). TrkB receptor activation is abolished by ANA-12 (Cazorla et al. 2011), a non-competitive inhibitor. In order to understand if meningeal response was directly regulated by the activation of the neurotrophic receptor TrkB, we administrated ANA-12 inhibitor to CD1 mice 3 days before and at the 3rd day of EE exposure (Figure 3.4A) (Moy et al. 2019). With this aim, we proceeded by comparing the effect of EE exposure and EE exposure plus ANA-12 inhibitor in the following experimental groups: EE ANA-12 (animals exposed to EE and injected with ANA-12 inhibitor), EE VEH (animals exposed to EE and injected with the vehicle), NO EE VEH (single-housed animals without EE, receiving vehicle injections), NO EE ANA-12 (single-housed animals without EE, receiving ANA-12 inhibitor) (Figure 3.4A).

At first, we assessed through immunofluorescence and confocal analysis if ANA-12 was able to ablate the increase of DCX^+ immature neurons caused by EE on the hippocampal neurogenesis. We detected no statistically significant differences between NO EE VEH and EE ANA-12 animals (number of DCX^+ cells per 2mm of DG area: NO EE VEH: 366.1 ± 16.16, n=3; EE VEH: 547.1 ± 25.39, n=3; EE ANA-12: 370.7 ± 27.76, n=3; NO EE ANA-12: 386.6 ± 24.68, n=3; NO EE VEH vs EE VEH, p= 0.0030; EE VEH vs EE ANA-12, p= 0.0036; EE VEH vs NO EE ANA-

12, p= 0.0063) (Figure 3.4B,C), suggesting the ablating effect of ANA-12 on the hippocampal neurogenesis.

We then proceeded to analyse the effect of ANA-12 on the expression of TrkB/BDNF in the meninges. To this aim, we performed RT-PCR on meningeal tissue lysates from EE VEH, EE ANA-12 and NO EE VEH animals and we evaluated the *NTRK2* (gene name for TrkB) and *BDNF* gene expression levels. We found that *NTRK2* significantly increased its gene expression following EE and decrease in animals that received EE treatment with ANA-12 administration (log2 Fold Change: NO EE VEH: 0 ± 0.26, n=4; EE VEH: 0.76 ± 0.14, n=5; EE ANA-12: 0.22 ± 0.16, n=5; NO EE VEH vs EE VEH, p=0.0272) (Figure 3.4D). As regard *BDNF* gene expression in meninges, RT-PCR indicated no change following EE or EE plus ANA-12 administration (log2 Fold Change: NO EE VEH: 0 ± 0.96, n=4; EE VEH: 0.98 ± 0.64, n=5; EE ANA-12: 0.44 ± 0.42, n=5) (Figure 3.4E). To deeply investigate the effect of ANA-12, we than performed western blot analysis on meninges from the three different experimental groups. We noted that, in EE VEH animals, TrkB increased the expression of truncated 1 isoform (TrkB.T1, 90KDa) (Tomassoni-Ardori et al. 2019) which decreased to undetectable control level following ANA-12 administration (Figure 3.4F). Among the different groups, full length TrkB (130KDa) didn't change its expression. To further confirm the increase in the expression of TrkB signaling pathway in meninges following EE, we assessed the expression of the neurotrophin receptor p75 using western blot: p75 receptor cross links with TrkB receptor to activate the response to BDNF signaling (Formaggio et al. 2010; Meeker and Williams 2015). Indeed, we found that p75 increased in EE VEH animals and decreased in EE ANA-12 group (p75/total proteins (Fold

Change): NO EE VEH: 1 ± 0.36, n=3; EE VEH: 4.08 ± 1.38, n=2; EE ANA-12: 2.03 ± 0.4, n=3; NO EE VEH vs EE VEH, p=0.0695) (Figure 3.4F).

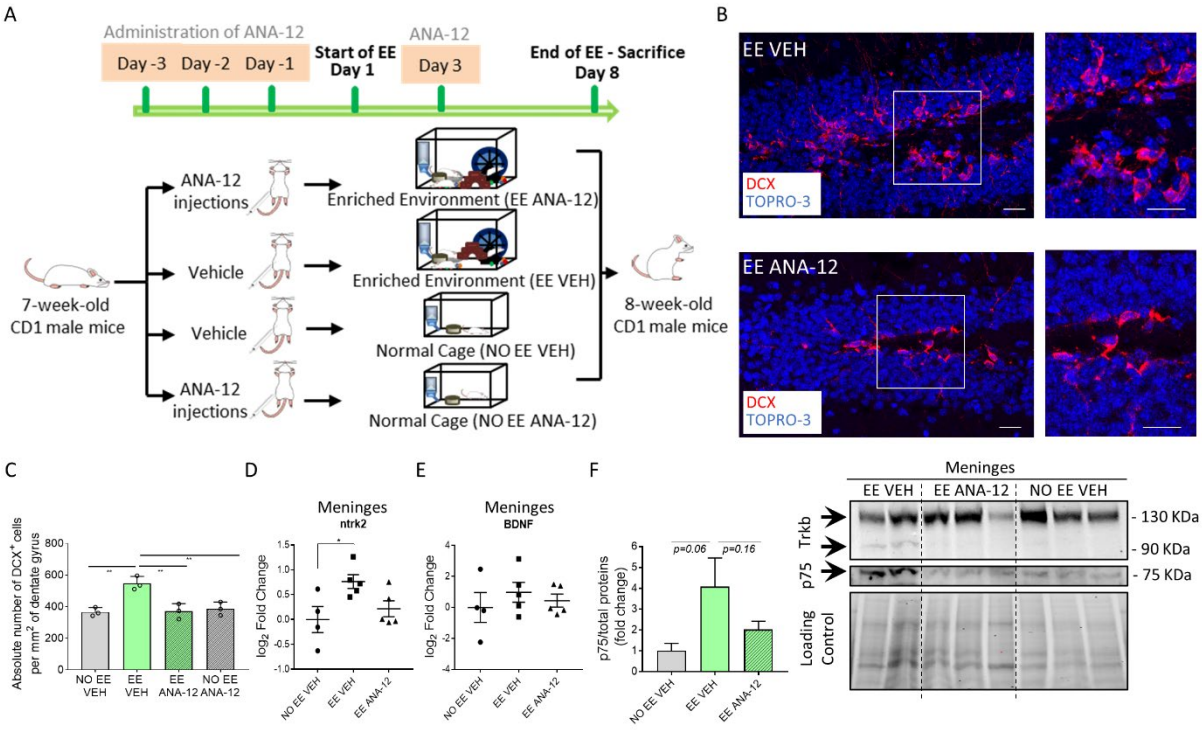

FIGURE 3.4 – ANA-12 INHIBITS HIPPOCAMPAL NEUROGENESIS AND IMPACTS BDNF-TRKB SIGNALING IN MENINGES

(A) Schematic representation of the experimental design used for EE exposure and TrkB inhibitor ANA-12 administration in CD1 mice. (B) Sagittal brain sections of CD1 mice showing hippocampal DCX$^+$ (red) cells in animals exposed to EE and administered only vehicle (EE VEH) and animals exposed to EE and administered with the TrkB inhibitor ANA-12 (EE ANA-12). A white box highlights a dentate gyrus (DG) zone reported as a magnification on the right panel. (C) Graph showing the number of DCX$^+$ cells per mm2 of the DG in animals subjected to EE or not and administered with vehicle or ANA-12 (NO EE VEH, EE VEH, EE ANA-12, NO EE ANA-12). (D) Graph depicting gene expression analysis for *NTRK2* (TrkB) in NO EE VEH, EE VEH and EE ANA-12 mice. Expression levels are reported as log2 Fold Change in respect with NO EE VEH. (E) Graph depicting gene expression analysis for *BDNF* in NO EE VEH, EE VEH and EE ANA-12 mice. Expression levels are reported as log2 Fold Change in respect with NO EE VEH. (F) Graph showing the differential fold change in protein expression for p75 protein in NO EE VEH, EE VEH and EE ANA-12 mice in respect with NO EE VEH (left panel). Representative western blotting analysis of mouse brain meningeal protein extracts which shows the presence of TrkB and p75 proteins in EE VEH, EE ANA-12 and NO EE VEH samples (right). In EE VEH samples one additional TrkB protein isoform was identified. Data are presented as mean ± SEM; * = p value ≤ 0.05, ** = p value ≤ 0.01. In pictures B nuclei are in blue (TOPRO-3 nuclear staining). Pictures B are maximum intensity projections of z-stack confocal images. Scale bars represent 20 µm.

We then investigated how meningeal niche react to the administration of ANA-12 inhibitor following EE exposure.

Immunofluorescence and confocal analysis revealed a decreased number of GLAST$^+$ and β3-Tubulin$^+$ cells in EE-treated group after the administration of ANA-12 (number of GLAST$^+$ cells

per 2 mm of cross-sectioned meninges: NO EE VEH: 5.667 ± 1.167, n=3; EE VEH: 14 ± 0.5, n=3; EE ANA-12: 9 ± 0.7638, n=3; NO EE ANA-12: 6.333 ± 1.014, n=3; NO EE VEH vs EE VEH, p= 0.0008; EE VEH vs EE ANA-12, p= 0.0181; EE VEH vs NO EE ANA-12, p= 0.0014; number of β3-Tubulin$^+$ cells per 2 mm of cross-sectioned meninges, NO EE VEH: 12.33 ± 1.202, n=3; EE VEH: 24.5 ± 2.363, n=3; EE ANA-12: 9.167 ± 0.8819, n=3; NO EE ANA-12: 7.22 ± 1.848, n=3; NO EE VEH vs EE VEH, p= 0.0053; EE VEH vs EE ANA-12, p= 0.0012; EE VEH vs NO EE ANA-12, p= 0.0005) (Figure 3.5A-D) . RT-PCR analysis further confirm for the expression of GLAST gene (*SLC1A3*) and β3-Tubulin gene (*TUBB3*) in EE VEH, EE ANA-12 and NO EE VEH animal groups (*SLC1A3* log2 Fold Change: NO EE VEH: 0 ± 0.23, n=4; EE VEH: 0.6 ± 0.34, n=5; EE ANA-12: 0.5 ± 0.22, n=5; *TUBB3* log2 Fold Change: NO EE VEH: 0 ± 0.64, n=4; EE VEH: 0.63 ± 0.42, n=5; EE ANA-12: 0.28 ± 0.33, n=5) (Figure 3.5E,F).

In order to confirm TrkB signaling modulation of meningeal neural progenitors following EE, we assessed the expression of DCX, a different immature neuron marker. DCX$^+$ cells are extremely rare in meninges of adult mice (Bifari et al. 2015), however, through western blot analysis, we were able to observe an increase of DCX protein following EE. This increment was partially reduced in EE with ANA-12 mice (DCX/total proteins (Fold Change): NO EE VEH: 1.25 ± 0.74, n=3; EE VEH: 3.58 ± 0.39, n=2; EE ANA-12: 2.14 ± 0.6, n=3) (Figure 3.5G).

These data suggested that ANA-12 inhibitor may interfere with the capacity of the immature neurons in meninges to react to EE.

Since we noted changes in the fractones and macrophages content following EE, we investigate whether ANA-12 inhibitor could have an effect on the trophic and immune state of the meningeal niche. Interestingly, immunofluorescence analysis revealed that the increase in meningeal fractones observed after EE exposure was reduced in EE ANA-12 animals, suggesting its regulation by TrkB/BDNF signaling (number of fractones per 2 mm of cross-sectioned meninges: NO EE VEH: 47.67 ± 3.632, n=3; EE VEH: 89.17 ± 1.302, n=3; EE ANA-12: 66.17 ± 6.333, n=3; NO EE ANA-12: 56.5 ± 4.093, n=3; NO EE VEH vs EE VEH, p= 0.0006; EE VEH vs EE ANA-12, p= 0.0207; EE VEH vs NO EE ANA-12, p= 0.0027) (Figure 3.5H-I). On the contrary, no significant changes were identified in CD68$^+$ cell number in meninges (Figure 3.5J-K).

Overall, these results suggested that the meningeal niche response to neurogenic stimuli was mediated by the neurotrophic receptor TrkB.

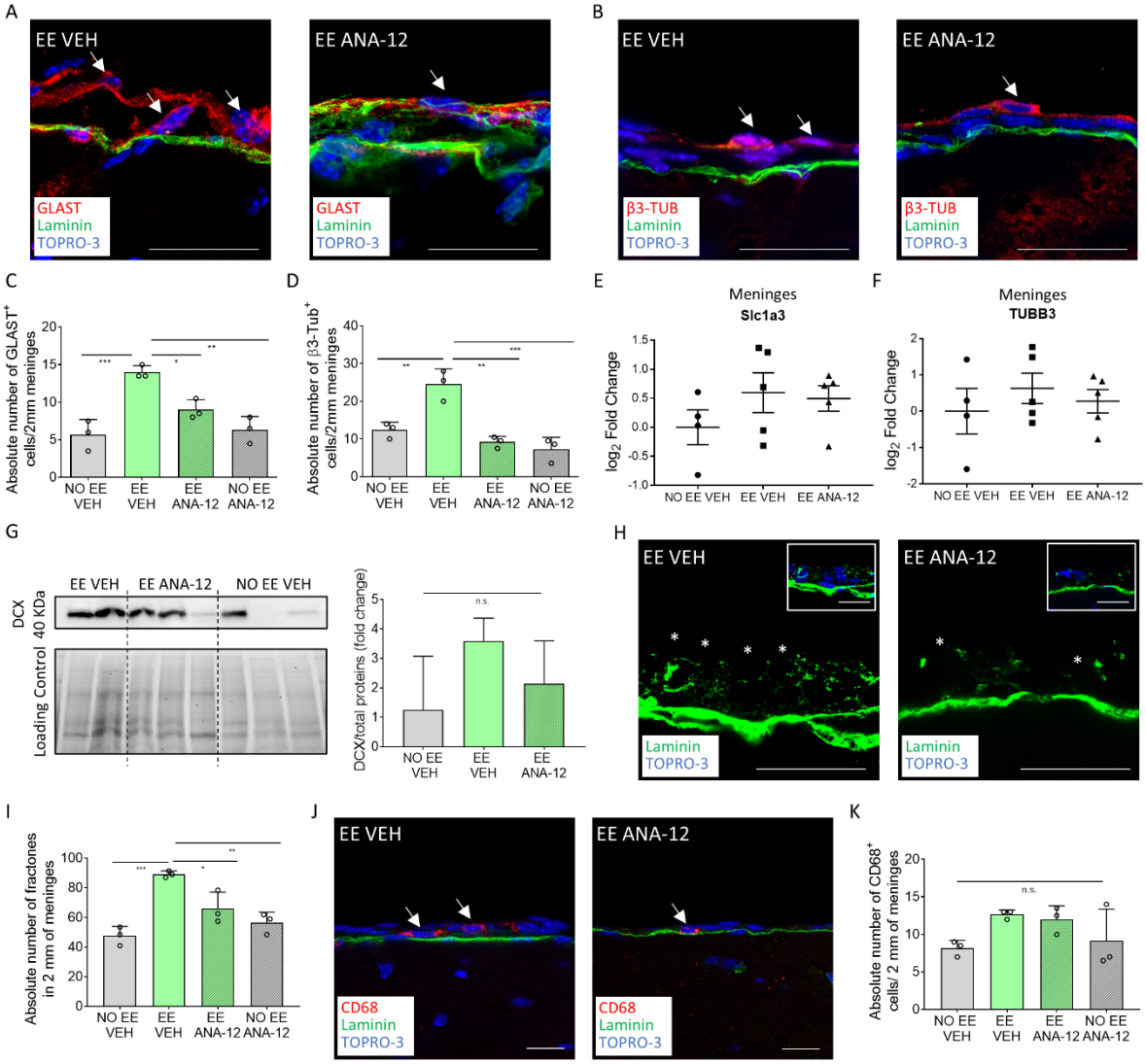

FIGURE 3.5 – ANA-12 ADMINISTRATION REVERTS EE-INDUCED CHANGES IN THE MENINGEAL NICHE

(A) Sagittal brain sections of CD1 mice showing GLAST⁺ (red) cells above meningeal basal lamina (green) in EE VEH and EE ANA-12 mice. (B) Sagittal brain sections of CD1 mice showing β3-Tubulin+ (red) cells above meningeal basal lamina (green) in EE VEH and EE ANA-12 mice. (C) Graph showing the number of GLAST⁺ cells in 2mm of retrosplenial brain meninges of NO EE VEH, EE VEH, EE ANA-12 and NO EE ANA-12 animals. (D) Graph showing the number of β3-Tubulin⁺ cells in 2mm of retrosplenial brain meninges of NO EE VEH, EE VEH; EE ANA-12 and NO EE ANA-12 animals. (E) Graph depicting gene expression analysis for *SLC1A3* (GLAST) in NO EE VEH, EE VEH and EE ANA-12 mice. Expression levels are reported as log2 Fold Change in respect with NO EE VEH. (F) Graph depicting gene expression analysis for *TUBB3* (β3-Tubulin) in NO EE VEH, EE VEH and EE ANA-12 mice. Expression levels are reported as log2 Fold Change in respect with NO EE VEH. (G) Representative western blotting analysis of mouse brain meningeal protein extracts which shows the presence of DCX protein in EE VEH, EE ANA-12 and NO EE VEH samples (left panel). Graph showing the differential fold change in protein expression for DCX protein in NO EE VEH, EE VEH and EE ANA-12 mice with respect witch NO EE VEH (right panel). (H) Sagittal brain sections of CD1 mice showing fractones (*) identified via laminin (green) staining in brain meninges of EE VEH and EE ANA-12 mice. An insert illustrates laminin staining (fractones) below meningeal nuclei (TOPRO-

3). (I) Graph showing the number of $CD68^+$ cells in 2mm of retrosplenial brain meninges of NO EE VEH, EE VEH, EE ANA-12 and NO EE ANA-12 animals. (J) Sagittal brain sections of CD1 mice showing CD68 + (red) cells in brain meninges of EE VEH and EE ANA-12 mice. (K) Graph showing the number of fractones in 2mm of retrosplenial brain meninges of NO EE VEH, EE VEH; EE ANA-12 and NO EE ANA-12 animals. Data are presented as mean ± SEM; n.s. = not statistically significant, * = p value ≤ 0.05, ** = p value ≤ 0.01, *** = p value ≤ 0.001. In pictures A, B, H and J nuclei are in blue (TOPRO-3 nuclear staining). Pictures J are single plane confocal images. Pictures A, B and H are maximum intensity projections of z-stack confocal images. Scale bars represent 20 µm. White arrows indicate positive cells while asterisks indicate fractones.

3.1.4 Fluoxetine administration induces meningeal niche response

To assess if the meningeal niche was responsive to other neurogenic stimuli different from EE, we investigated the effect of long-term antidepressant treatment on young mice meninges. It is known that antidepressants are able to carry out their therapeutic function, amelioration of anxiety/depression-related behaviour, via a neurogenic boost induced in the patients' hippocampi (Khodanovich et al. 2018; Malberg et al. 2000; Samuels and Hen 2011; Wang et al. 2008).

According to this, we decided to exposed CD1 mice (4 weeks old) to chronic (4 weeks) administration of fluoxetine, one of the most prescribed antidepressant drugs belonging to the SSRI category, as described by other groups (Figure 3.6A) (David et al. 2009; Khodanovich et al. 2018; Samuels and Hen 2011).

To achieve this goal, we performed anxiety/Obsessive Compulsive Disorder (OCD)-evaluating behavioural test (the Marble Burying Test, MBT) to confirm the effectiveness of the fluoxetine treatment on animal (de Brouwer et al. 2019; Kraeuter et al. 2019). Following 4 weeks of drug administration, the percentage of marbles buried by treated animals (FLUOX) was significantly lower when compared with controls (percentage of marbles buried over the total marble number, CTRL: 86.67% ± 7.2, n=4; FLUOX: 35.83% ± 12.84, n=8; p=0.0246) (Figure 3.6B, C). The consistent reduction in the number of marbles buried in the treated group suggested that fluoxetine exerted its pharmacological effect and was able to reduce OCD-like behaviour. Fluoxetine and other SSRI antidepressants are known to induce hippocampal neurogenesis in DG (Samuels and Hen 2011). To further confirm if the antidepressant treatment was properly effective, we performed immunofluorescence and confocal analysis for the proliferation marker Ki67 and the newborn immature neuron marker doublecortin, DCX (Figure 3.6D-G). In line with previous observations, we found that the number of $Ki67^+$ and DCX^+ cells of the DG were significantly higher in fluoxetine-treated mice compared to control mice (number of $Ki67^+$ cells per mm2 of DG area, CTRL: 2.322 ± 1.592, n=3; FLUOX: 14.33 ± 1.963, n=3;

p=0.0090) (number of DCX^+ cells per mm2 of DG area, CTRL: 331.3 ± 37.04, n=3 ; FLUOX: 484.1 ± 25.58, n=3; p=0.0274) (Figure 3.6F, G). These data confirmed the fluoxetine treatment effectiveness, supporting that antidepressant can induce cell differentiation in the hippocampus, as already reported by literature (David et al. 2009; Khodanovich et al. 2018; Samuels and Hen 2011).

We then evaluated the fluoxetine effect on meninges by analysing the mouse brain retrosplenial meningeal cell number and proliferation following 4 weeks of treatment. According to EE exposure results, the number of meningeal nuclei, identified by the nuclear marker TOPRO-3, as well as the number of proliferating cells, identified by the marker Ki67, didn't change following the fluoxetine administration (Figure 3.6H, I, N, O). We proceeded performing immunofluorescence and confocal analysis for NSCs and we found that, while $GLAST^+$ cells showed a trend of increase, β3-$Tubulin^+$ cells increased significantly in the treated group compared to the control (number of $GLAST^+$ cells per 2 mm of cross-sectioned meninges: CTRL: 9.667 ± 0.3333, n=3; FLUOX: 12.67 ± 2.848, n=3; p=0.3545; number of β3-$Tubulin^+$ cells per 2 mm of cross-sectioned meninges: CTRL: 15.67 ± 2.848, n=3; FLUOX: 31.19 ± 3.641, n=3; p=0.0284) (Figure 3.6J, K, P, Q). These data suggested that meningeal niche responded to fluoxetine increasing number of meningeal immature neurons, as we previously described in the paradigm of EE.

Alike what we observed after EE exposure, the number of fractones (identified by Laminin) resulted significantly higher in fluoxetine-treated group compared to controls (number of fractones per 2 mm of cross-sectioned meninges: CTRL: 58.33 ± 3.844, n=3; FLUOX: 82.67 ± 7.446, n=3; p= 0.0440) (Figure 3.6L, R) as well as we found an increased number of $CD68^+$ macrophages in fluoxetine treated mice, albeit the difference was not statistically significant (Figure 3.6M, S).

Taken together, these results showed that meningeal niche is able to react to fluoxetine treatment by increasing macrophages and trophic ECM fractones, as described before for EE meningeal response.

Overall, these results suggested that meningeal niche may react not only to EE exposure, but also to other pharmacological neurogenic stimuli like fluoxetine. Further studies will be necessary to clarify the role of TrkB signaling in meningeal response to pharmacological neurogenic stimuli.

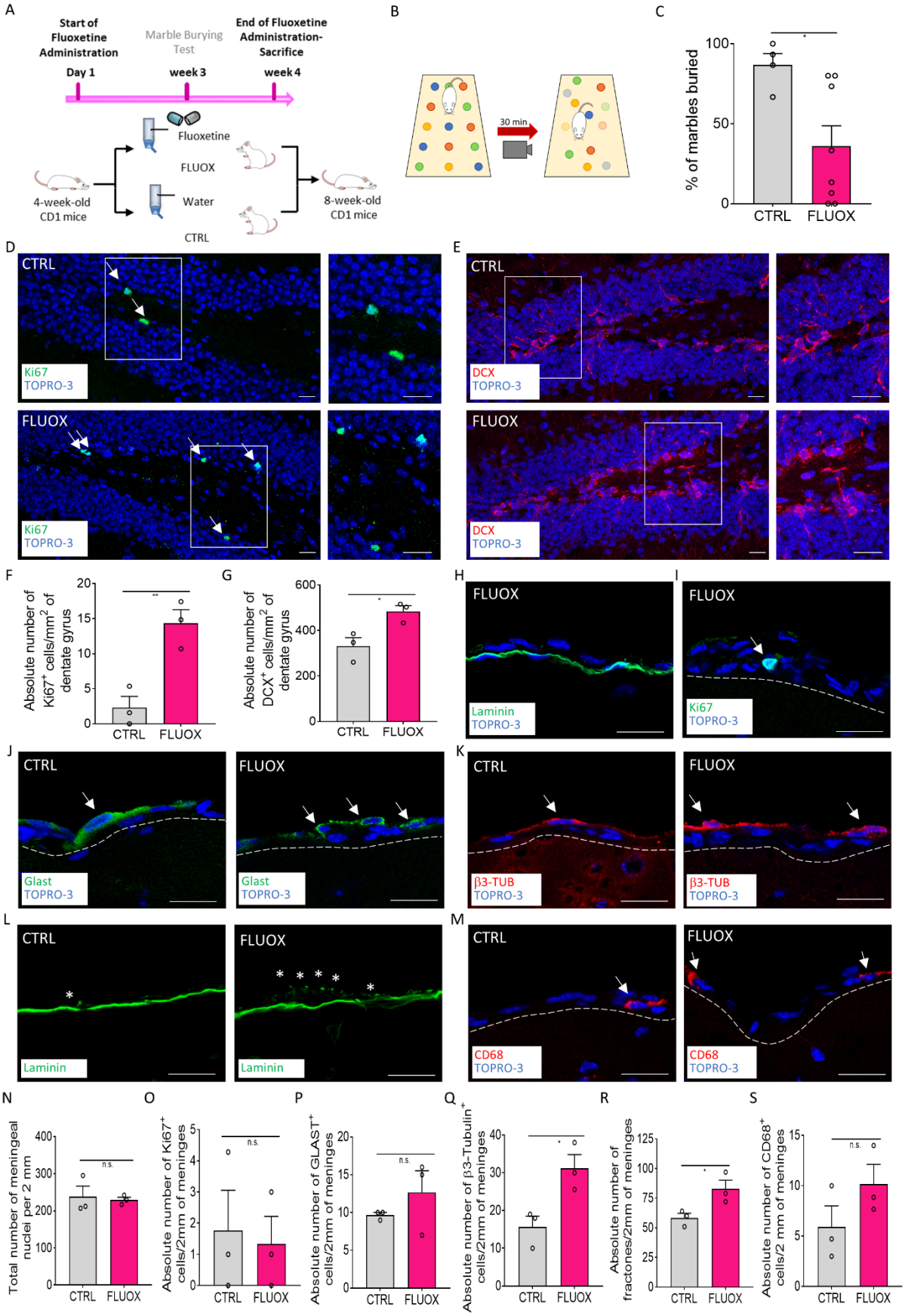

FIGURE 3.6 –MENINGEAL NICHE RESPONDS TO FLUOXETINE TREATMENT

(A) Schematic representation of the experimental design used for fluoxetine administration. (B) Schematic representation of behavioral testing for OCD-like behavior via Marble Burying Test (MBT). (C) Graph showing the percentage of marbles buried by treated (FLUOX) and non-treated (CTRL) animals. (D, E) Sagittal brain sections of CD1 mice, showing the presence of $Ki67^+$ cells (green) and DCX^+ cells (red) in hippocampal dentate gyri (DG) in CTRL and FLUOX animals. A white box highlights a DG zone reported as a magnification on the right panel. (F) Graph showing the number of $Ki67^+$ cells per mm2 of DG in CTRL and FLUOX animals. (G) Graph showing the number of DCX^+ cells per mm2 of DG in CTRL and FLUOX animals. (H) Sagittal brain section of CD1 mice, showing brain meningeal nuclei and meningeal basal laminin (green) in a FLUOX animal. (I) Sagittal brain section of CD1 mice showing a brain meningeal $Ki67^+$ (green) cell in a FLUOX animal. Meninges are delineated via white dashes. (J) Sagittal brain sections of CD1 mice showing brain meningeal $GLAST^+$ cells in CTRL and FLUOX mice. Meninges are delineated via white dashes. (K) Sagittal brain sections of CD1 mice showing brain meningeal $\beta3\text{-Tubulin}^+$ (red) cells in CTRL and FLUOX mice. Meninges are delineated via white dashes. (L) Sagittal brain sections of CD1 mice showing fractones (*) identified via laminin (green) staining in brain meninges of CTRL and FLUOX mice. (M) Sagittal brain sections of CD1 mice showing brain meningeal $CD68^+$ (red) cells in CTRL and FLUOX mice. Meninges are delineated via white dashes. (N-S) Graphs showing the number of (N) nuclei, (O) $Ki67^+$ cells, (P) $GLAS^+$+ cells, (Q) $\beta3\text{-Tubulin}^+$ cells, (R) fractones, (S) $CD68^+$ cells in 2 mm of retrosplenial brain meninges of CTRL and FLUOX animals. Data are presented as mean ± SEM; n.s. = not statistically significant, * = p value ≤ 0.05, ** = p value ≤ 0.01. In pictures D, E, H, I, J, K and M nuclei are in blue (TOPRO-3 nuclear staining). Pictures H, I, J, K, L and M are single plane confocal images. Pictures D and E are maximum intensity projections of z-stack confocal images. Scale bars represent 20 µm. White arrows indicate positive cells while asterisks indicate fractones.

3.2 AIM 2: Meningeal niche in a murine model of Multiple sclerosis

3.2.1 Meningeal niche Response to EAE

To validate the second hypothesis of this work about the meningeal modulation in pathological condition, we exploit the use of EAE animal model to study the effect of MS in meningeal niche. The establishment of the animal model for the disease and the subsequent score assignments were conducted in collaboration with the group coordinated by Professor Gabriela Constantin, Department of Medicine, section of General Pathology, University of Verona. Briefly, C57Bl/6J 8-10-week-old female and male mice (n=12) were immunized with an emulsion containing MOG35-55 peptide in CFA supplemented with Mycobacterium tuberculosis and also PTX (Vinci Biochem, Italy) in order to induce the disease. Animals were observed daily up to a period of 50 days post-transfer/post-immunization and associated to an EAE score according to literature (Constantin et al. 1999; Stromnes and Goverman 2006). The grading scale of 0–5 score with the clinical severity of EAE-induced mice used in this work is reported in Table 4. From the immunization process, we obtained n=X EAE animals (also called MOG) and n=X control animals (also called CTRL+CFA).

Brain meningeal niche responds to the inflammatory environment of EAE

As already reported in the literature, the EAE model of MS is characterized by the presence of immunity cells that actively participate in the development of the disease (Caravagna et al. 2018; Christy et al. 2013; Russi et al. 2018). In order to confirm the presence of immune cells characterizing the EAE model, we performed immunofluorescence and confocal analysis at the peak stage of pathology for different markers: CD163 for meningeal macrophages, CD3 for T cell and Ly6G for neutrophils.

We compared the number of meningeal $CD163^{+}$ cells between control and EAE mice. We found an increasing percentage of CD163 marker in EAE brain meninges (CTRL+CFA: 3,434 ± 0,5657%, MOG: 7,042 ± 0,9809%) and meningeal substructures (CTRL + CFA: 3.695 ± 0.7% vs MOG peak 10.37 ± 1.6%) (Figure 3.7C-E), indicating a reaction of meningeal niches to the inflammation (Bevan et al. 2018). On the other hand, the quantification of CD3 marker (Figure 3.7F-H) suggest no difference between control and EAE group in meninges. In meningeal substructures, instead, we found an increase of T cells (CTRL + CFA: 1.548 ± 0.03% vs MOG 5.43 ± 0.7%; p= 0.022) (Figure 3.9H). We also quantified the presence of Ly6G, a marker which is expressed in granulocytes and peripheral neutrophils. According to literature, neutrophils are among the first cells able to enter in the CNS during EAE (Christy et al. 2013), and in fact we detected their presence in the pre-onset stage (Russi et al. 2018) whereas they were absent in control mice (CTRL + CFA 0 ± 0% vs MOG 1.766 ± 0.05%; p= 0.073) (Figure 3.9I). On the other hand, we didn't detect neutrophils within brain meninges at peak stage, but we found their presence in meningeal substructures of EAE mice (CTRL + CFA 0.5194 ±0.1% vs MOG 4.451 ± 0.2%; p= 0.0001) (Figure 3.7J, K).

Taken together, these results suggest that meningeal niche respond to EAE inflammatory conditions and that meningeal substructures are a site of accumulation of meningeal macrophages, T cells and neutrophils at peak stage of EAE disease.

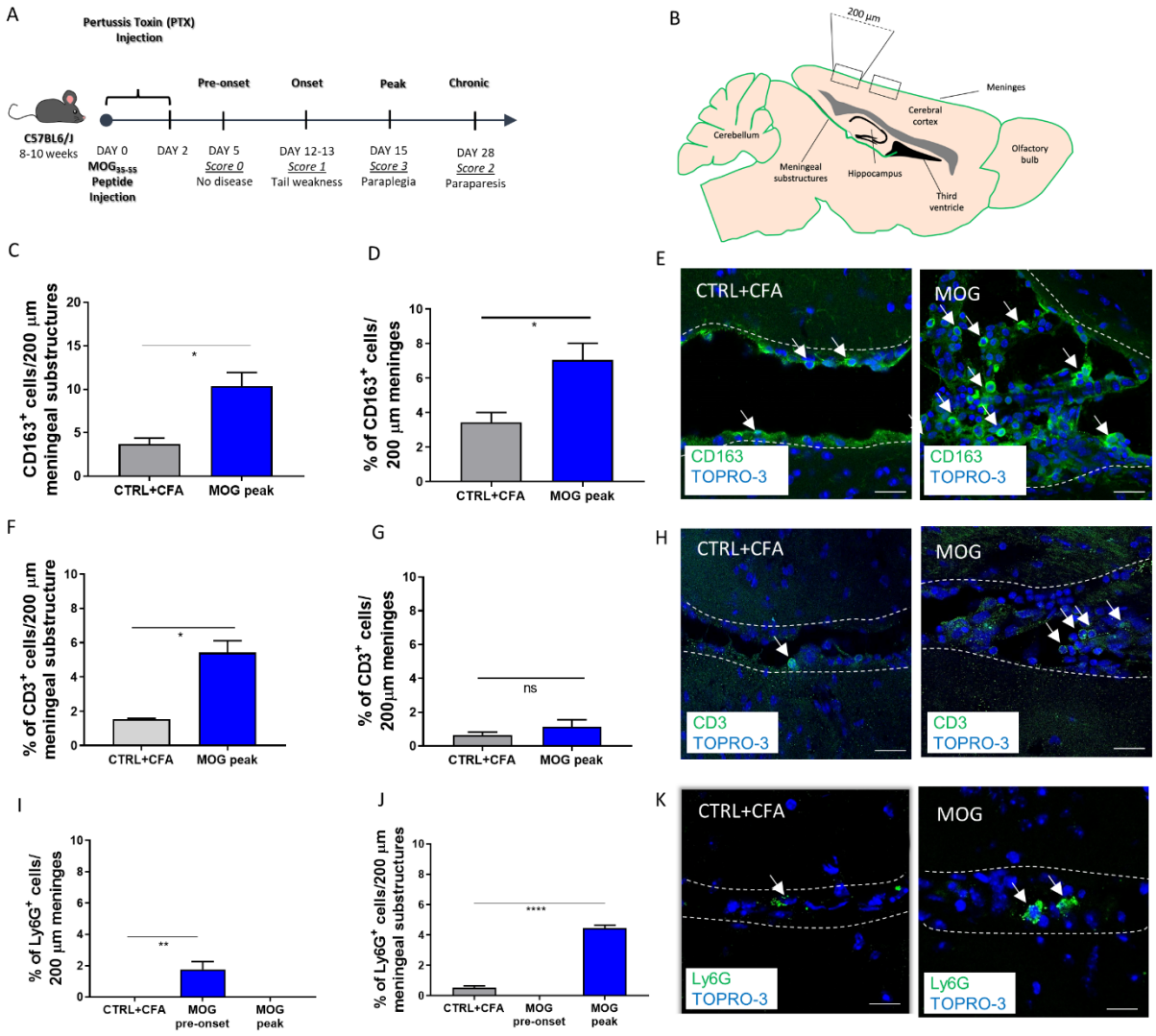

FIGURE 3.7 - IMMUNE CELLS IN EAE AND CONTROL MICE

(A) Schematic representation of the experimental design used for EAE induction. (B) Scheme depicting the sagittal section of mouse brain highlighting the specific regions where brain meninges and meningeal substructures were analyzed. (C, D) The graphs compare the percentage of $CD163^+$ cells in meninges and meningeal substructures respectively between EAE and control mice. (E) Sagittal brain section of control and EAE mouse brain, showing $CD163^+$ cells are present in meningeal substructures. (F, G) Graphs represent the percentage of double positive $CD3^+$ cells in 200µm of meninges and meningeal substructures at peak stage. (H) Sagittal brain section of control and EAE mouse brain, showing $CD3^+$ cells are present in meningeal substructures. (I, J) Graphs represent the percentage of double positive $Ly6G^+$ cells in 200µm of meninges and meningeal substructures at pre-onset and peak stage. (K) Sagittal brain section of control and EAE mouse brain, showing $Ly6G^+$ cells are present in meningeal substructures. White dashed lines delineate meninges above the brain parenchyma. $CD163^+$, $CD3^+$, $Ly6G^+$ cells in (E, H, K) are shown in green, while nuclei are in blue (TOPRO-3 nuclear staining). Data are presented as mean ± SEM; ns = not significant, * $p \leq 0.05$, *** $p \leq 0.001$. All the pictures are single plane confocal images. Scale bars represent 20 µm.

It has been described that neural precursor cells present in meninges are able to react following injury and disease (Decimo et al. 2011; Nakagomi et al. 2012). Moreover,

leptomeninges could have a fundamental role in T cells infiltration of CNS during autoimmune inflammation or immune surveillance (Schläger et al. 2016). Since it has not yet been well investigated, we specifically investigated how meningeal niche react during the progression of multiple sclerosis disease and, to this aim, we first focused our analyses on NSCs populations that have been recently described in leptomeninges (Bifari et al. 2017). We analysed EAE mouse brain meninges and meningeal substructures (Figure 3.8A) at different stage of pathology: pre-onset (5 days post-immunization = dpi), onset (12 dpi), peak (15 dpi) and chronic (28 dpi).

As reported by Decimo et al. 2012, meninges react to inflammation by increasing the number of cells. Accordingly, to this evidence, we analysed the number of meningeal cells (identified by the nuclear marker TOPRO-3) and proliferative cells (stained for Ki67 marker) in all the stages of the disease. We counted the number of positive cells for Ki67 marker among the total number of meningeal or meningeal substructures cells in 200 μm of meninges or meningeal substructures. The results showed an immediate increase of cells proliferation in EAE mouse brain meninges compared to control animals (CTRL + CFA: 1.21 ± 0.37%, MOG pre-onset 5.04 ± 0.64%, p= 0.02; MOG onset: 4.84 ± 0.90%, p= 0.013; MOG peak: 8.69 ± 0.92%, p= 0.0001; MOG chronic: 5.91 ± 0.66%, p= 0.0059) (Figure 3.8D), whereas in meningeal substructures a significantly increase of cells proliferation was found starting from the onset of EAE disease (CTRL + CFA: 1.86 ± 0.47%, MOG pre-onset 2.599 ± 1.07%, MOG onset: 13.77 ± 0.48%, p= 0.012; MOG peak: 11.19 ± 3.17%, p= 0.053; MOG chronic: 6.237 ± 0.59%) (Figure 3.8D,E).

We then characterized the reaction of meningeal neural precursors toward the inflammatory environment by performing immunofluorescence and confocal analysis on specific marker such as PDGFrβ for NSCs, GLAST for radial glia-like cells and DCX for immature neurons. As shown in Figure 3.8G, meninges were characterized by a significant steady higher number of PDGFrβ$^+$ cells at pre-onset, onset and peak of disease development in EAE compared to control mice; a slight reduction in PDGFrβ$^+$ cells was, instead, observed at chronic stage of disease (CTRC + CFA: 4.82 ± 0.2%, MOG pre-onset: 8.395 ± 1.10%, MOG onset: 8.164 ± 1.1%, MOG peak: 8.396 ± 0.7%, MOG chronic: 4.17 ± 0.3%). On the other side, within meningeal substructures (Figure 3.8H), PDGFrβ$^+$ cells are significantly increased mainly at pre-onset of disease and slightly decreased through the other stages of analysis (CTRL + CFA: 6.312 ± 0.5%,

MOG pre-onset: 11.6 ± 0.3%, MOG onset: 8.437 ± 0.3%, MOG peak: 8.874 ± 0.4%, MOG chronic: 5.332 ± 0.8%).

Interestingly, we observed PDGFrβ$^+$ cells in close contact (considered as cells distance <10 µm (Nagl et al. 2016)) with macrophages identified by CD68 marker and meningeal macrophages identified by CD163 marker (Figure 3.8I), suggesting the existence of a possible crosstalk between these NSC and immune cell populations.

We then evaluated, in meninges and in meningeal substructures, the distribution of radial glia-like NSCs by analyzing GLAST marker and the presence of DCX+ immature neurons. We observed a non-significant increase of GLAST$^+$ cells in meninges at peak of disease and a slightly decrease in chronic stage (CTRL + CFA: 4.551 ± 0.4, MOG pre-onset: 4.692 ± 0.2%, MOG onset: 6.324 ± 0.8, MOG peak: 6.827 ± 0.6%, MOG chronic: 3.861 ± 0.3%) (Figure 3.8J). Even in meningeal substructures there were no differences between control and EAE mouse (CTRL + CFA: 1.281 ± 0.15, MOG pre-onset: 2.345 ± 0.96%, MOG onset: 2.29 ± 0.33, MOG peak: 0.593 ± 0.22%, MOG chronic: 1.764 ± 0.34%) (Figure 3.8K). Contrary, compared to control mice, EAE mice showed a statistically significant increase of DCX$^+$ cells in meninges at pre-onset and onset stages of disease (CTRL +CFA: 1.729 ± 0.3%, MOG pre-onset: 8.091 ± 1.5%, MOG onset: 7.051 ± 1.6%) (Figure 3.8M). Instead, within meningeal substructures, significant differences were found at onset and peak stages of disease (CTRL + CFA: 1.264 ± 0.3%, MOG onset: 7.121 ± 1.7%, MOG peak: 7.209 ± 1.1%) (Figure 3.8N). Interestingly, these results suggest a reaction of DCX$^+$ cells in meninges at very early stages of pathology and a later reaction in the meningeal substructures.

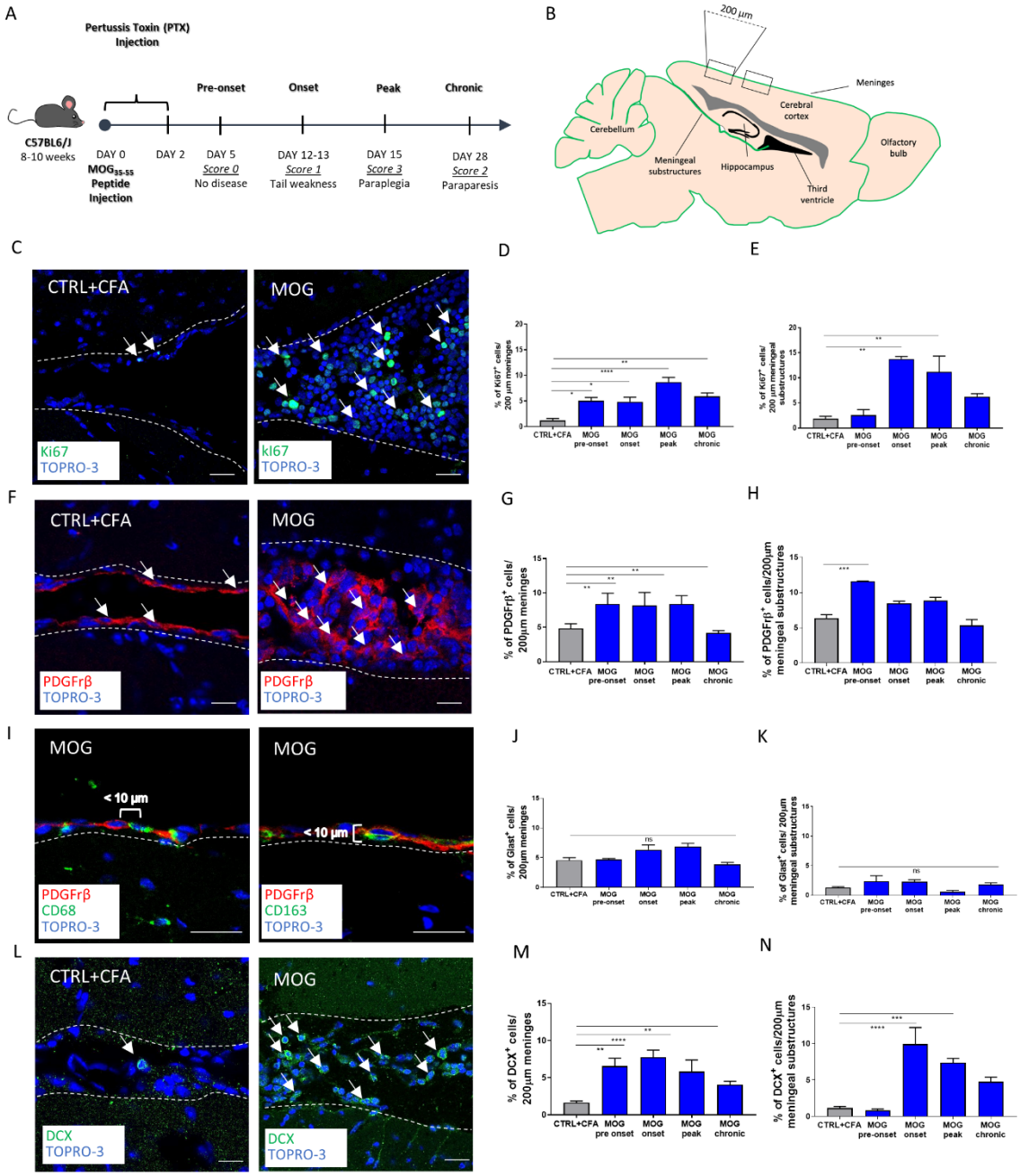

FIGURE 3.8 – NSCS INCREASED IN NUMBER IN EAE DEVELOPMENT

(A) Schematic representation of the experimental design used for EAE induction. (B) Scheme depicting the sagittal section of mouse brain highlighting the specific regions where brain meninges and meningeal substructures were analyzed. (C) Sagittal brain sections of CTRL and MOG mice showing Ki67$^+$ (green) cells in meningeal substructures. (D, E) Graphs showing the percentage of Ki67$^+$ cells in 200µm of meninges and meningeal substructures. (F) Sagittal brain sections of CTRL and MOG mice showing PDGFrβ$^+$ (red) cells in meningeal substructures. (G, H) Graphs showing the percentage of PDGFrβ$^+$ cells in 200µm of meninges and meningeal substructures. (I) Sagittal brain sections of MOG mice showing PDGFrβ$^+$ (red) cells in close contact with CD68 (green) and PDGFrβ$^+$ (red) cells in close contact with CD163 (green) in meninges. (J, K) Graphs showing the percentage of GLAST$^+$ cells in 200µm of meninges and meningeal substructures. (L) Sagittal brain sections of CTRL and MOG mice showing DCX$^+$ (green) cells in meningeal substructures. (M, N) Graphs showing the percentage of DCX$^+$ cells in 200µm of meninges and meningeal substructures. White dashed lines delineate meningeal substructures. PDGFrβ$^+$ cells in (F, I) are shown in red, Ki67$^+$ cells in (C) and DCX$^+$ cells in (L) are shown

in green, $CD68^+$ and $MHCII^+$ cells in (I) are shown in green while nuclei are in blue (TOPRO-3 nuclear staining). Data are presented as mean ± SEM; ∗∗∗∗p ≤ 0.0001, ∗∗∗p ≤ 0.001, ∗∗p ≤ 0.01, ∗p ≤ 0.05; ns = not significant. All the pictures are single plane confocal images. Scale bars represent 20 µm (C, F, I, L).

In order to deeply investigate the role of NSCs in EAE and their possible interaction with the immune populations, we performed immunofluorescence and confocal analysis for antigen presenting cells, monocytes and macrophages, identified by MHCII and CD68 markers, respectively. We observed a significant change in the percentage of $MHCII^+$ cell numbers and also in $CD68^+$ cell numbers, both in meninges and in meningeal substructures.

Interestingly, we found a significant increase of double positive cells for DCX and MHCII markers in meninges of EAE animals in comparison with controls (CTRL + CFA: 0.4655 ± 0.2%, MOG onset: 3.565 ± 0.5%, MOG chronic: 2.073 ± 0.7%) (Figure 3.9G). The same analysis was performed in meningeal substructures showing significant differences between control and EAE onset and peak stage (CTRL + CFA: 0.4774 ± 0.2%, MOG onset: 2.581 ± 0.4%, MOG peak: 2.095 ± 0.4%) (Figure 3.9H). These results show that $DCX^+/MHCII^+$ cells increase at pre-onset stage, and these are maintained during the disease progression.

Given the ability of DCX^+ cells to express MHCII marker, we also checked for double-positive DCX and CD68 cells. We found $DCX^+/CD68^+$ cells both in meninges and meningeal substructures: in meninges of EAE mice brain, they were detected at all stages of disease development (CTRL + CFA:0.2412 ± 0.1%, MOG pre-onset: 2.204 ± 0.3%, MOG onset: 2.939 ± 0.7, MOG peak: 2.405 ± 0.2%, MOG chronic: 2.017 ± 0.5%) (Figure 3.9I) while double-positive cells were only found at onset of disease in the meningeal substructure, with a statistically significant increment between EAE mouse meningeal substructures and control mouse (CTRL + CFA: 0.3788 ± 0.03%, MOG onset: 6.696 ± 2.5%) (Figure 3.9J).

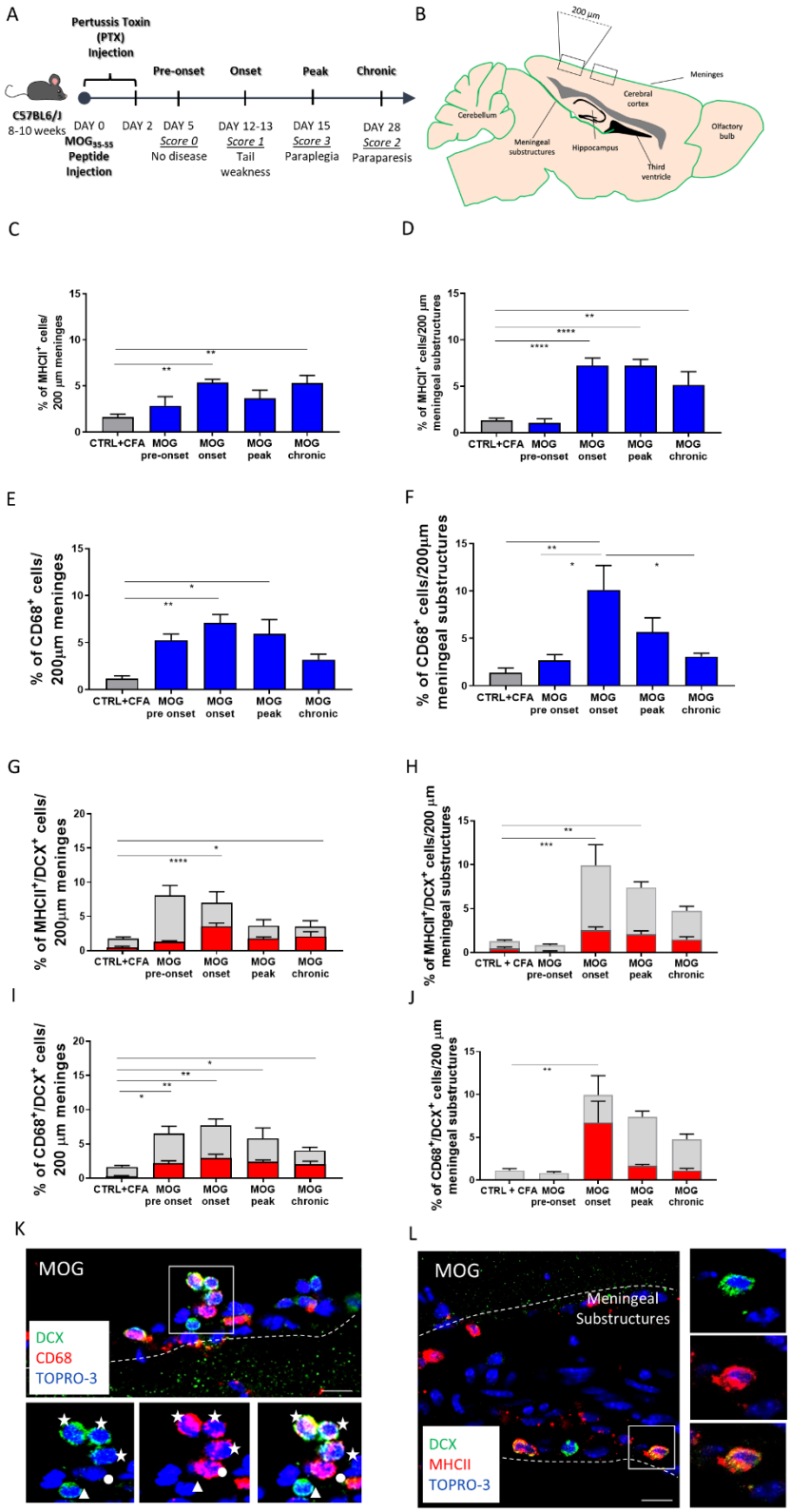

FIGURE 3.9 – IMMUNE CELLS INCREASED IN NUMBER IN EAE DEVELOPMENT

(A) Schematic representation of the experimental design used for EAE induction. (B) Scheme depicting the sagittal section of mouse brain highlighting the specific regions where brain meninges and meningeal

substructures were analyzed. (C, D) Graphs showing the percentage of MHCII+ cells in 200µm of meninges and meningeal substructures. (E, F) Graphs showing the percentage of CD68+ cells in 200µm of meninges and meningeal substructures. (G, H) Graphs represent the percentage of double positive $DCX^+/MHCII^+$ cells in 200µm of meninges and meningeal substructures at different stages: red bars represent $DCX^+/MHCII^+$ cells and grey bars $DCX^+/MHCII^-$ cells. (I, J) Graphs represent the percentage of double positive $DCX^+/CD68^+$ cells in 200µm of meninges and meningeal substructures at different stages: red bars represent $DCX^+/CD68^+$ cells and grey bars $DCX^+/CD68^-$ cells. (K, L) Sagittal brain section of EAE mouse, showing that DCX^+ cells are positive also for MHCII and CD68 markers in meningeal substructures of EAE mice. White dashed lines delineate meningeal substructures. CD68+ and MHCII+ cells in (K, L) are shown in red, DCX^+ cells in green, while nuclei are in blue (TOPRO-3 nuclear staining). Data are presented as mean ± SEM; ∗∗∗∗p ≤ 0.0001, ∗∗∗p ≤ 0.001, ∗∗p ≤ 0.01, ∗p ≤ 0.05; ns = not significant. All the pictures are single plane confocal images. Scale bars represent 20 µm (K, L).

Overall, our results show an increase of meningeal NPCs in EAE mice from the pre-onset to the peak of the disease in meninges and meningeal substructures. These results suggest a reaction of meningeal NPCs of EAE mice according to the inflammation conditions.

Spinal cord meningeal niche responds to the inflammatory environment of EAE

After a deep investigation of NSCs in mouse brain meninges, we proceeded the analysis on spinal cord. In accordance with the symptomatology of MS, the spinal cord was well characterized over time, but little is known about the markers that we specifically took in consideration for meningeal NSCs. According to the literature (Shrestha et al. 2017), meningeal inflammation, at the level of spinal cord, is initially clearer in the caudal subarachnoid space (SAS), so we performed all the analysis on the caudal (lumbar + sacral) portion of the spinal cord.

Alike the observation done for the brain meningeal tissue, we analysed the total number of cells in the spinal cord meninges during the progression of the EAE disease through immunofluorescence and confocal microscopy analysis by using the nuclear marker TOPRO-3. We counted the absolute number of nuclei in 200µm of spinal cord meninges and we found statistical difference between control and MOG animals (CTRL+CFA 231.3± 49.13, Pre-onset 215.2 ± 55.1, Onset 473.9 ± 143.9, Peak 643.4 ± 143 and Chronic 575.6 ± 172.7) (Figure 3.10D), highlighting the establishment of an inflammatory condition.

Then, we proceeded to characterize of the meningeal NPCs by counting the number of DCX^+ cells among the total number of meningeal cells in 200 µm of spinal cord meninges in all EAE stages. We found a marked increase of DCX^+ cells in spinal cord meninges following EAE, in particular at onset and peak stages of disease while a slight decrease was observed during the chronic phase (Figure 3.10F).

Since the fascinating findings of cells expressing an immune-neuronal like phenotype in brain meninges and meningeal substructures following the induction of EAE, we questioned about the presence of the same cell population even in the spinal cord. To solve this point, we performed a double staining to visualize possible $DCX^+/MHCII^+$ and $DCX^+/CD68^+$ cells (Figure 3.10J, K). Interestingly, we detected DCX/MHCII double positive cells in spinal cord meninges at all stages of disease with a distinct increment at the onset time-point of EAE cells (CTRL+CFA 1.069 ± 0.61, Pre-onset 0.975 ± 0.50, Onset 5.778 ±0.77, Peak 4.048 ± 0.74 and Chronic 3.14 ± 1.46) (Figure 3.10H). The same trend was found for $DCX^+/CD68^+$ cells (CTRL+CFA 0.17± 0.17, Pre-onset 0.424 ± 0.21, Onset 2.219 ±0.49, Peak 1.16 ± 0.41 and Chronic 0.22 ± 0.02) (Figure 3.10I).

Altogether, these results showed that even spinal cord meninges respond to inflammation following EAE induction, by changing the number of cells and showing a population of cells with an immune-neuronal like phenotype.

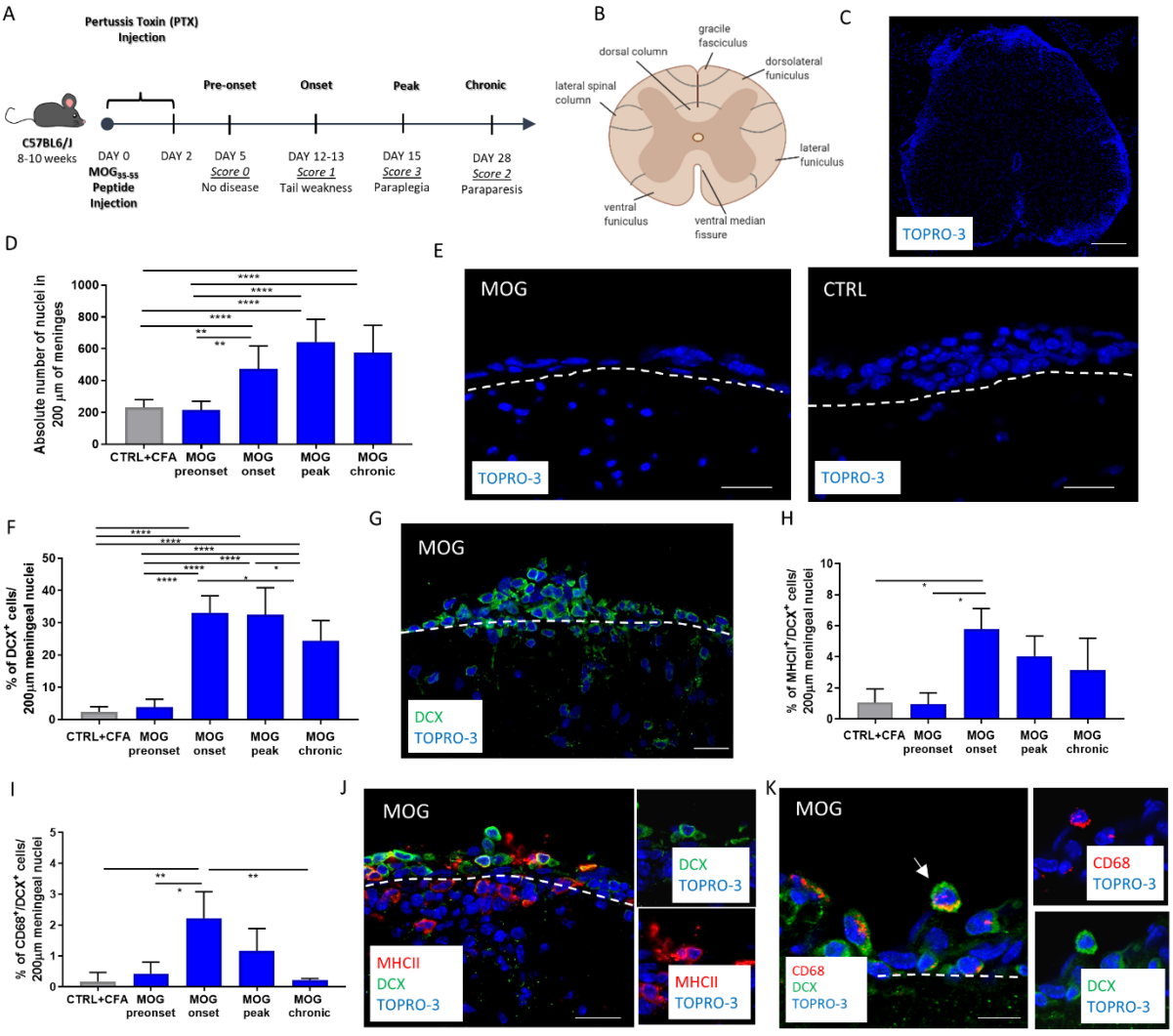

FIGURE 3.10 - NPCS INCREASED IN SPINAL CORD MENINGES

(A) Schematic representation of the experimental design used for EAE induction. (B, C) Scheme depicting the trasversal section of mouse spinal cord. (D) Graph showing the absolute number of nuclei in spinal cord meninges (E) Transversal spinal cord slice of EAE and control mouse showing the increase of nuclei in meninges. (F) Graph showing increase in percentage of DCX+ cells at the onset and peak of disease. (G) Transversal spinal cord section showing DCX+ meningeal cells in a MOG animal. (H) Graph showing increase in percentage of DCX+/MHCII+ cells in control and EAE mice. (I) Graph showing increase in percentage of DCX+/CD68+ cells in control and EAE mice. (J, K) Transversal spinal cord slice of EAE mouse showing DCX+/MHCII+ cells and DCX+/CD68+ cells in spinal cord meninges in EAE mice. White dashed lines delineate meninges above the spinal cord parenchyma. (C, J, K) DCX+ cells are in green, in (J, K) MHCII+ and CD68+ cells are in red, and nuclei are in blue (TOPRO-3 nuclear staining). Data are presented as mean ± SEM; * $p \leq 0.05$, ** $p \leq 0.01$, **** $p \leq 0.0001$. Scale bars represent 20 µm.

3.2.2 Meningeal substructures and spinal cord meninges as route of infiltrations of NSCs and immune cells into CNS parenchyma during EAE

Up to date, we showed that external brain meninges, meningeal substructures and spinal cord meninges acts as point of cells accumulation during EAE progression, and they could

represent novel entry points toward the brain parenchyma. Indeed, it has already been observed the migration of meningeal precursor cells from meninges toward the injured brain and spinal cord parenchyma (Decimo et al. 2011). One of the currently open questions in MS research regards the mechanism by which autoreactive immune cells first access to the uninflamed CNS (Russi and Brown 2015).

To analyse the possible infiltration through meninges we focused our attention on the parenchymal accumulation of NSCs and immune cells close to the meningeal layer. Specifically, we performed haematoxylin and eosin staining on sagittal brain (Figure 3.11B) and transversal spinal cord (Figure 3.13B) slices of EAE mice at chronic stage of the disease and we analysed the presence of infiltrating cells, identified as a pool of at least 5 cells immediately adjacent (100 µm wide range from meninges and meningeal substructures) to the meninges that visibly protrude from the meningeal space.

Meningeal substructures represented an entry point toward the brain parenchyma

A qualitative analysis of cell infiltrations at the level of external meninges and meningeal substructures revealed the consistent presence of cell infiltrations at brain parenchymal areas next to meningeal substructures, while no infiltrations were found in external brain meninges. Thus, for the following analysis, we focused our attention on the meningeal substructures.

NSCs in meninges are characterized by the expression of specific markers like PDGFrβ and GLAST for NSCs and DCX for immature neurons (Bifari et al. 2009; Decimo et al. 2012a). To assess the possible contribution of meningeal NSCs to brain degeneration we analysed meningeal NSCs infiltrations to the parenchyma during EAE. To this aim, we performed qualitative analyses, at each stage of the disease (pre-onset, onset, peak and chronic), of cell infiltrations. For the qualitative assessment of NSC infiltrations we analysed 5 section/mouse of brain external meninges above the cortex and meningeal substructures in all stage of disease with n=3 for EAE mouse and n=3 for control.

Meningeal substructures cells infiltrations were evaluated at different brain regions like midbrain, retrosplenial area in the cortex, thalamus, hippocampus and fornix. Different infiltrations of neural precursor cells were observed in EAE mice at onset and peak stages of disease in different sites along the meningeal substructures. Cellular infiltrations were found along meningeal substructures close to the dentate gyrus and, at the peak stage, at the level of cerebral cortex, in the retrosplenial area and in the midbrain at superior colliculus (Figure

3.11C-E). No infiltration of NPs was observed in control mice or in EAE animals at the pre-onset stage of disease.

In order to assess the infiltration of immune cells after EAE induction, we also evaluated the presence of antigen presenting cells ($MHCII^+$), macrophage and monocyte ($CD68^+$), starting from the onset of disease. Likewise, to the NSCs infiltrations analysis, qualitative analysis of brain immune cells infiltrations revealed the presence of pool of immune cells mainly localised at specific brain parenchymal areas next to meningeal substructures, while no infiltration was observed at the external meninges. Specifically, we detected $MHCII^+$ cells at the onset stage in the fornix region while, during peak phase, cells were observed primarily in the midbrain at the level of pretectal nucleus. At the onset of disease, we found $CD68^+$ cells localised in the pretectal nucleus at the level of midbrain while at the peak of disease we found them at the midbrain at the level of the superior colliculus and the pretectal nucleus and in the retrosplenial area (Figure 3.11G, H). During the chronic phase, the principal points of cells infiltrations were the thalamus, the midbrain at the level of pretectal nucleus and the hippocampus.

As we observed the presence of cells with an immune-neural like phenotype both in brain and spinal cord meningeal tissue, we then assessed by immunofluorescence and confocal microscopy analysis whether double positive $DCX^+/MHCII^+$ and $DCX^+/CD68^+$ cells were also presence across brain external meninges and meningeal substructures (Figure 3.11I, J). Qualitative analyses of cell infiltrations were performed at all time point (pre-onset, onset, peak and chronic).

We detected infiltrations of DCX/MHCII double positive cells starting at the onset phase of EAE disease at the level of the fimbria. At the peak stage, along the progress of the disease, we observed more points of infiltration, particularly at the anterior pretectal nucleus. In the chronic stage of disease, we found greater points of cells infiltrations at the thalamus, in the pretectal nucleus and in the hippocampus.

We also detected that DCX/CD68 double positive cells started to infiltrate at the onset of disease throughout the meningeal substructures in the midbrain, at the level of the anterior pretectal nucleus (Figure 3.11J). In the peak phase the main point of infiltrations was found at the superior colliculus.

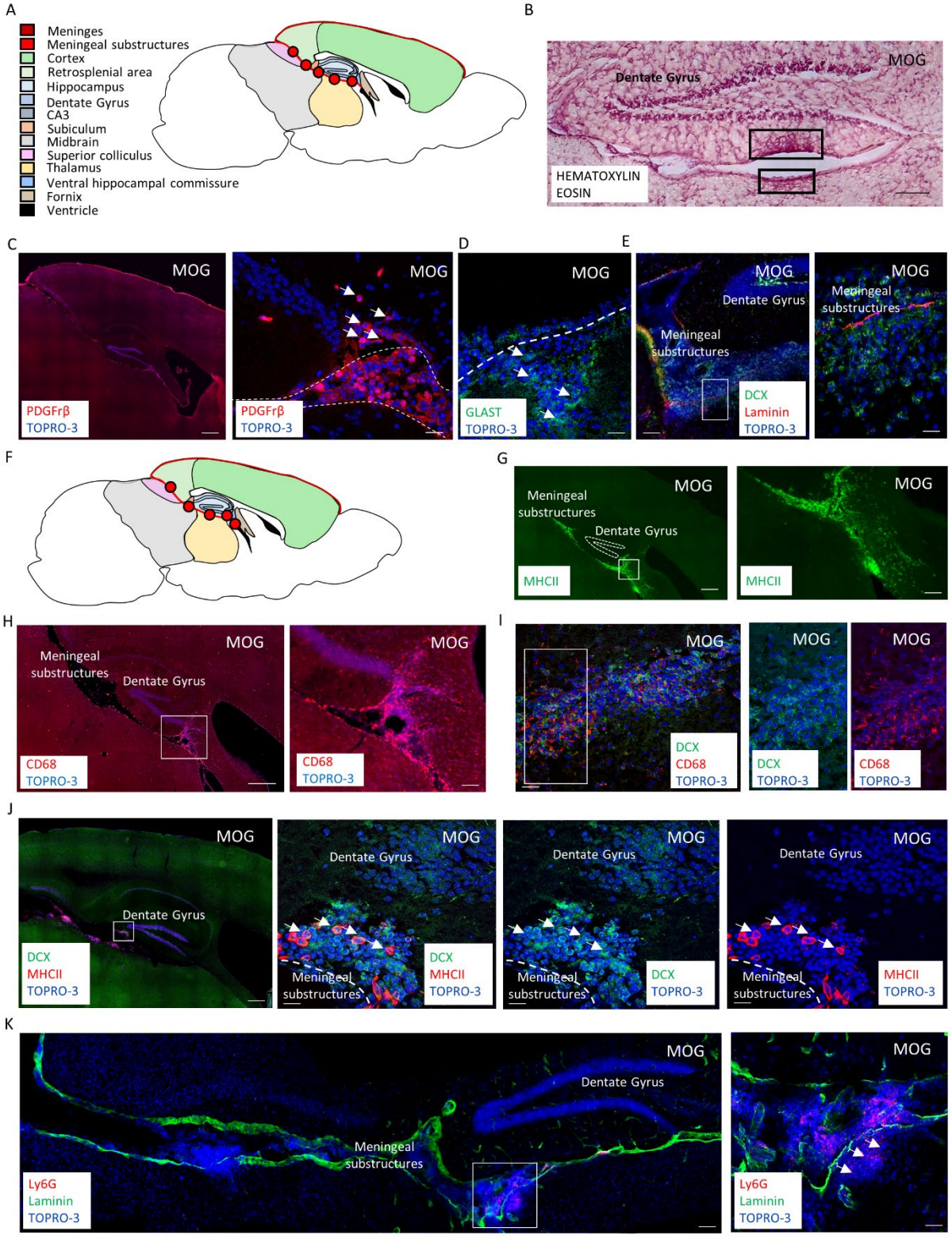

FIGURE 3.11 - NSCS AND IMMUNE CELLS IN EAE MICE INFILTRATE IN DIFFERENT POINTS ALONG THE MENINGEAL SUBSTRUCTURES

(A) Picture of sagittal mouse brain slice where the red spot highlights the preferential point of infiltrations of NPCs. (B) Sagittal section of EAE mouse brain with hematoxylin and eosin staining showing two points of cells infiltrations in hippocampal area. (C) Sagittal section of EAE mouse brain showing Infiltration of PDGFrβ^{+} cells

(left panel) and high magnification of white box showing an infiltration of PDGFrβ$^+$ cells at the level of dentate gyrus (right panel). (D) Sagittal section of EAE mouse brain showing Infiltration of GLAST$^+$. (E) Sagittal brain section of EAE mouse showing infiltration of DCX+ cells from meningeal substructures, delimitated by laminin, to Thalamus (left panel) and high magnification of the white square showing the point of infiltration in the Thalamus (right panel). (F) Sagittal brain section of EAE mouse showing infiltration of Ly6G+ cells from meningeal substructures, delimitated by laminin (left panel) and high magnification of the white square showing the point of infiltration in the Thalamus (right panel). (G) Picture of sagittal mouse brain slice where the red spot highlights the preferential point of infiltrations of immune cells. (H) Sagittal brain section of EAE mouse showing infiltration of CD68$^+$ cells from meningeal substructures (left panel) and high magnification of the white square showing the point of infiltration in the ventral hippocampal commissure (right panel). (I) Sagittal brain section of EAE mouse showing infiltration of DCX$^+$/CD68$^+$ cells from meningeal substructures (left panel) and high magnification of the white square showing the point of infiltration (right panel). (J) Sagittal brain section of EAE mouse showing infiltration of DCX$^+$/MHCII$^+$ cells from meningeal substructures (left panel) and high magnification of the white square showing the point of infiltration in dentate gyrus (right panel). (K) Sagittal brain section of EAE mouse showing infiltration of Ly6G$^+$ cells from meningeal substructures (left panel) and high magnification of the white square showing the point of infiltration in Thalamus (right panel). White dashed lines delineate meningeal substructures. PDGFrβ, Laminin, Ly6G, CD68 and MHCII in (C, E H, I, J, K) are shown in red, GLAST, laminin and DCX are in green in (D, E, G, H, I, J, K), while nuclei are in blue (TOPRO-3 nuclear staining). Scale bars represent 500μm and 20 μm.

Taken together, these results demonstrated that both neuronal precursors and immunological cells infiltrate the brain parenchyma in different sites, close to the meningeal substructures.

The principal point of cells infiltration was represented by the hippocampus. Thus, we investigated the presence of demyelinated lesion at the level of hippocampus through immunofluorescence and confocal analysis using the myelin basic protein (MBP) marker. We quantified the myelin content through ImageJ software assigning a threshold according to the positivity of the staining and we detected a decrease in myelin amount at the chronic stage of disease (Figure 3.12A, B). Furthermore, we performed analyses to characterize the hippocampal area after the onset of EAE. To this aim, we looked for GFAP, an astrocyte marker used to examine the distribution of astrocytes and the hypertrophy of astrocytes in response to neural degeneration, and Iba1, a calcium-binding protein expressed by activated microglia, shown to be increase after injury, cerebral ischemia and demyelination (Decimo et al. 2011; Nakagomi et al. 2011; Nakagomi et al. 2012). According to literature (Bhargava et al. 2021), we found an increase in percentage of GFAP$^+$ and Iba1$^+$ area in onset and peak stage of disease, the same stage on which we observed major cells infiltration (Figure 3.12C-F).

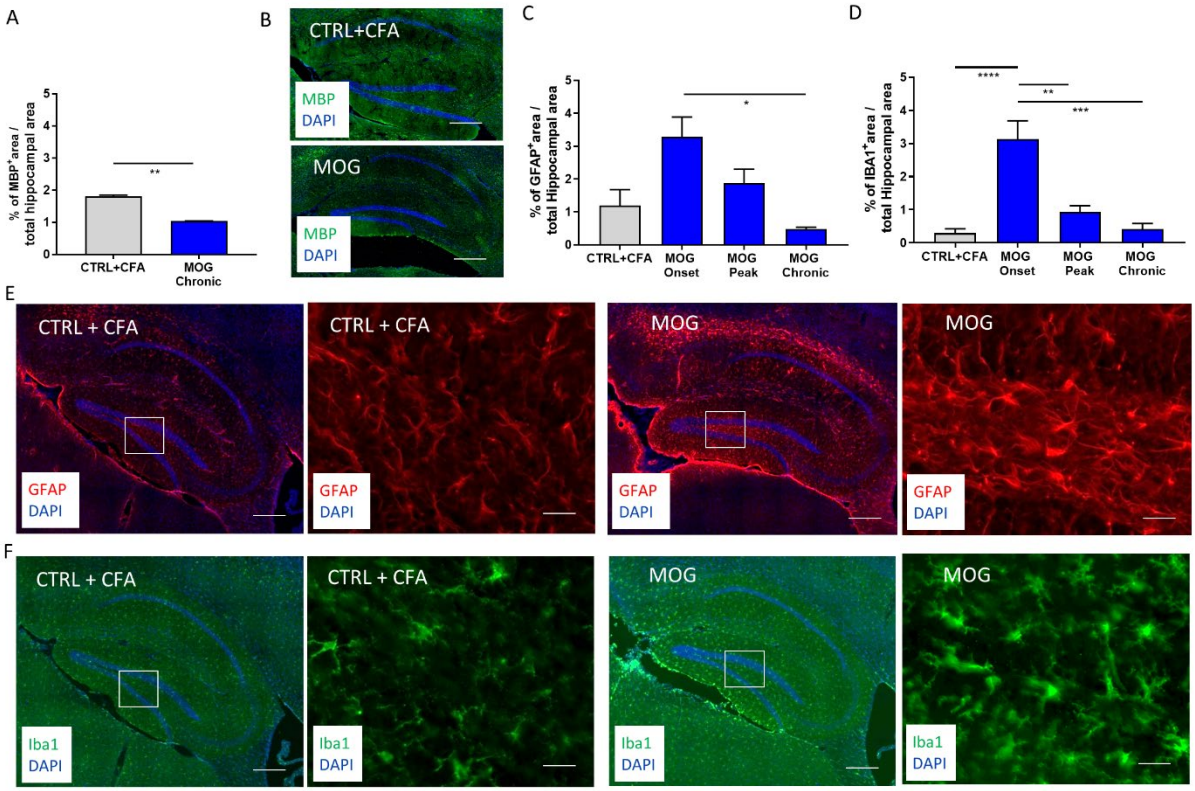

FIGURE 3.12 - MYELIN DECREASED AT THE CHRONIC STAGE FOLLOWING THE INDUCTION OF EAE IN THE HIPPOCAMPUS

(A) Graph showing the percentage of MBP positive area in control mice and in EAE mice at chronic stage. (B) Sagittal brain sections of hippocampal region in control and EAE animal respectively showing myelin stained with MBP (Myelin Basic protein). (C) Graph showing increase in percentage of GFAP+ cells in control and EAE mice. (D) Graph showing increase in percentage of Iba1+ cells in control and EAE mice. (E) Sagittal brain section of control and EAE mouse showing hippocampal area stained with GFAP marker (left panel) and high magnification of the white square (right panel). (F) Sagittal brain section of control and EAE mouse showing hippocampal area stained with Iba1 marker (left panel) and high magnification of the white square (right panel). MBP and Iba1 are shown in green, GFAP is shown in red, and nuclei are in blue (DAPI). Scale bars represent 200 µm. Data are presented as mean ± SEM; * $p \leq 0.05$, ** $p \leq 0.01$, *** $p \leq 0.001$, **** $p \leq 0.0001$.

Taken together these results show that meningeal substructures could represent a possible entry route for the brain parenchyma infiltrating cells during the development of EAE disease. Furthermore, we observed that cells infiltration starts at the onset of disease, concurrently to the strong inflammation detected with GFAP and Iba1 markers. Moreover, the remarkable involvement of the hippocampal area as access point for almost all the cell types we have analysed is further supported by the decrement in the level of myelin protein in the hippocampal area at chronic stage of disease.

Spinal cord meninges represented an entry point toward the spinal cord parenchyma

Once described the cellular phenotypes present during the development of EAE and assessed the spatio-temporal dissemination of cells infiltrations in the brain, we then performed the same qualitative analysis on the spinal cord of control (n=3) and EAE (n=3) mice by characterizing 18 caudal sections/mouse in all stage of disease.

As results, we found that cell infiltrations, defined as at least 5 cells immediately adjacent to the meninges that visibly protrude from the meningeal space, in the spinal cord parenchyma were distributed along meninges, as in the ventral as in the dorsal portion of spinal cord. Cell infiltrations begin to be detectable at the onset stage of EAE disease and persisted in the peak and chronic phases. We divided spinal cord according to the anatomical structures of transversal sections.

We found DCX^+ cell infiltrations in all EAE animals: DCX^+ cells massively infiltrated in spinal cord parenchyma in transversal sections of spinal cord, in particular at the level of lateral funiculus, dorsolateral funiculus, ventral funiculus and ventral median fissure, both at the onset and peak stages (Figure 3.13C).

We proceeded with the analyses of immune cells, and we observed that infiltration of $MHCII^+$ cells in EAE mice started at the onset of disease involving different points across all the meninges. Cell infiltrations are easily identified along the transversal section of spinal cord slice, as is shown in the Figure 3.13E. Infiltrations at the onset and peak of disease were found mainly in the ventral funiculus, dorsolateral funiculus and lateral funiculus.

We performed immunofluorescence and confocal microscopy analysis on transversal section of spinal cord slice for CD68 marker (Figure 3.13F). We detected infiltrations starting at the onset of disease till the peak and chronic stages. The infiltrations observed were allocated across the meninges that is wrapped around the spinal cord, both in the ventral and in the dorsal part. At the onset of the pathology, we observed infiltrations manly at the level of dorsolateral funiculus. At the peak of disease, more points of infiltrations were found in the ventral funiculus, at dorsal funiculus and dorsolateral funiculus.

Furthermore, we performed immunofluorescence and confocal microscopy analysis on both longitudinal and transversal spinal cord slice to characterize infiltrations of cells expressing both neuronal and immunological phenotype. We were able to detect DCX/MHCII double positive cells infiltrations at the onset, peak and chronic stage of the disease (Figure 3.13G). We observed many points of infiltrations between the different animals, such as ventral, dorsolateral and lateral funiculus of spinal cord. Infiltrations of DCX/CD68 double positive

cells were spreads across all the spinal cord meninges and were identified starting at the onset of disease, mainly in ventral funiculus, dorsolateral funiculus and lateral funiculus (Figure 3.13H).

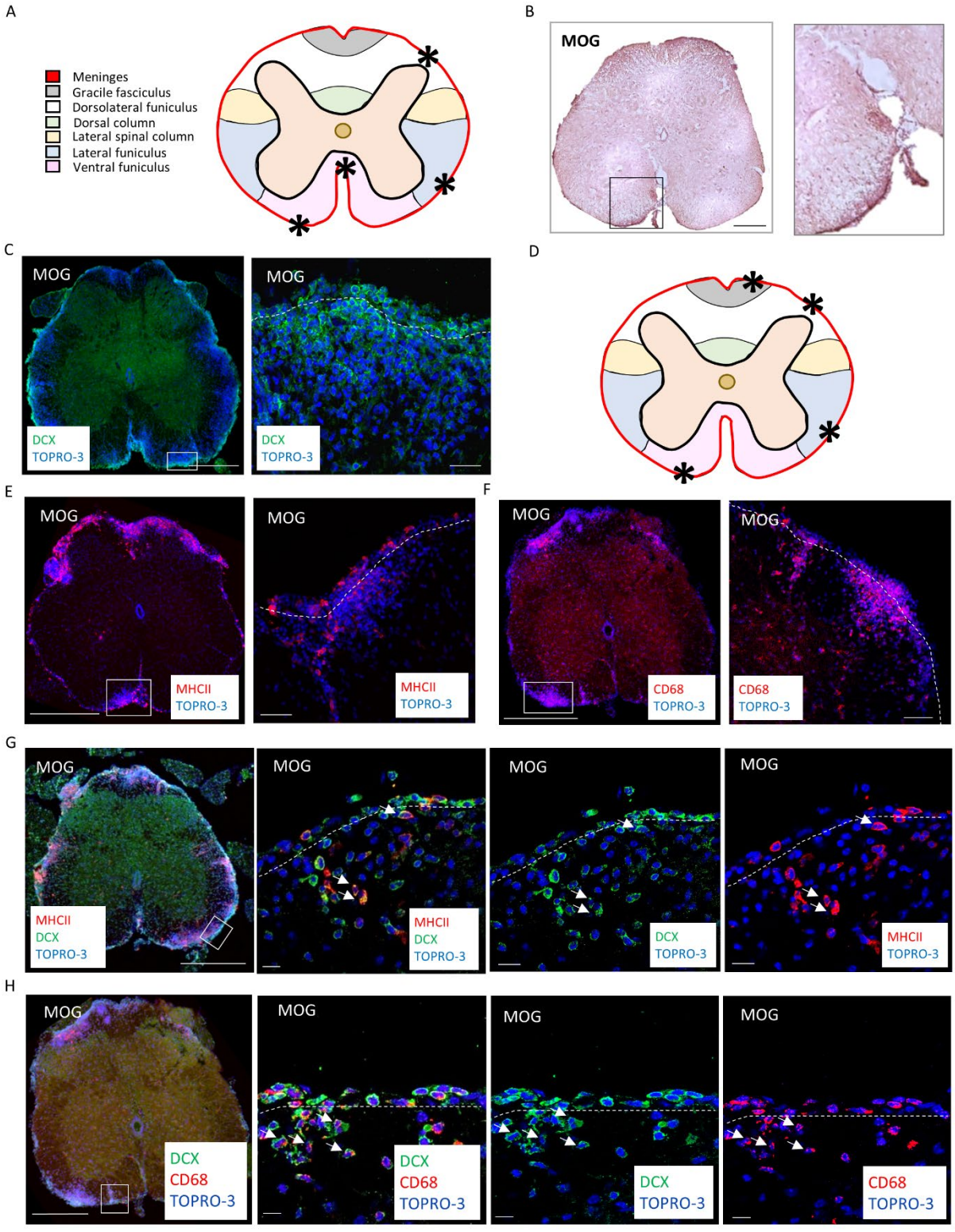

FIGURE 3.13 - NPCS AND IMMUNE CELLS FROM MENINGEAL LAYER INFILTRATE INSIDE THE SPINAL CORD PARENCHYMA

(A) Picture of transversal mouse spinal cord slice where the asterisk highlights the preferential point of infiltrations of NPCs. (B) Transversal spinal cord slice of EAE mouse spinal cord with hematoxylin and eosin staining showing points of cells infiltrations. (C) Transversal spinal cord section of EAE mouse, showing DCX^+ cells infiltration into spinal cord at onset stages (left panel) and high magnification of the white square showing the point of infiltration (right panel). (D) Picture of transversal mouse spinal cord slice where the asterisk highlights the preferential point of infiltrations of immune cells. (E) Transversal spinal cord section of EAE mouse, showing $MHCII^+$ cells infiltration into spinal cord at onset stages (left panel) and high magnification of the white square showing the point of infiltration (right panel). (F) Transversal spinal cord section of EAE mouse, showing $CD68^+$ cells infiltration into spinal cord at onset stages (left panel) and high magnification of the white square showing the point of infiltration (right panel). (G) Transversal spinal cord section of EAE mouse, showing $DCX^+/MHCII^+$ cells infiltration into spinal cord at onset stages (left panel) and high magnification of the white square showing the point of infiltration (right panel). (H) Transversal spinal cord section of EAE mouse, showing $DCX^+/CD68^+$ cells infiltration into spinal cord at onset stages (left panel) and high magnification of the white square showing the point of infiltration (right panel). DCX^+ cells are in green, $MHCII^+$ and $CD68^+$ cells are in red and, nuclei are in blue (TOPRO-3nuclear staining). Meninges are delineated with a dashed line. Scale bars represent respectively 500 µm and 20 µm.

Taken together these results show that the entire meninges of spinal cord are involved as possible entry route for the infiltrating cells in parenchyma during the development of EAE disease.

3.2.3 Meningeal cell population heterogeneity in EAE

Characterisation of meningeal cell population phenotype changes during EAE disease by single cell RNA sequencing

In order to deeply investigate the phenotype of meningeal NSCs during the progress of the EAE, we performed scRNAseq analysis on two distinct experimental group: C57BL/6J mice injected with CFA (2 groups each of n=3) and immunised MOG mice at onset and peak of disease (2 groups each of n=6) (Figure 3.14A). The grading scale of 0–5 score with the clinical severity of EAE mice is reported in Table 4.

Brain meninges and meningeal substructures from EAE and CTRL animals were collected and dissociated. After verifying the viability of the cells, single cell sequencing was performed by the Technological Platform Center of Verona University through 10X Genomics kit (see Material and Methods).

As a result of the quality control performed on the total amount of extracted cells from the brain meninges, we applied a quality control at 10% of mitochondrial DNA (mtDNA). This metric can identify whether there is a large amount of mitochondrial contamination from dead or dying cells and discard it from the analysis. We obtained, and further characterized,

116 high-quality cells for CTR1, 96 for CTR2, 897 for MOG1 and 495 for MOG2, with an average of 624 genes per cell for CTR1, 454 for CTR2, 1319 for MOG1 and 1470 for MOG2.

This part of the results was performed in collaboration with Professor Lucas Schirmer, Department of Neurology, Medical Faculty Mannheim, Heidelberg University. By using the uniform manifold approximation and projection (UMAP) clustering analysis, we found that cells clustered in five distinct cellular population groups: immune cells (comprehensive of T cells, B cells, neutrophils, macrophages, dendritic cells and NK cells), endothelial cells, pericytes, erythroid cells and stromal cells (Figure 3.14B).

Thanks to UMAP clustering analysis we were able to distinguish the populations between conditions, CTRL and EAE (Figure 3.14C) and between samples, CTRL1, CTRL2, MOG1 and MOG2 (Figure 3.14D). From these graphs, according to cell number of each sample we can appreciate the distribution and localization of cells belong to the different groups. We also were able to show through a dot plot, the scaled expression of selected signature genes for each cluster and the percentage of cells in each cluster with more than one read of the corresponding gene (Figure 3.14E). Finally, for a clearer interpretation we plotted the number of cells per cluster in EAE and control animals. This allowed us to understand if the cells for each population were present in both groups (CTRL and EAE) or not (Figure 3.14F).

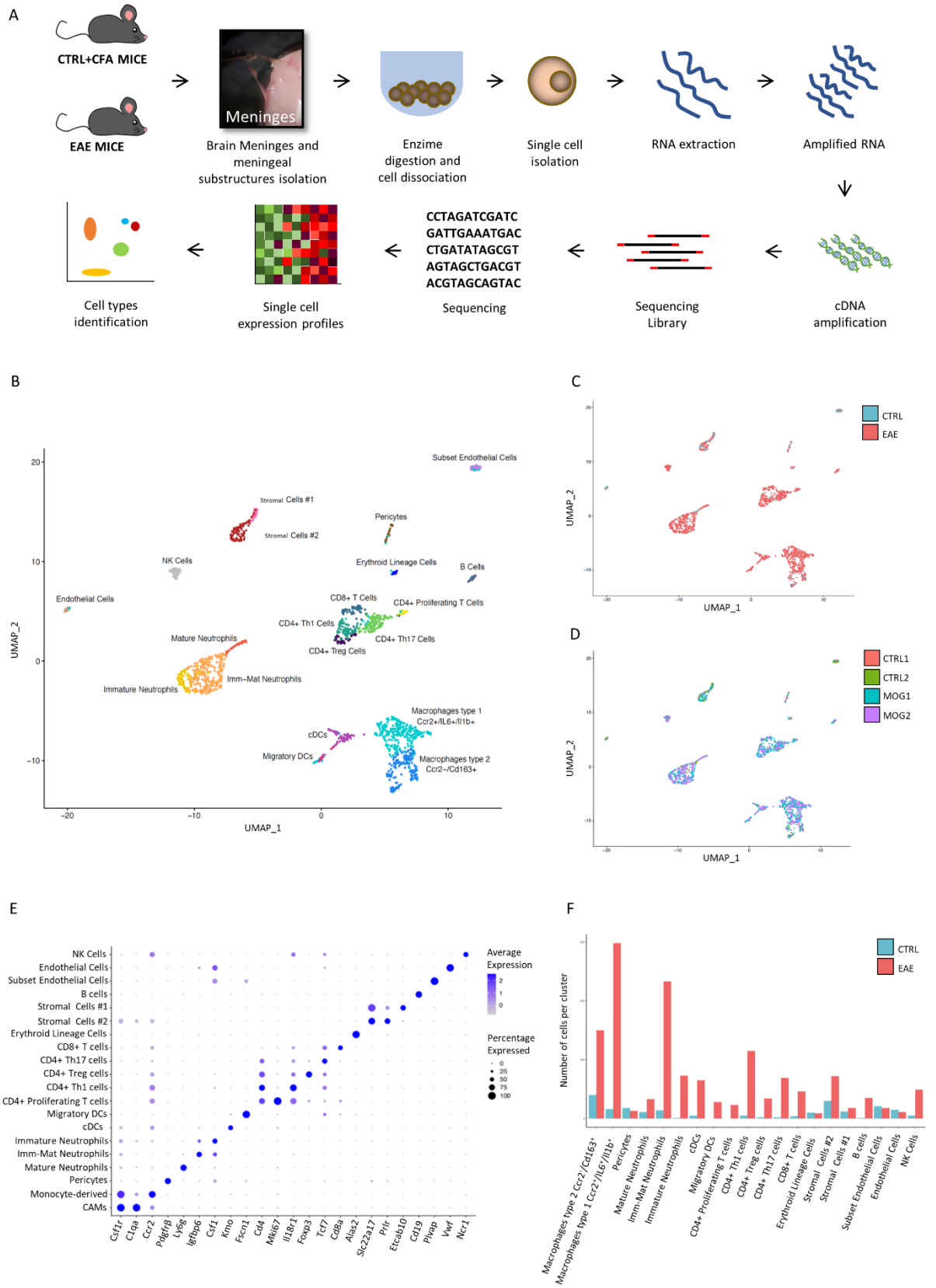

FIGURE 3.14 - SCRNASEQ ANALYSIS OF BRAIN MENINGES FROM EAE AND CONTROL ANIMALS

(A) Schematic representation of the experimental design used for scRNAseq. (B) UMAP of brain meninges from control and EAE animals coloured by cell type. (C) UMAP of brain meninges from control and EAE animals coloured by conditions: blue for CTRL and red for EAE. (D) UMAP of brain meninges from control and EAE animals coloured by samples: red for CTRL1, green for CTRL2, blue for MOG1 and violet for MOG2. (E) Dot plot showing

the scaled expression of selected signature genes for each cluster, colored by the average expression of each gene in each cluster scaled across all clusters. Dot size represents the percentage of cells in each cluster with more than one read of the corresponding gene. (F) Scheme representing the number of cells per cluster in EAE and control animals.

According to the features that characterized stromal cells in meninges (Pikor et al. 2017; Wei et al. 2021), stromal cell cluster might be the one that better represents the cells that we studied previously. Thus, we focused the attention on stromal cells cluster and, by deeply analysing this cell population, we identified seven different subclusters (from 0 to 6) (Figure 3.15). Each subcluster was characterized by the expression of specific genes, that is genes involved in regulation of oligodendrocyte differentiation, neuronal synaptic plasticity, and glycolytic process like *ENPP2*, *SLC4A10* and *ZBTB20* in subcluster 0; genes involved in different processes of cell division, translation and chromatin organization in subcluster 1;genes like *CD81*, *CD63* and *JUNB* that are involved in cell migration and T cell regulation were identified in subcluster 2; subcluster 3 was characterised by mitochondrial genes such as *MT-ND4I*, *MT-ND2* and *MT-ATP6*; genes involved in neuronal and apoptotic processes, like *RASA1*, *MED15* and *ADAM17*, were identified in subcluster 4; subcluster 5 was characterized by the expression of genes such as *AKAP11*, *PPP4R1* and *ZFYVE19*, associated to different processes like cellular protein localization, cell division and protein phosphorylation; lastly, subcluster 6 was represented by genes involved in cell cycle, cellular response to DNA damage and catabolic process.

Among those cell subpopulation group, the subcluster 0 revealed to be the most attracting ones since cells belonging to this group expressed some genes also present in neural cells. A synthetic list and brief description of the most interesting genes found in the subcluster 0 with neuronal phenotype affinity is reported below. Specifically, we identified the *ENPP2* gene, encoding for Hydrolyzes lysophospholypids that is involved in several motility-related processes, such as neurite outgrowth, and in the positive regulation of oligodendrocyte differentiation. *SLC4A10* gene, instead, played an important role in regulating intracellular pH, it contributed to the secretion of cerebrospinal fluid, it reduced the excitability of CA1 pyramidal neurons and modulated short-term synaptic plasticity. *PRLR* gene encoded for the anterior pituitary hormone prolactin receptor and *NSG2* gene is associated to the assembly of clathrin and thus involved in the formation of the neuronal vesicle. *HTR2C* gene encoded for G-protein coupled receptor for serotonin that regulates neuronal activity via the activation

of short transient receptor potential calcium channels in the brain, it plays a role in the regulation of appetite and feeding behaviour, responses to anxiogenic stimuli and stress. *ZBTB20* is a transcription factor that may be involved in haematopoiesis, oncogenesis, and immune responses. It plays a role in postnatal myogenesis, it may be involved in the regulation of satellite cells self-renewal and it is a neural commitment of stem cells. *LRP6* gene encoded for a cell-surface coreceptor of the Wnt-Fzd-LRP5-LRP6 complex that trigger beta-catenin signaling.

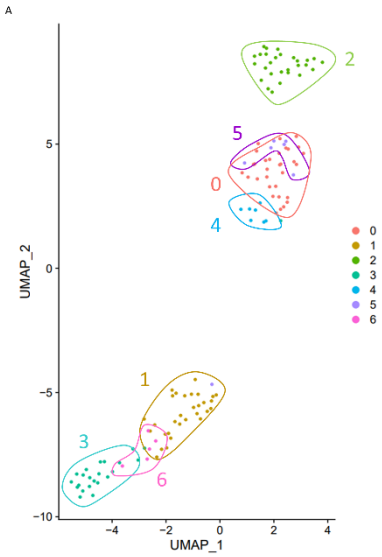

FIGURE 3.15 - UMAP OF STROMAL CELL CLUSTER FROM EAE AND CONTROL ANIMALS
(A) UMAP of stromal cell cluster from control and EAE animals coloured by inferred cluster identity.

After this in-depth analysis, with the aim to identify a relationship between stromal cell cluster and immune cell cluster, we performed a ligand-receptor analysis. Through this latter we defined a link between stromal cells and neutrophils and between neutrophils and macrophages (Figure 3.16A). We found that all stromal cells strongly expressed *SLC22A17* gene while neutrophils, and mainly the more immature neutrophils population, expressed *LCN2* gene (Figure 3.16B). *SLC22A17* gene encode for a cell surface receptor for *LCN2*, a biomarker for inflammation involved in cellular processes such as cell growth, migration/invasion, differentiation, death/survival and iron delivery (Chi et al. 2020; Nam et al. 2014). As concern the relationship between macrophages and neutrophils, we found that the more mature part of neutrophils strongly expressed *CSF1* gene while macrophages expressed *CSF1R* gene (Figure 3.16C). *CSF1* gene encoded for the Colony-stimulating factor that bind *CSF1R* on the surface of macrophages. *CSF1R* modulates proliferation, migration, differentiation, and survival of microglia and macrophages in health and disease. In

pathological condition, neutrophils produce *CSF1*, that in turn stimulates macrophages increasing the inflammation and neurodegeneration (Hagan et al. 2020).

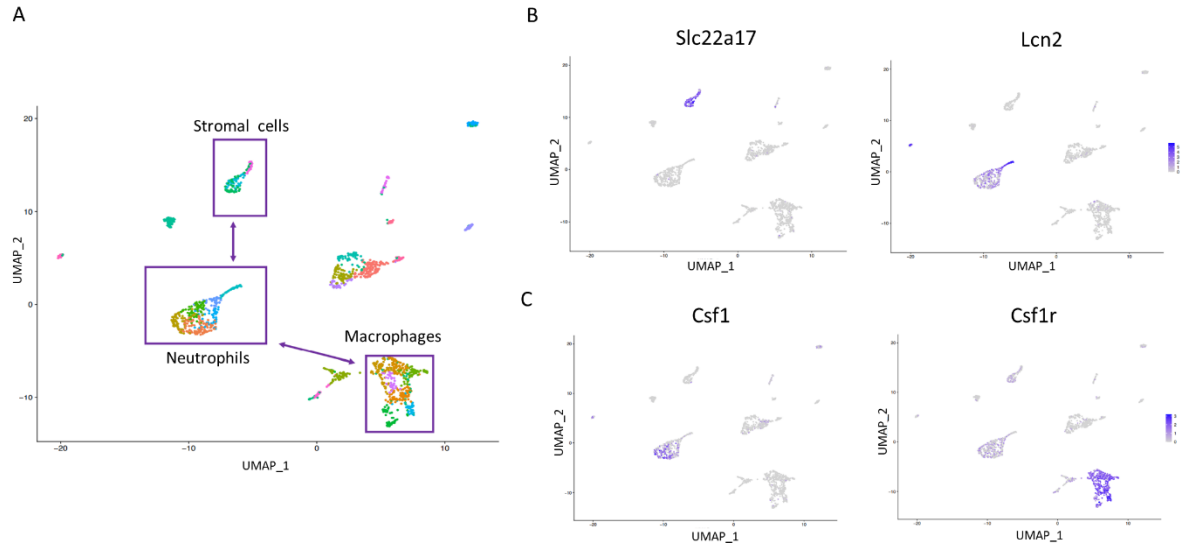

FIGURE 3.16 - LIGAND-RECEPTOR ANALYSIS OF NEUTROPHIL POPULATION

(A) UMAP of brain meninges from control and EAE animals, violet squares identify the populations involved in ligand-receptor analysis. (B) UMAP of brain meninges from control and EAE animals with the expression of *SLC22A17* and *LCN2* gene. (C) UMAP of brain meninges from control and EAE animals with the expression of *CSF1* and *CSF1R* gene.

Based on those interesting evidence, we proceeded with a supervised trajectory analysis of neutrophil populations. We used specific markers and cellular stages to recognize the different phases of neutrophil maturation from (Xie et al.): neutrophils that belonged to G0–4 stage mainly originated from bone marrow (BM), while neutrophils belonging to G5a–c mainly originated from peripheral tissue samples. According to this classification, we were able to characterize the neutrophil population from an immature to a more mature state using (Figure 3.17A).

G1 to G2 cells underwent active proliferation, with cell division stopping abruptly thereafter and we recognized them through the expression of *SMC2* and *SERPINB1A* genes (Figure3.17C). We detected a cluster of G3 cells, following G2 expansion, expressing secondary granule genes such as *CAMP* and *NGP* (Figure 3.17D). In BM, neutrophil differentiation is concluded with a more mature G4 population highly expressing *MMP8* (encoding a key granule protein for neutrophil-mediated host defences) and *RETNLG* genes (Figure3.17E). As regards G5a stage, the youngest stage of the peripheral tissue, it shared similarities with G3/G4 and it is characterized by *CCL6* and *TMCC1* gene expression

(Figure3.17F). G5b neutrophils expressed a set of interferon-stimulated genes (ISGs), such as *IFLT3* and *IFLT1* genes (Figure3.17G). Trajectory analysis showed that G5a and G5b neutrophils gradually developed into G5c neutrophils, with the latter expressing the more apoptotic genes like *BCL2A1B* and *CLEC4N* genes (Figure 3.17H).

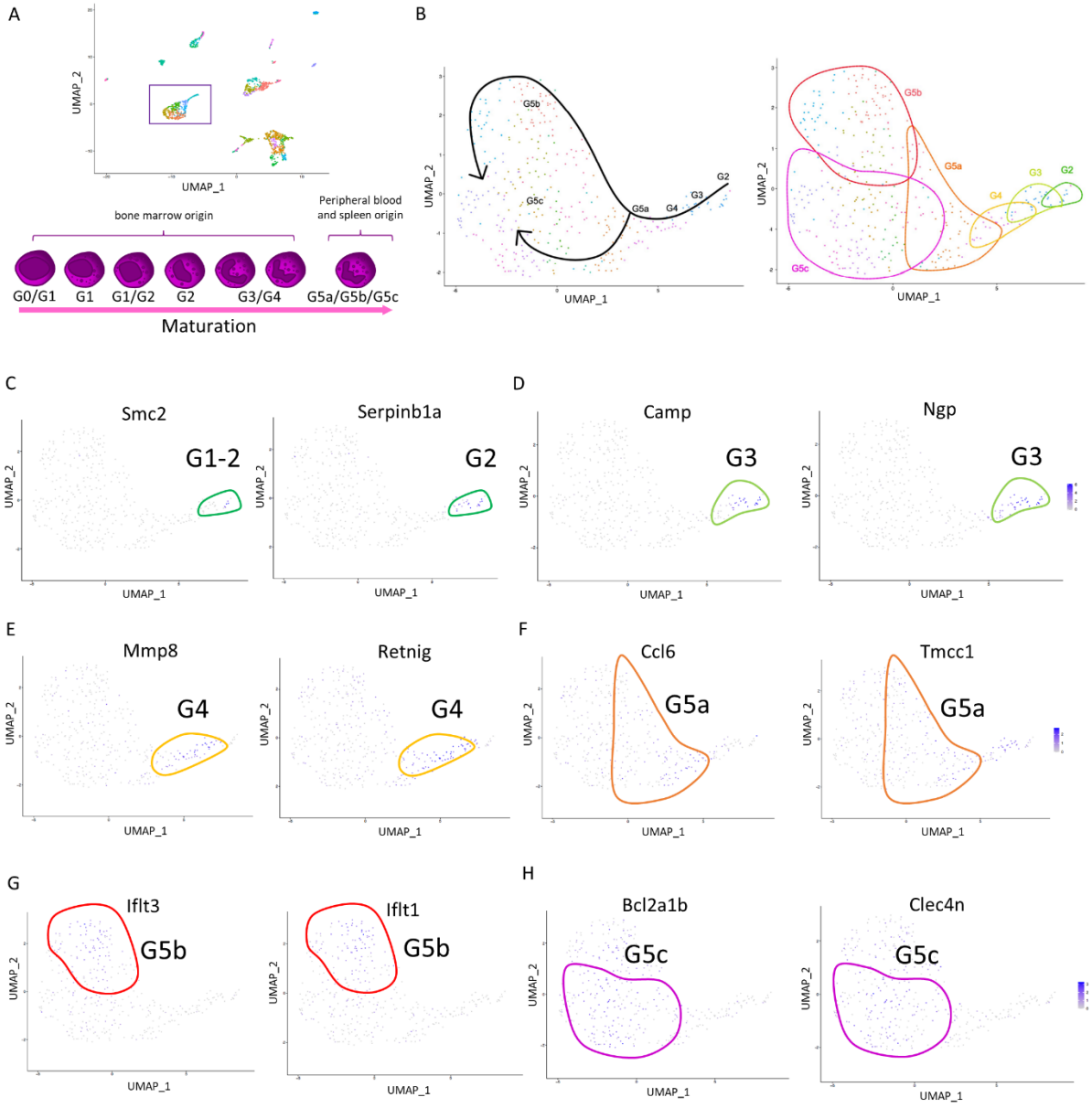

FIGURE 3.17 - TRAJECTORY ANALYSIS OF NEUTROPHIL POPULATION

(A) UMAP of brain meninges from control and EAE animals, violet square identifies neutrophil population involved in trajectory analysis and the maturation scheme of neutrophils. (B) UMAP of neutrophil population from control and EAE animals Coloured by inferred cluster identity. (C) UMAP of neutrophil population from control and EAE animals with the expression of *SMC2* and *SERPINB1A* gene that identify G2 maturation stage. (D) UMAP of neutrophil population from control and EAE animals with the expression of *CAMP* and *NGP* gene that identify G3 maturation stage. (E) UMAP of neutrophil population from control and EAE animals with the expression of *MMP8* and *RETNLG* gene that identify G4 maturation stage. (F) UMAP of neutrophil population

from control and EAE animals with the expression of *CCL6* and *TMCC1* gene that identify G5a maturation stage. (G) UMAP of neutrophil population from control and EAE animals with the expression of *IFLT3* and *IFLT1* gene that identify G5b maturation stage. (H) UMAP of neutrophil population from control and EAE animals with the expression of *BCL2A1B* and *CLEC4N* gene that identify G5c maturation stage.

Overall, these results showed highly heterogeneity of cell populations present in meninges during EAE and confirmed a crosstalk between immune cells and NSCs identified by stromal cluster. More analyses are ongoing to describe the specific pathological phenotype of meningeal NSCs.

3.2.4 Immune-regulation properties of meningeal NSCs

Assessment of in vitro meninges NPCs-immune cells interactions

In order to better investigate the relationship between immune cells (T cells, TMPs) and brain meningeal NSCs, we performed co-culture *in vitro* experiment in physiological and pathological conditions.

We hypothesised that meningeal NSCs interaction with Naïve T cells could drive the immune-cell activation. To assess this idea, we tested *in vitro* PDGFrβ cells, stained with CMAC dye, interaction with two different types of immune cells: Naïve T cells from control C57Bl/6J WT mice (CTRL) and resting TMPs from EAE mice. Firstly, we performed different NPCs:Naïve T cells ratio (1:1, 1:10, 1:100) with increasing number of T Naïve cells from CTRL seeded (Figure 3.18A-D). After 48h in co-culture condition, results of FACS analysis showed an increase of CD25, activation marker for T cells, percentage in $CD4^+$ and $CD8^+$ (markers for T helper and cytotoxic T cells) cells in 1:1 ratio suggesting an activation of Naïve T cells (Figure 3.18C).

With the aim to understand the immune-activation effect of $PDGFr\beta^+$ cells on resting T cells from EAE mice, we performed NSCs-resting TMPs co-culture experiment. Experiments was performed using various concentration ratios PDGFrβ:resting TMPs (1:10, 1:100) (Figure 3.18E-G). FACS analysis showed an increase in percentage of CD25 and CD69 (early marker for T cells) marker in $CD4^+$ and $CD8^+$ cells (Figure 3.18G). We also observed a decrease of CD62L marker for L-selectin, a cell adhesion molecule, in $CD8^+$ cells (Figure 3.18F) according with the activation of these cells in the co-culture (Klinger et al. 2009). These results may suggest an activation of resting T cells by $PDGFr\beta^+$ cells.

Taken together these data showed an increased expression of markers associated with activated T cells suggesting the ability of $PDGFr\beta^+$ cells to interact and activate both Naïve T cells in physiological and resting T cells in pathological conditions.

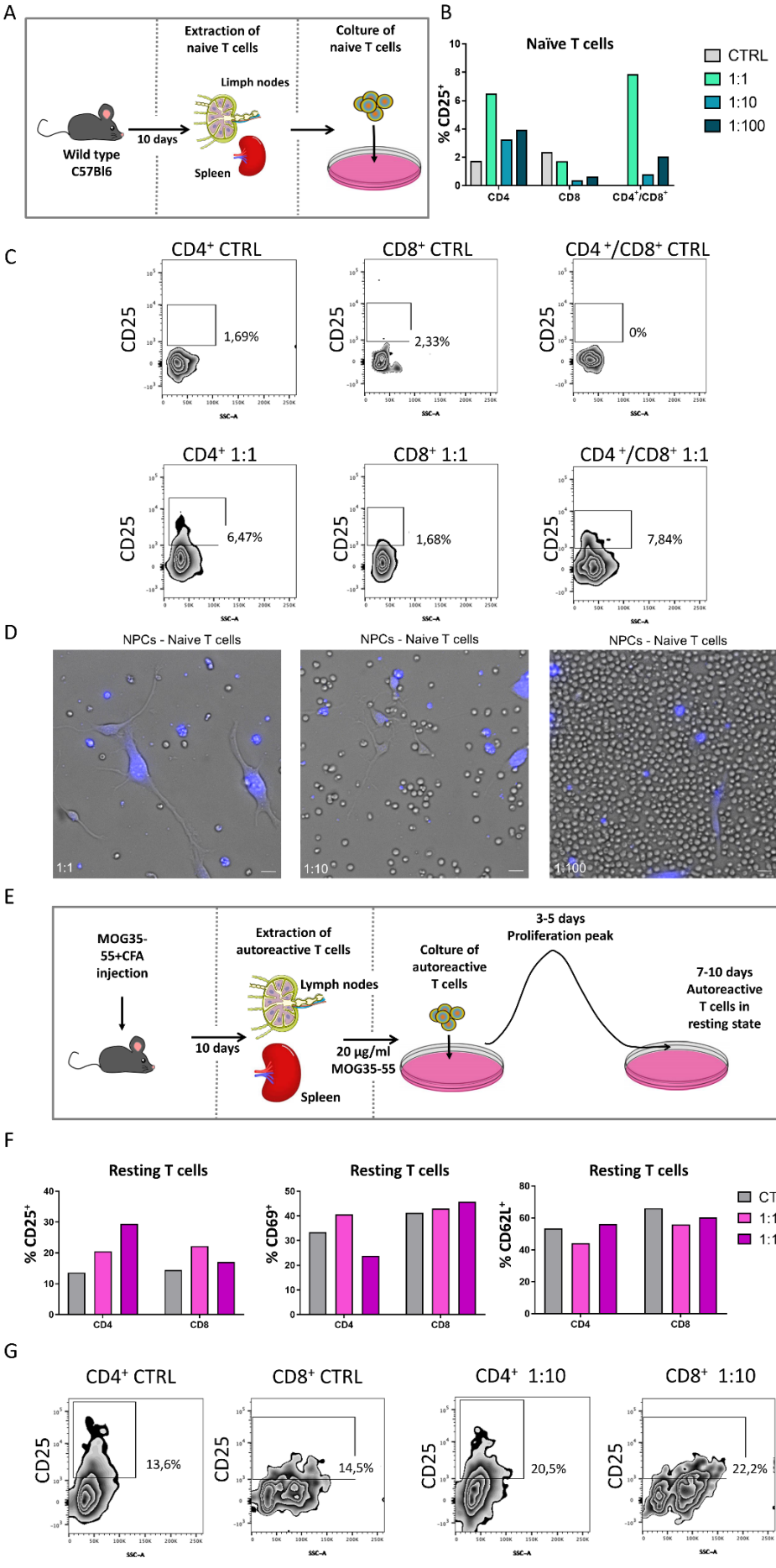
A
Extraction of naive T cells
Colture of naive T cells
Limph nodes
10 days
Wild type C57Bl6
Spleen
B
Naïve T cells
% CD25+
CD4
CD8
CD4+/CD8+
CTRL
1:1
1:10
1:100
C
CD4+ CTRL
CD8+ CTRL
CD4 +/CD8+ CTRL
CD25
1,69%
2,33%
0%
CD4+ 1:1
CD8+ 1:1
CD4 +/CD8+ 1:1
6,47%
1,68%
7,84%
SSC-A
D
NPCs - Naive T cells
1:1
1:10
1:100
E
MOG35-55+CFA injection
10 days
Extraction of autoreactive T cells
Lymph nodes
Spleen
20 µg/ml MOG35-55
Colture of autoreactive T cells
3-5 days Proliferation peak
7-10 days Autoreactive T cells in resting state
F
Resting T cells
% CD25+
% CD69+
% CD62L+
CD4
CD8
CTRL
1:10
1:100
G
CD4+ CTRL
CD8+ CTRL
CD4+ 1:10
CD8+ 1:10
13,6%
14,5%
20,5%
22,2%

FIGURE 3.18 - CO-COLTURE REVEAL AN INTERACTION BETWEEN T CELLS AND NSCS

(A) Schematic representation of the experimental design used to obtain naive T cells. (B) Graph of $CD4^+$ and $CD8^+$ naïve T cells expressing CD25 in different ratios 1:1, 1:10, 1:100. (C) FACS analysis of co-culture Naïve T cells and $PDGFr\beta^+$ cells in DMEM medium incubated with CD4, CD8, CD25 and measured using APC (CD4), PE/Cy7 (CD8), PE (CD25). Control of Naïve T cells population distribution expressing $CD25^+$: $CD4^+$ cells, $CD8^+$ cells and $CD4^+/CD8^+$ cells (Top panels). Co-culture distributions of $PDGFr\beta^+$:Naïve T cells ratios: $PDGFr\beta^+$:$CD4^+$ naïve T cells 1:1, $PDGFr\beta^+$:$CD8^+$ naïve T cells 1:1 and $PDGFr\beta^+$:$CD4^+/CD8^+$ naïve T cells 1:1, respectively (Bottom panels). (D) Increasing concentration of Naive T cells and fixed concentration of PDGFrβ cells: 1:1 ratio (50.000 NSCs:50.000 Naive T cells), 1:10 ratio (50.000 NSCs: 500.000 Naive T cells), 1:100 ratio (50.000 NSCs:5.000.000 Naive T cells) respectively. (E) Schematic representation of the experimental design used to obtain resting T cells. (F) Graphs of $CD4^+$ and $CD8^+$ resting T cells expressing CD25, CD69, CD62L, respectively, in different $PDGFr\beta^+$:resting T cells ratios 1:10, 1:100. (G) FACS analysis of co-culture resting T cells and $PDGFr\beta^+$ cells in DMEM medium incubated with CD4, CD8, CD25, CD62L and measured using APC (CD4), PE/Cy7 (CD8), FITC (CD69), PE (CD62L). Control of CD4+ resting T cells expressing CD25 (First panel). Control of $CD8^+$ resting T cells expressing CD25 (Second panel). Co-culture population distributions in 1:10 $PDGFr\beta^+$:resting T cells ratios: $PDGFr\beta^+$:$CD4^+$ resting T cells 1:10 expressing CD25 (Third panel), $PDGFr\beta^+$:$CD8^+$ resting T cells 1:10 expressing CD25 (Fourth panel). All conditions were cultured in DMEM. Blue cells are NSCs stained with CMAC dye (D). Scale bars represent 20µm

Characterisation of meningeal neural cell population phenotype changes during EAE disease progression by Fluorescent Activated-Cell Sorting

Based on these data, we proceeded to investigate how NSCs are modified in EAE pathogenesis.

With this aim, we confirm the modifications of meningeal cell phenotype, through FACS analysis, of cells isolated from control (n=5) and EAE (n=6) mouse brain between the onset and peak stages of disease. We stained the meningeal cells by different specific markers: PDGFrβ for neural stem cells and MHCII for antigen presenting cells.

Interestingly, comparing FACS results from MOG and control mice, we identified an increase of PDGFrβ (3,1% of positive cells in MOG sample over 600.000 events analysed in comparison with the 1,4% in the control sample) and MHCII (1,6% of positive cells in MOG sample over 600.000 events analysed in comparison with the 0,9% in the control sample) cells (Figure 3.19).

These results showed the increase of meningeal neuronal and MHCII cell population during disease development, further supporting the data obtained *in vivo*.

Furthermore, the data obtained from FACS analysis, showed marked increase of double positive cells in EAE animals, with 2,2% of $MHCII^+/PDGFr\beta^+$ positive cells over 600.000 events compared to the 0,3 % in control animals. Suggesting that meningeal NSCs may become antigen presenting cells during EAE (Figure 3.19).

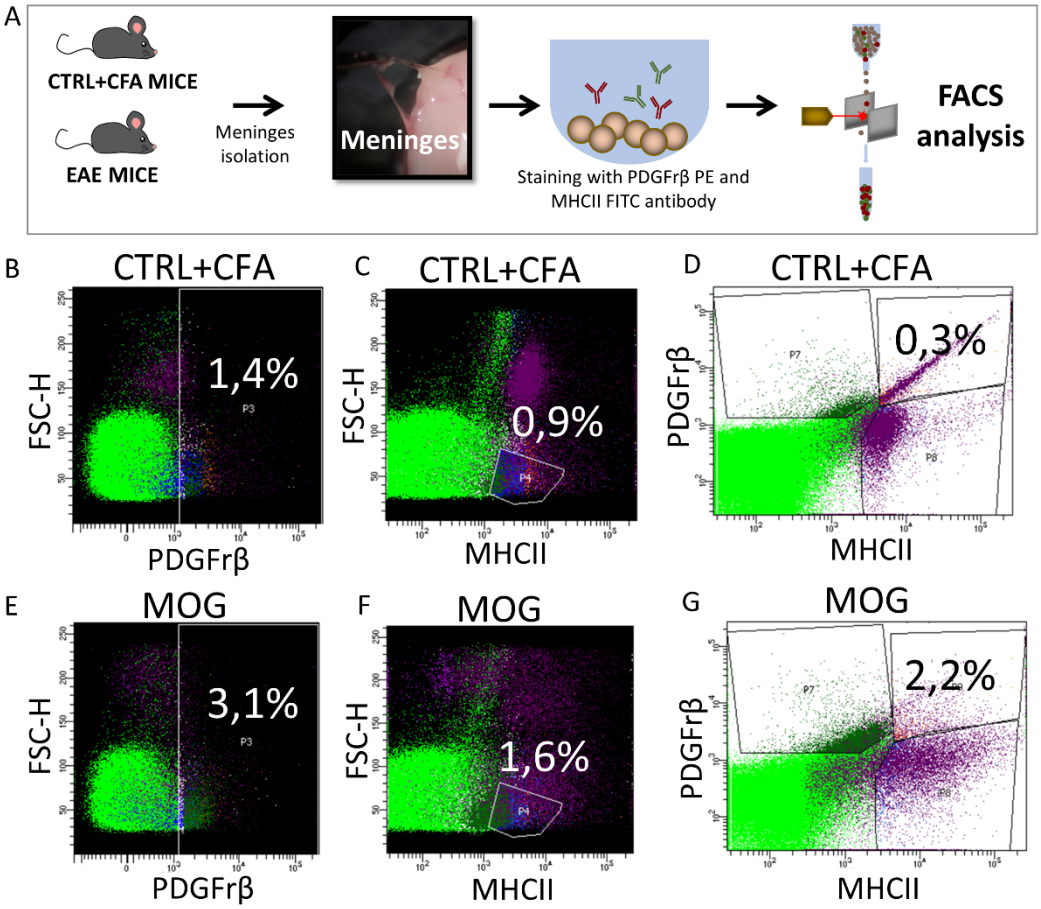

FIGURE 3.19 – NSCS INCREASED IN NUMBER IN EAE PATHOGENESYS

(A) Schematic representation of the experimental design used for FACS analysis. (B, E) FACS analysis results showing increase in the percentage of PDGFrβ$^+$ and (C, F) MHCII$^+$ cells in EAE animals (MOG) respects to the controls (CTRL). (D, G) FACS analysis results showing increase in the percentage of PDGFrβ$^+$/MHCII$^+$ cells in EAE animals (MOG) respects to the controls (CTRL).

CHAPTER 4 – DISCUSSION

4.1 Meningeal niche respond to EE stimulus

The primary finding of this thesis project is that meningeal tissue, and in particular the resident neural stem cells, response to neurogenic stimuli like EE.

It is known in literature that pro neurogenic paradigms such as EE and anti-depressant treatments affect hippocampal neurogenesis. However, the effect on meninges, a novel less-known NSC niche, is still unexplored (David et al. 2009; Eisinger and Zhao 2018; Kempermann 2019). Based on this evidence, here we investigated, for the first time, the role of meninges in a physiological context of EE. As widely reported in literature (Kempermann et al. 1997), we first confirmed the efficacy of pro-neurogenic stimuli on hippocampal neurogenesis through immunofluorescence and confocal analysis. As result, we stated an increased number of immature DCX^+ neurons after EE treatment. We subsequently studied how the meningeal niche reacts to the same neurogenic stimulus.

In literature it has already been shown that the meningeal niche is able to react and respond to different types of stimuli both in physiological and pathological conditions. Administration of FGF-2 and NGF in meninges induced hyperplastic changes within the meninges of the rat and monkey (Day-Lollini et al. 1997; Parr et al. 2007). Injuries, including spinal cord injury (SCI) (Decimo et al. 2011), progressive ataxia (Kumar et al. 2014) and brain stroke (Nakagomi et al. 2012) were able to increase the number of meningeal-derived doublecortin (DCX) positive immature neurons.

Strikingly, after exposure to EE, we found an increase in $GLAST^+$ stem cells and immature $\beta3\text{-Tubulin}^+$ neurons in meninges. These data suggested that meninges are able to react to the EE stimulus increasing the neural part of the niche. However, the meningeal response to EE partially differs from the hippocampal one (David et al. 2009; Kempermann 2019; Ming and Song 2011; Sohur et al. 2006; Wang et al. 2008), as no apparent increase in cellular proliferation was observed.

As previously described in the cerebral cortex, in addition to the effects on immature neurons and NSCs, pro-neurogenic stimuli are also capable of significantly remodelling the extracellular matrix (Slaker et al. 2016). In line with this, we observed in animals subjected to EE an increase of fractones (Mercier 2016), specialized ECM components of the neurogenic

niche able to retain trophic factors (Kerever et al. 2007), suggesting an overall remodelling of the meningeal niche.

4.2 Meningeal cells responsive to EE belong to the GLAST population

In order to investigate whether immature neurons reacting to EE were derived from neuronal progenitors relying in the meninges or other brain regions, we took advantage of an inducible transgenic mouse model for radial-glia (RG) cells tracing (Mori et al. 2006; Nakamura et al. 2006). Through immunofluorescence and confocal analysis, we observed GFP^+ radial glia derived neural precursors cells co-expressing TrkB and β3-Tubulin increased after EE exposure, even though no change in cell number of meningeal retrosplenial cortex was observed. With these results, we showed, for the first time, the presence of neurons with RG origin in the adult mouse brain, so far only demonstrated in the healthy newborn mouse (Bifari et al. 2017). In this context, the increase in the number of immature neurons observed in the meninges after EE stimulation may be due to: i) differentiation of endogenous RG cells already present in the meninges, ii) other populations of meningeal neural progenitors not investigated in this study (including $Nestin^+$ and $PDGFr\beta^+$ cells (Bifari et al. 2017)) or iii) neural precursors that migrate from other neurogenic niches in the brain to the meninges.

4.3 TrkB/BDNF signaling modulate meningeal niche response to EE

The mechanism underlying the effects of pro-neurogenic stimuli is still not fully understood. The pivotal role played by BDNF, a member of the neurotrophin family that plays a fundamental role in neuronal development and plasticity (Bjorkholm and Monteggia 2016), has been demonstrated (Casarotto et al. 2021; David et al. 2009; Eisinger and Zhao 2018). Trying to investigate the mechanism that guide the EE effects on meningeal niche, we examined the role of BDNF using ANA-12, a small molecule that acts as a non-competitive inhibitor of TrkB (Cazorla et al. 2011). Through immunofluorescence, western blot and RT-PCR, we were able to observe that the effects on the high expression of $\beta3\text{-Tubulin}^+$ immature neurons and TrkB induced by EE were partially reduced by the administration of ANA-12. Furthermore, the number of $CD68^+$ macrophages was not altered by the TrkB inhibitor, while a statistical reduction in the number of meningeal fractones was observed suggesting that the activity of macrophages to generate ECM is affected by this mechanism (Kerever et al. 2007).

4.4 Fluoxetine administration induces meningeal niche response

With the aim to explore if the meningeal niche was able to respond to other stimuli than EE, we evaluated the effect of fluoxetine, an antidepressant that acts as a neurogenic stimulus on DG (David et al. 2009; Wang et al. 2008). After confirming the response of the hippocampal niche to the stimulus, we focused on meningeal niche. Similarly to EE exposure observations, as a reaction to fluoxetine administration, we found an increase of GLAST$^+$ neural precursors and β3-Tubulin$^+$ immature neurons, along with no proliferation in meninges. Alike to EE exposure, also fluoxetine treatment led to a significantly higher number of fractones in meninges of treated mice, together with a slight increase in CD68$^+$ macrophages. These data confirm a reaction of meningeal niche to a different pro-neurogenic stimulus, but we didn't explore the molecular mechanism behind this response. Previous studies have shown the role of TrkB in anxiety (Bergami et al. 2008) and fluoxetine treatment (Casarotto et al. 2021). However, further studies will be necessary to elucidate the molecular mechanisms driving the meningeal response to pharmacological neurogenic stimuli including antidepressant treatment.

4.5 Immune cells of meningeal niche respond to EAE

In order to provide a comprehensive characterization of the meningeal niche responsiveness in different scenarios, we then explored whether meninges could react also in pathological conditions (Decimo et al. 2011; Nakagomi et al. 2011; Nakagomi et al. 2012) as reported for other classical NSCs niches like SVZ niche during different type of disease such as ischemia (Kojima et al. 2010) and Multiple Sclerosis (Nait-Oumesmar et al. 2007).

As second purpose, we therefore explored the meningeal niche response to neurodegenerative disease such as Multiple Sclerosis (MS). The more used animal model for MS is the Experimental Autoimmune Encephalomyelitis (EAE) that supports the autoimmunity hypothesis of disease development (Procaccini et al. 2015) and it is characterized by demyelination, axonal loss and gliosis. As already reported in literature, the EAE model is characterized also by the presence of immunity cells that actively participate in the development of the disease (Caravagna et al. 2018; Christy et al. 2013; Russi et al. 2018). By means of immunofluorescence and confocal analysis, we characterized the immune cells present in the leptomeninges of EAE mouse brain. Among cell populations, we found, at the peak stage of the disease, the presence of T cells (CD3$^+$ cells) in meninges of both control and

EAE mice, confirming the role of meninges in the CNS immune surveillance (Louveau et al. 2018). On the other hand, we observed that these cells, together with meningeal macrophages ($CD163^+$ cells) (Kim et al. 2006) significantly migrated toward EAE meningeal substructures at peak stage, compared to control animals. Cells of the adaptive and innate immune systems in the brain parenchyma and in the meningeal spaces contribute to physiologic functions but when the equilibrium is broken, they contribute in CNS to the disease course and to neurodegenerative and neurobehavioral disorders (Healy et al. 2020). In EAE animals the immunological homeostasis is lost and the T cells accumulation and their aberrant activation lead to the neurodegenerative disease (Grigoriadis and van Pesch 2015), instead, in control animals, no alterations of meningeal niche were detected.

Neutrophils ($Ly6G^+$ cells) have been described as one of the major sources of pro-inflammatory cells that are responsible of EAE initiation, axonal demyelination and axonal degeneration in the first acute stage of EAE development (De Bondt et al. 2020; Wu et al. 2010). According to this, we observed $Ly6G^+$ cells accumulated in meninges before the onset of clinical sign of EAE (De Bondt et al. 2020), while their presence in meningeal substructures started few days later and coincided with the peak of disease. These immune populations and their relative increase in the meninges, demonstrate the presence of inflammation and the development of pathology in the mouse model.

4.6 Meningeal NSC niche respond to EAE

Currently, NSCs studies mainly focus on neurodegenerative field due to the biological proprieties of undifferentiated and proliferating cells (2019). Beside the well-known protective function as a physical barrier and neural precursors reservoir for the formation of new neurons, meninges are also involved in the reaction to injuries and insults (Decimo et al. 2011; Decimo et al. 2020; Nakagomi et al. 2011; Nakagomi et al. 2012). In fact, they are becoming more relevant in MS field.

In order to identify the modifications of the leptomeningeal niche and of the meningeal NSCs-T cell interactions in EAE pathological conditions, we performed immunofluorescence and confocal analysis on control and EAE animals. First, in EAE brain meninges from pre-onset stage and in meningeal substructures from onset stage of disease, we detected an increase of cell proliferation through ki67 marker. We also observe an increase in cell nuclei number in spinal cord meninges of EAE animals in comparison with controls during onset stage of

disease. These results, according to literature, demonstrated a reaction of meningeal niche to the inflammatory environment of EAE (Decimo et al. 2012a; van Olst et al. 2021). Among neural precursor populations, we investigated PDGFrβ$^+$ and GLAST$^+$ stem cells, and DCX$^+$ immature neurons in both brain meninges and meningeal substructures. We noted, in meninges and meningeal substructures, an early increase of PDGFrβ$^+$ cells at the pre-onset stage of EAE mice, which is maintained until peak stages with a slightly decrease at chronic stage. This evidence highlights that PDGFrβ$^+$ cells may have a role in the initiation and progression of EAE development. On the other hand, no differences were found in the number of Glast$^+$ cells between EAE and control mice. Interestingly, we found a significant increase of DCX$^+$ cells at pre-onset stage in meninges and at onset stages in meningeal substructures and spinal cord meninges, suggesting an initial role of these cells in meninges and a later accumulation of immature neurons in meningeal substructures and spinal cord meninges.

A striking observation was the detection of DCX$^+$ cells able to express MHCII marker in brain and spinal cord meninges, suggesting their potential ability to interact and subsequently re-activate myelin-specific auto-reactive T cells. DCX$^+$/MHCII$^+$ cells slightly increased with a high statistical significance at onset of disease in meninges and meningeal substructures. Additionally, we also detected the presence of DCX$^+$/CD68$^+$ cells, further supporting the potential role of DCX$^+$ cells as antigen-presenting cells (APCs). As previously discussed, professional APCs have a key role for the MS/EAE pathology due to their ability to re-activate T cells causing the infiltration of auto-reactive T cells within CNS parenchyma (Constantinescu et al. 2011; Jordão et al. 2019).

In literature it has already been reported the presence of DCX$^+$ cells expressing immunological markers (Unger et al. 2018). The presence of this non-canonical DCX$^+$ cells expressing the phagocytic marker CD68 has been found near amyloid plaques in the brain of an Alzheimer Disease mouse model. In this context, it is strongly suggested that DCX cells have phagocytic activity and that they contribute to amyloid plaque clearance (Unger et al. 2018). However, the exact origin of these DCX$^+$/CD68$^+$ cells need to be deeply understood and further analyses are still required. Despite this, Mauffrey and colleagues showed the extraordinary ability of DCX$^+$ cells to migrate from SVZ and infiltrate in sites that are colonized by cancer cells. At this level, DCX cells initiate neurogenesis during tumour formations, helping the tumour growth

(Mauffrey et al. 2019). This study revealed a unique crosstalk between the CNS and tumours and indicate neural targets for the treatment of cancer.

4.7 Meningeal substructures and spinal cord meninges as route of infiltrations into CNS parenchyma

MS studies, in mouse animal model, have shown conspicuous multifocal perivascular infiltrates, mainly including lymphocytes, monocytes and macrophages (Jordão et al. 2019; Wu et al. 2010) that provoke a massive destructive inflammation (Miljkovic and Spasojevic 2013; Pol et al. 2019). Recently, it has been proposed T cell trafficking within leptomeninges, during EAE (Schläger et al. 2016). Thus, leptomeninges may have a key role as checkpoint at which activated T cells are licensed to infiltrate into CNS parenchyma and non-activated T cells are preferentially released into the CSF, reaching areas of antigen availability (Schläger et al. 2016; Yasuda et al. 2019).

Interestingly, by investigating the external brain meninges, meningeal substructures and spinal cord meninges of EAE animal model, we observed that those sites actually act as point of cells accumulation during EAE development. In leptomeninges extravascular brain-reactive T cells have been found to express different factors such as proinflammatory cytokines, tumour necrosis factor, proteases, chemokines and adhesion molecules, included LFA-1 and VLA-4. These latter required for the attachment and migration of effector T-cell trough the leptomeninges into the CNS Parenchyma (Grigoriadis and van Pesch 2015; Schläger et al. 2016). Furthermore, meninges represent an important site of accumulation for many activated lymphocytes, as well as dendritic cells, neutrophils, mast cells, B cells and plasma cells.

In this contest, we analysed the presence of NSCs and immune cells infiltrations, at each time point of disease development, at the level of brain meninges, meningeal substructures and spinal cord meninges.

We observed that in brain, NSCs (PDGFrβ$^+$, GLAST$^+$, PDGFrβ$^+$/GLAST$^+$ and DCX$^+$), immune cells (CD68$^+$ and MHCII$^+$) and also immune like-NSCs (DCX$^+$/CD68$^+$ and DCX$^+$/MHCII$^+$) infiltrate only along the meningeal substructures, which projected inside brain parenchyma underneath the hippocampus, but not through external brain meninges. Along the meningeal projections, we identified specific points of cells infiltrations, including the retrosplenial area, the superior colliculus, the midbrain and the subiculum. Noteworthy, all these brain regions are involved in a wide range of cognitive functions, able to receive visual signals and also to help with the

orientation of the eyes and head (Savage et al. 2017), which are all compromised in MS. Further, we found cells infiltrating from meninges to hippocampus inside dentate gyrus, CA3, ventral hippocampal commissure, thalamus, and the fornix which are all key brain areas involved in cognitive and memory functions as well.

By means of behavioural test, several studies in literature correlate the demyelination observed in the areas of hippocampus, dentate Gyrus and CA3 with the cognitive decline in EAE mice (Aharoni et al. 2019). According to these findings, we detected a reduction of myelin content in hippocampal area together with microglia and astrocyte reaction to EAE.

Overall, our results are in line with the already described cells infiltration in EAE mice brain at the level of cerebellum, cerebral cortex and subcortical regions (thalamus and striatum) (Waiczies et al. 2012). However, it is the first time that such a specific characterisation is performed on brain areas along meningeal substructures presenting cells infiltrations.

Contrarily, at the level of spinal cord, we observed that cells infiltrations were diffused along all meninges both in ventral and in the dorsal sections without showing a preferential point of cells infiltration. This result is in accordance with other studies in which infiltrations are shown to be not spatially restricted but more dispersed in the spinal cord tissue (Shrestha et al. 2017).

4.8 Meningeal cell population heterogeneity in EAE

In this work, for the first time, we performed a scRNAseq on meningeal tissue without sorting cells for a specific marker. Thus meningeal tissue was collected and analysed for a more informative and complete result that described all the features of meningeal cells in EAE animals in comparison with controls. We performed scRNAseq in order to describe deeply meningeal NSCs in EAE conditions and to better investigate neural-immune phenotype of meningeal cells that was detected in previous analysis. From scRNAseq analysis emerged different cluster of cellular population: immune cells (comprehensive of T cells, B cells, neutrophils, macrophages, dendritic cells and NK cells), endothelial cells, pericytes, erythroid cells and stromal cells. Among them, we mainly focused the attention on the stromal cell cluster. Indeed, from a deep analysis of the entire cluster, we identified a subpopulation of the stromal cells (the group 0) that was characterized by the expression of genes like *ENPP2, SLC4A10, PRLR, NSG2, HTR2C* and *ZBTB20*, all involved in the regulation of neuronal activity

and differentiation process. This genes signature suggests that the neural cells of interest may be included in the stromal cell cluster.

Strictly, through a ligand-receptor analysis, we were able to determinate a link between stromal cells and neutrophils and between neutrophils and macrophages. We found that all stromal cells strongly expressed *SLC22A17* gene while the more immature part of neutrophils expressed *LCN2* gene. Neutrophils play a key role in the immune system by participating in inflammatory response and adaptive immunity (Nam et al. 2014). In the present study the expression of the LCN2 receptor, *SLC22A17* (Chi et al. 2020), was detected in stromal cells of EAE meninges, which suggested that it could contribute to the neutrophils entrance into the meninges. Furthermore, neutrophils are involved in the differentiation and proliferation of naïve T cells by inducing the activation of antigen presenting cells, such as macrophages and dendritic cells (Nam et al. 2014). Here, we found that the more mature part of neutrophils strongly expressed *CSF1* gene while macrophages expressed *CSF1R* gene. *CSF1* gene on neutrophils encoded for a cytokine involved in the production, differentiation, and function of macrophages (Lin et al. 2019), *CSF1R* on macrophages, instead, encoded for the relative receptor. This data suggested that neutrophils can act as a booster to macrophages and monocytes by activating them and promoting the invasion of meningeal tissue (Hagan et al. 2020).

Due to the correlation found between stromal cells and neutrophils, we proceeded with a supervised trajectory analysis of neutrophil populations and we characterized them from an immature to a more mature state, both involved in EAE pathogenesis and performing numerous functions (De Bondt et al. 2020). As described in literature, we detected neutrophils that belonged to G0–4 stage mainly originating from bone marrow (BM), and neutrophils belonging to G5a–c mainly originating from peripheral tissue (Xie et al. 2020). Despite their involvement in EAE pathogenesis, the role of neutrophils in MS is still not yet well defined. The unsolved question is whether neutrophils exhibit a predominantly proinflammatory function or are implicated in the resolution of chronic inflammatory responses in MS.

Our results showed an extended heterogeneity of cell populations in meninges during EAE and confirmed a crosstalk between immune cells and NSCs, identified by stromal cluster. However, further studies are necessary to describe the specific pathological phenotype of meningeal NSCs.

4.9 Immune-regulation properties of meningeal NSCs

Our preliminary data on SCID mice, immunocompromised animals, showed that in the absence of lymphocytes, NSCs are highly affected in number and proliferation, suggesting the presence of a strong relationship between immune system and NPCs (Saino et al. 2010). According to this, with the aim to study the relationship between NSCs and immune cells under physiological condition, we performed an *in vitro* co-culture experiment with PDGFrβ$^+$ cells and naïve T cells. The observed increased expression of CD25 marker, which is a marker associated to activated T cells, in naïve T cells reflects the ability of NSCs to activate immune cells. We also found the ability of PDGFrβ$^+$ cells to re-activate resting myelin-specific auto-reactive T cells (TMPs), deriving from EAE mouse, further suggesting an ability to modulate immune responses *in vitro* (Conforti et al. 2014). Interestingly, this result is supported also by a cell-cell contact between PDGFrβ$^+$ cells and monocytes/macrophages (CD68$^+$ cells) and meningeal macrophages (CD163$^+$ cells) showed in *ex vivo* experiments.

Lastly, FACS analysis on meningeal cells isolated from control and EAE mouse brain showed an increase of double positive cells for PDGFrβ and MHCII marker in EAE animals. This result suggests that meningeal NSCs may become antigen presenting cells during EAE and it is in line with *in vitro* study showing that, once primed by inflammatory stimuli (INF-γ and TNF-α), leptomeningeal NSCs acquire an immune regulatory functions, and up-regulate molecules important for immune cell interactions (MHCII, CD40, PDL-1) and adhesion molecules (ICAM-1 and VCAM-1)(Di Trapani et al. 2013).

4.10 Final conclusions

In this thesis we described and characterised meninges in different paradigms: in physiological condition under pro-neurogenic stimuli and in pathological condition in a neurodegenerative disease. We found that in both conditions meningeal NSC niche is able to react modulating meningeal neural populations present in the niche.

The main output of this project is the identification of novel players, neural precursor cells, governing the complex events that act during the pro neurogenic stimulation and in pathological conditions, and the pharmacological potentiality that those cells represent.

The generation of immature neurons in the cerebral meninges after exposure to neurogenic stimuli as in pathological condition is a completely new and largely misunderstood result. The main question that arises in this context is: what is the function of these cells? In recent years,

the presence of neuroblasts in a quiescent state (no expression of Ki67, no incorporation of BrdU) has been described expressing markers of neural precursors (such as GLAST) or of migrating cells (such as DCX) (Benedetti et al. 2020; La Rosa et al. 2019; Pino et al. 2017). Those quiescent cells were found in classical NSC niches, like the subgranular (Fuentealba et al. 2015; Jhaveri et al. 2015) and the subventricular zone (Ottone et al. 2014), but also in newly described niches like the cortex, the striatum and the meninges themselves (Bifari et al. 2017; Fuentealba et al. 2015; Kempermann 2017; Luzzati et al. 2014; Pino et al. 2017).

Interestingly, here we found that meningeal stand-by neuroblasts participate to brain plasticity after pro-neurogenic stimulation in physiological condition, giving the possibility to modulate these quiescent precursors in order to boost endogenous regeneration.

In pathological condition, instead, meningeal neural precursors expressed molecules that are usually associated with immune system suggesting an existence of crosstalk between NSCs and immune cells. Additionally, the identification through scRNAseq analysis of the relationship between NSCs and immunity could represent a valuable source of information to identify new pharmacological target for MS and may be promising for the development of a therapy.

As a whole, meninges appear as a potential pharmacological target for regenerative medicine of the CNS. The meninges are a source of adult, somatic, endogenous NSCs that could be modulated by drugs. The modulation of this neurogenic population could be a novel therapeutic strategy to boost endogenous regeneration in neurodegenerative diseases and mood disorders, based on a potential “ready to use” widespread NSC potential located outside the brain parenchyma.

CHAPTER 5 – REFERENCES

(2019) Global, regional, and national burden of neurological disorders, 1990-2016: a systematic analysis for the Global Burden of Disease Study 2016. Lancet Neurol 18: 459-480.

Adeeb N, Deep A, Griessenauer CJ, Mortazavi MM, Watanabe K, Loukas M, Tubbs RS, Cohen-Gadol AA (2013) The intracranial arachnoid mater : a comprehensive review of its history, anatomy, imaging, and pathology. Childs Nerv Syst 29: 17-33.

Adeeb N, Mortazavi MM, Tubbs RS, Cohen-Gadol AA (2012) The cranial dura mater: a review of its history, embryology, and anatomy. Childs Nerv Syst 28: 827-37.

Agrawal S, Anderson P, Durbeej M, van Rooijen N, Ivars F, Opdenakker G, Sorokin LM (2006) Dystroglycan is selectively cleaved at the parenchymal basement membrane at sites of leukocyte extravasation in experimental autoimmune encephalomyelitis. Journal of Experimental Medicine 203: 1007-1019.

Aharoni R, Schottlender N, Bar-Lev DD, Eilam R, Sela M, Tsoory M, Arnon R (2019) Cognitive impairment in an animal model of multiple sclerosis and its amelioration by glatiramer acetate. Sci Rep 9: 4140.

Baek IS, Park JY, Han PL (2015) Chronic Antidepressant Treatment in Normal Mice Induces Anxiety and Impairs Stress-coping Ability. Exp Neurobiol 24: 156-68.

Balcombe J, Barnard N, Sandusky C (2004) Laboratory Routines Cause Animal Stress. Contemporary topics in laboratory animal science.

Baranzini SE, Oksenberg JR (2017) The Genetics of Multiple Sclerosis: From 0 to 200 in 50 Years. Trends Genet 33: 960-970.

Barber M, Andrews WD, Memi F, Gardener P, Ciantar D, Tata M, Ruhrberg C, Parnavelas JG (2018) Vascular-Derived Vegfa Promotes Cortical Interneuron Migration and Proximity to the Vasculature in the Developing Forebrain. Cereb Cortex 28: 2577-2593.

Bartholomaus I, Kawakami N, Odoardi F, Schlager C, Miljkovic D, Ellwart JW, Klinkert WE, Flugel-Koch C, Issekutz TB, Wekerle H, Flugel A (2009) Effector T cell interactions with meningeal vascular structures in nascent autoimmune CNS lesions. Nature 462: 94-8.

Belbasis L, Bellou V, Evangelou E, Ioannidis JP, Tzoulaki I (2015) Environmental risk factors and multiple sclerosis: an umbrella review of systematic reviews and meta-analyses. Lancet Neurol 14: 263-73.

Belmadani A, Ren D, Bhattacharyya BJ, Rothwangl KB, Hope TJ, Perlman H, Miller RJ (2015) Identification of a sustained neurogenic zone at the dorsal surface of the adult mouse hippocampus and its regulation by the chemokine SDF-1. Hippocampus 25: 1224-41.

Benarroch EE (2013) Adult neurogenesis in the dentate gyrus: general concepts and potential implications. Neurology 81: 1443-52.

Benedetti B, Dannehl D, Konig R, Coviello S, Kreutzer C, Zaunmair P, Jakubecova D, Weiger TM, Aigner L, Nacher J, Engelhardt M, Couillard-Despres S (2020) Functional Integration of Neuronal Precursors in the Adult Murine Piriform Cortex. Cereb Cortex 30: 1499-1515.

Berard JL, Wolak K, Fournier S, David S (2010) Characterization of relapsing-remitting and chronic forms of experimental autoimmune encephalomyelitis in C57BL/6 mice. Glia 58: 434-45.

Bergami M, Rimondini R, Santi S, Blum R, Goetz M, M. C (2008) Deletion of TrkB in adult progenitors alters newborn neuron integration into hippocampal circuits and increases anxiety-like behavior. PNAS 105.

Bevan RJ, Evans R, Griffiths L, Watkins LM, Rees MI, Magliozzi R, Allen I, McDonnell G, Kee R, Naughton M, Fitzgerald DC, Reynolds R, Neal JW, Howell OW (2018) Meningeal inflammation and cortical demyelination in acute multiple sclerosis. Ann Neurol 84: 829-842.

Bhargava P, Kim S, Reyes AA, Grenningloh R, Boschert U, Absinta M, Pardo C, Van Zijl P, Zhang J, Calabresi PA (2021) Imaging meningeal inflammation in CNS autoimmunity identifies a therapeutic role for BTK inhibition. Brain 144: 1396-1408.

Bifari F, Berton V, Pino A, Kusalo M, Malpeli G, Di Chio M, Bersan E, Amato E, Scarpa A, Krampera M, Fumagalli G, Decimo I (2015) Meninges harbor cells expressing neural precursor markers during development and adulthood. Front Cell Neurosci 9: 383.

Bifari F, Decimo I, Chiamulera C, Bersan E, Malpeli G, Johansson J, Lisi V, Bonetti B, Fumagalli G, Pizzolo G, Krampera M (2009) Novel stem/progenitor cells with neuronal differentiation potential reside in the leptomeningeal niche. J Cell Mol Med 13: 3195-208.

Bifari F, Decimo I, Pino A, Llorens-Bobadilla E, Zhao S, Lange C, Panuccio G, Boeckx B, Thienpont B, Vinckier S, Wyns S, Bouche A, Lambrechts D, Giugliano M, Dewerchin M, Martin-Villalba A, Carmeliet P (2017) Neurogenic Radial Glia-like Cells in Meninges Migrate and Differentiate into Functionally Integrated Neurons in the Neonatal Cortex. Cell Stem Cell 20: 360-373 e7.

Bjorkholm C, Monteggia LM (2016) BDNF - a key transducer of antidepressant effects. Neuropharmacology 102: 72-9.
Borrell V, Marín O (2006) Meninges control tangential migration of hem-derived Cajal-Retzius cells via CXCL12/CXCR4 signaling. Nat Neurosci 9: 1284-93.
Brocke S, Gijbels K, Steinman L (1994) Chapter 1 - Experimental Autoimmune Encephalomyelitis in the Mouse. In: Cohen IR, Miller A (eds) Autoimmune Disease Models. Academic Press, San Diego, pp 1-14
Brown AP, Dinger N, Levine BS (2000) Stress Produced by Gavage Administration in the Rat. Contemporary topics in laboratory animal science.
Caravagna C, Jaouën A, Desplat-Jégo S, Fenrich KK, Bergot E, Luche H, Grenot P, Rougon G, Malissen M, Debarbieux F (2018) Diversity of innate immune cell subsets across spatial and temporal scales in an EAE mouse model. Sci Rep 8: 5146.
Casarotto PC, Girych M, Fred SM, Kovaleva V, Moliner R, Enkavi G, Biojone C, Cannarozzo C, Sahu MP, Kaurinkoski K, Brunello CA, Steinzeig A, Winkel F, Patil S, Vestring S, Serchov T, Diniz C, Laukkanen L, Cardon I, Antila H, Rog T, Piepponen TP, Bramham CR, Normann C, Lauri SE, Saarma M, Vattulainen I, Castren E (2021) Antidepressant drugs act by directly binding to TRKB neurotrophin receptors. Cell 184: 1299-1313 e19.
Catala M (1998) Embryonic and fetal development of structures associated with the cerebro-spinal fluid in man and other species. Part I: The ventricular system, meninges and choroid plexuses. Arch Anat Cytol Pathol 46: 153-69.
Cazorla M, Premont J, Mann A, Girard N, Kellendonk C, Rognan D (2011) Identification of a low-molecular weight TrkB antagonist with anxiolytic and antidepressant activity in mice. J Clin Invest 121: 1846-57.
Chau KF, Springel MW, Broadbelt KG, Park HY, Topal S, Lun MP, Mullan H, Maynard T, Steen H, LaMantia AS, Lehtinen MK (2015) Progressive Differentiation and Instructive Capacities of Amniotic Fluid and Cerebrospinal Fluid Proteomes following Neural Tube Closure. Dev Cell 35: 789-802.
Chi Y, Remsik J, Kiseliovas V, Derderian C, Sener U, Alghader M, Saadeh F, Nikishina K, Bale T, Iacobuzio-Donahue C, Thomas T, Pe'er D, Mazutis L, Boire A (2020) Cancer cells deploy lipocalin-2 to collect limiting iron in leptomeningeal metastasis. Science 369: 276-282.
Choe Y, Huynh T, Pleasure SJ (2014) Migration of oligodendrocyte progenitor cells is controlled by transforming growth factor β family proteins during corticogenesis. J Neurosci 34: 14973-83.
Choe Y, Siegenthaler JA, Pleasure SJ (2012) A cascade of morphogenic signaling initiated by the meninges controls corpus callosum formation. Neuron 73: 698-712.
Christy AL, Walker ME, Hessner MJ, Brown MA (2013) Mast cell activation and neutrophil recruitment promotes early and robust inflammation in the meninges in EAE. J Autoimmun 42: 50-61.
Comi G, Bar-Or A, Lassmann H, Uccelli A, Hartung HP, Montalban X, Sørensen PS, Hohlfeld R, Hauser SL (2021) Role of B Cells in Multiple Sclerosis and Related Disorders. Ann Neurol 89: 13-23.
Conforti A, Scarsella M, Starc N, Giorda E, Biagini S, Proia A, Carsetti R, Locatelli F, Bernardo ME (2014) Microvescicles derived from mesenchymal stromal cells are not as effective as their cellular counterpart in the ability to modulate immune responses in vitro. Stem Cells Dev 23: 2591-9.
Constantin G, Laudanna C, Brocke S, Butcher EC (1999) Inhibition of experimental autoimmune encephalomyelitis by a tyrosine kinase inhibitor. J Immunol 162: 1144-9.
Constantinescu CS, Farooqi N, O'Brien K, Gran B (2011) Experimental autoimmune encephalomyelitis (EAE) as a model for multiple sclerosis (MS). British Journal of Pharmacology 164: 1079-1106.
Dang TC, Ishii Y, Nguyen V, Yamamoto S, Hamashima T, Okuno N, Nguyen QL, Sang Y, Ohkawa N, Saitoh Y, Shehata M, Takakura N, Fujimori T, Inokuchi K, Mori H, Andrae J, Betsholtz C, Sasahara M (2019) Powerful Homeostatic Control of Oligodendroglial Lineage by PDGFRalpha in Adult Brain. Cell Rep 27: 1073-1089 e5.
Davare MA, Lal S, Peckham JL, Prajapati SI, Gultekin SH, Rubin BP, Keller C (2014) Secreted meningeal chemokines, but not VEGFA, modulate the migratory properties of medulloblastoma cells. Biochem Biophys Res Commun 450: 555-60.
David DJ, Samuels BA, Rainer Q, Wang JW, Marsteller D, Mendez I, Drew M, Craig DA, Guiard BP, Guilloux JP, Artymyshyn RP, Gardier AM, Gerald C, Antonijevic IA, Leonardo ED, Hen R (2009) Neurogenesis-dependent and -independent effects of fluoxetine in an animal model of anxiety/depression. Neuron 62: 479-93.
Day-Lollini PA, Stewart GR, Taylor MJ, Johnson RM, Chellman GJ (1997) Hyperplastic Changes within the Leptomeninges of the Rat and Monkey in Response to Chronic Intracerebroventricular Infusion of Nerve Growth Factor. Experimental Neurology 145.

De Bondt M, Hellings N, Opdenakker G, Struyf S (2020) Neutrophils: Underestimated Players in the Pathogenesis of Multiple Sclerosis (MS). Int J Mol Sci 21.
de Brouwer G, Fick A, Harvey BH, Wolmarans W (2019) A critical inquiry into marble-burying as a preclinical screening paradigm of relevance for anxiety and obsessive-compulsive disorder: Mapping the way forward. Cogn Affect Behav Neurosci 19: 1-39.
Decimo I, Bifari F, Krampera M, Fumagalli G (2012a) Neural stem cell niches in health and diseases. Curr Pharm Des 18: 1755-83.
Decimo I, Bifari F, Rodriguez FJ, Malpeli G, Dolci S, Lavarini V, Pretto S, Vasquez S, Sciancalepore M, Montalbano A, Berton V, Krampera M, Fumagalli G (2011) Nestin- and doublecortin-positive cells reside in adult spinal cord meninges and participate in injury-induced parenchymal reaction. Stem Cells 29: 2062-76.
Decimo I, Dolci S, Panuccio G, Riva M, Fumagalli G, Bifari F (2020) Meninges: A Widespread Niche of Neural Progenitors for the Brain. Neuroscientist: 1073858420954826.
Decimo I, Fumagalli G, Berton V, Krampera M, Bifari F (2012b) Meninges: from protective membrane to stem cell niche. Am J Stem Cells 1: 92-105.
Deczkowska A, Baruch K, Schwartz M (2016) Type I/II Interferon Balance in the Regulation of Brain Physiology and Pathology. Trends Immunol 37: 181-192.
Dendrou CA, Fugger L, Friese MA (2015) Immunopathology of multiple sclerosis. Nat Rev Immunol 15: 545-58.
Di Trapani M, Bassi G, Ricciardi M, Fontana E, Bifari F, Pacelli L, Giacomello L, Pozzobon M, Féron F, De Coppi P, Anversa P, Fumagalli G, Decimo I, Menard C, Tarte K, Krampera M (2013) Comparative study of immune regulatory properties of stem cells derived from different tissues. Stem Cells Dev 22: 2990-3002.
Dobson R, Giovannoni G (2019) Multiple sclerosis - a review. Eur J Neurol 26: 27-40.
Dolci S, Pino A, Berton V, Gonzalez P, Braga A, Fumagalli M, Bonfanti E, Malpeli G, Pari F, Zorzin S, Amoroso C, Moscon D, Rodriguez FJ, Fumagalli G, Bifari F, Decimo I (2017) High Yield of Adult Oligodendrocyte Lineage Cells Obtained from Meningeal Biopsy. Front Pharmacol 8: 703.
Duman RS, Monteggia LM (2006) A neurotrophic model for stress-related mood disorders. Biol Psychiatry 59: 1116-27.
Eisinger BE, Zhao X (2018) Identifying molecular mediators of environmentally enhanced neurogenesis. Cell Tissue Res 371: 7-21.
Etchevers HC, Vincent C, Le Douarin NM, Couly GF (2001) The cephalic neural crest provides pericytes and smooth muscle cells to all blood vessels of the face and forebrain. Development 128: 1059-68.
Feizi N, Focaccetti C, Pacella I, Tucci G, Rossi A, Costanza M, Pedotti R, Sidney J, Sette A, La Rocca C, Procaccini C, Matarese G, Barnaba V, Piconese S (2021) CD8(+) T cells specific for cryptic apoptosis-associated epitopes exacerbate experimental autoimmune encephalomyelitis. Cell Death Dis 12: 1026.
Ferguson JM (2001) Mechanism of Action of Antidepressant Medications. Primary Care Companion J Clin Psychiatry 3: 22-27.
Fletcher JM, Lalor SJ, Sweeney CM, Tubridy N, Mills KH (2010) T cells in multiple sclerosis and experimental autoimmune encephalomyelitis. Clin Exp Immunol 162: 1-11.
Forbes TA, Goldstein EZ, Dupree JL, Jablonska B, Scafidi J, Adams KL, Imamura Y, Hashimoto-Torii K, Gallo V (2020) Environmental enrichment ameliorates perinatal brain injury and promotes functional white matter recovery. Nat Commun 11: 964.
Formaggio E, Fazzini F, Dalfini AC, Di Chio M, Cantu C, Decimo I, Fiorini Z, Fumagalli G, Chiamulera C (2010) Nicotine increases the expression of neurotrophin receptor tyrosine kinase receptor A in basal forebrain cholinergic neurons. Neuroscience 166: 580-9.
Frischer JM, Weigand SD, Guo Y, Kale N, Parisi JE, Pirko I, Mandrekar J, Bramow S, Metz I, Bruck W, Lassmann H, Lucchinetti CF (2015) Clinical and pathological insights into the dynamic nature of the white matter multiple sclerosis plaque. Annals of Neurology 78: 710-721.
Fuentealba LC, Rompani SB, Parraguez JI, Obernier K, Romero R, Cepko CL, Alvarez-Buylla A (2015) Embryonic Origin of Postnatal Neural Stem Cells. Cell 161: 1644-55.
Gay FW, Drye TJ, Dick GW, Esiri MM (1997) The application of multifactorial cluster analysis in the staging of plaques in early multiple sclerosis. Identification and characterization of the primary demyelinating lesion. Brain 120 (Pt 8): 1461-83.
Ghasemi N, Razavi S, Nikzad E (2017) Multiple Sclerosis: Pathogenesis, Symptoms, Diagnoses and Cell-Based Therapy. Cell J 19: 1-10.
Glatigny S, Bettelli E (2018) Experimental Autoimmune Encephalomyelitis (EAE) as Animal Models of Multiple Sclerosis (MS). Cold Spring Harb Perspect Med 8.

Götz M, Stoykova A, Gruss P (1998) Pax6 controls radial glia differentiation in the cerebral cortex. Neuron 21: 1031-44.
Grigoriadis N, van Pesch V (2015) A basic overview of multiple sclerosis immunopathology. Eur J Neurol 22 Suppl 2: 3-13.
Hagan N, Kane JL, Grover D, Woodworth L, Madore C, Saleh J, Sancho J, Liu J, Li Y, Proto J, Zelic M, Mahan A, Kothe M, Scholte AA, Fitzgerald M, Gisevius B, Haghikia A, Butovsky O, Ofengeim D (2020) CSF1R signaling is a regulator of pathogenesis in progressive MS. Cell Death Dis 11: 904.
Hartmann D, Sievers J, Pehlemann FW, Berry M (1992) Destruction of meningeal cells over the medial cerebral hemisphere of newborn hamsters prevents the formation of the infrapyramidal blade of the dentate gyrus. J Comp Neurol 320: 33-61.
Hauser SL (2020) Progress in Multiple Sclerosis Research: An Example of Bedside to Bench. Jama 324: 841-842.
Healy LM, Yaqubi M, Ludwin S, Antel JP (2020) Species differences in immune-mediated CNS tissue injury and repair: A (neuro)inflammatory topic. Glia 68: 811-829.
Hemmer B, Kerschensteiner M, Korn T (2015) Role of the innate and adaptive immune responses in the course of multiple sclerosis. Lancet Neurol 14: 406-19.
Hemmer B, Nessler S, Zhou D, Kieseier B, Hartung HP (2006) Immunopathogenesis and immunotherapy of multiple sclerosis. Nat Clin Pract Neurol 2: 201-11.
Horakova D, Kalincik T, Dusankova JB, Dolezal O (2012) Clinical correlates of grey matter pathology in multiple sclerosis. BMC Neurol 12: 10.
Howard J, Trevick S, Younger DS (2016) Epidemiology of Multiple Sclerosis. Neurol Clin 34: 919-939.
Hu Y, Ota N, Peng I, Refino CJ, Danilenko DM, Caplazi P, Ouyang W (2010) IL-17RC Is Required for IL-17A– and IL-17F–Dependent Signaling and the Pathogenesis of Experimental Autoimmune Encephalomyelitis. The Journal of Immunology 184: 4307-4316.
International Multiple Sclerosis Genetics C, Wellcome Trust Case Control C, Sawcer S, Hellenthal G, Pirinen M, Spencer CC, Patsopoulos NA, Moutsianas L, Dilthey A, Su Z, Freeman C, Hunt SE, Edkins S, Gray E, Booth DR, Potter SC, Goris A, Band G, Oturai AB, Strange A, Saarela J, Bellenguez C, Fontaine B, Gillman M, Hemmer B, Gwilliam R, Zipp F, Jayakumar A, Martin R, Leslie S, Hawkins S, Giannoulatou E, D'Alfonso S, Blackburn H, Martinelli Boneschi F, Liddle J, Harbo HF, Perez ML, Spurkland A, Waller MJ, Mycko MP, Ricketts M, Comabella M, Hammond N, Kockum I, McCann OT, Ban M, Whittaker P, Kemppinen A, Weston P, Hawkins C, Widaa S, Zajicek J, Dronov S, Robertson N, Bumpstead SJ, Barcellos LF, Ravindrarajah R, Abraham R, Alfredsson L, Ardlie K, Aubin C, Baker A, Baker K, Baranzini SE, Bergamaschi L, Bergamaschi R, Bernstein A, Berthele A, Boggild M, Bradfield JP, Brassat D, Broadley SA, Buck D, Butzkueven H, Capra R, Carroll WM, Cavalla P, Celius EG, Cepok S, Chiavacci R, Clerget-Darpoux F, Clysters K, Comi G, Cossburn M, Cournu-Rebeix I, Cox MB, Cozen W, Cree BA, Cross AH, Cusi D, Daly MJ, Davis E, de Bakker PI, Debouverie M, D'Hooghe M B, Dixon K, Dobosi R, Dubois B, Ellinghaus D, Elovaara I, Esposito F, Fontenille C, Foote S, Franke A, Galimberti D, Ghezzi A, Glessner J, Gomez R, Gout O, Graham C, Grant SF, Guerini FR, Hakonarson H, Hall P, Hamsten A, Hartung HP, Heard RN, Heath S, Hobart J, Hoshi M, Infante-Duarte C, Ingram G, Ingram W, Islam T, Jagodic M, Kabesch M, Kermode AG, Kilpatrick TJ, Kim C, Klopp N, Koivisto K, Larsson M, Lathrop M, Lechner-Scott JS, Leone MA, Leppa V, Liljedahl U, Bomfim IL, Lincoln RR, Link J, Liu J, Lorentzen AR, Lupoli S, Macciardi F, Mack T, Marriott M, Martinelli V, Mason D, McCauley JL, Mentch F, Mero IL, Mihalova T, Montalban X, Mottershead J, Myhr KM, Naldi P, Ollier W, Page A, Palotie A, Pelletier J, Piccio L, Pickersgill T, Piehl F, Pobywajlo S, Quach HL, Ramsay PP, Reunanen M, Reynolds R, Rioux JD, Rodegher M, Roesner S, Rubio JP, Ruckert IM, Salvetti M, Salvi E, Santaniello A, Schaefer CA, Schreiber S, Schulze C, Scott RJ, Sellebjerg F, Selmaj KW, Sexton D, Shen L, Simms-Acuna B, Skidmore S, Sleiman PM, Smestad C, Sorensen PS, Sondergaard HB, Stankovich J, Strange RC, Sulonen AM, Sundqvist E, Syvanen AC, Taddeo F, Taylor B, Blackwell JM, Tienari P, Bramon E, Tourbah A, Brown MA, Tronczynska E, Casas JP, Tubridy N, Corvin A, Vickery J, Jankowski J, Villoslada P, Markus HS, Wang K, Mathew CG, Wason J, Palmer CN, Wichmann HE, Plomin R, Willoughby E, Rautanen A, Winkelmann J, Wittig M, Trembath RC, Yaouanq J, Viswanathan AC, Zhang H, Wood NW, Zuvich R, Deloukas P, Langford C, Duncanson A, Oksenberg JR, Pericak-Vance MA, Haines JL, Olsson T, Hillert J, Ivinson AJ, De Jager PL, Peltonen L, Stewart GJ, Hafler DA, Hauser SL, McVean G, Donnelly P, Compston A (2011) Genetic risk and a primary role for cell-mediated immune mechanisms in multiple sclerosis. Nature 476: 214-9.
Jhaveri DJ, O'Keeffe I, Robinson GJ, Zhao QY, Zhang ZH, Nink V, Narayanan RK, Osborne GW, Wray NR, Bartlett PF (2015) Purification of neural precursor cells reveals the presence of distinct, stimulus-specific subpopulations of quiescent precursors in the adult mouse hippocampus. J Neurosci 35: 8132-44.

Jones EG (1970) On the mode of entry of blood vessels into the cerebral cortex. Journal of anatomy 106: 507-520.
Jordão MJC, Sankowski R, Brendecke SM, Sagar, Locatelli G, Tai YH, Tay TL, Schramm E, Armbruster S, Hagemeyer N, Groß O, Mai D, Çiçek Ö, Falk T, Kerschensteiner M, Grün D, Prinz M (2019) Single-cell profiling identifies myeloid cell subsets with distinct fates during neuroinflammation. Science 363.
Karow M, Sánchez R, Schichor C, Masserdotti G, Ortega F, Heinrich C, Gascón S, Khan MA, Lie DC, Dellavalle A, Cossu G, Goldbrunner R, Götz M, Berninger B (2012) Reprogramming of pericyte-derived cells of the adult human brain into induced neuronal cells. Cell Stem Cell 11: 471-6.
Kempermann G (2017) A Back Door to Cortical Development. Cell Stem Cell 20: 295-296.
Kempermann G (2019) Environmental enrichment, new neurons and the neurobiology of individuality. Nat Rev Neurosci 20: 235-245.
Kempermann G, Kuhn HG, Gage FH (1997) More hippocampal neurons in adult mice living in an enriched environment. Nature 386.
Kerever A, Schnack J, Vellinga D, Ichikawa N, Moon C, Arikawa-Hirasawa E, Efird JT, Mercier F (2007) Novel extracellular matrix structures in the neural stem cell niche capture the neurogenic factor fibroblast growth factor 2 from the extracellular milieu. Stem Cells 25: 2146-57.
Khodanovich M, Kisel A, Kudabaeva M, Chernysheva G, Smolyakova V, Krutenkova E, Wasserlauf I, Plotnikov M, Yarnykh V (2018) Effects of Fluoxetine on Hippocampal Neurogenesis and Neuroprotection in the Model of Global Cerebral Ischemia in Rats. Int J Mol Sci 19.
Kim WK, Alvarez X, Fisher J, Bronfin B, Westmoreland S, McLaurin J, Williams K (2006) CD163 identifies perivascular macrophages in normal and viral encephalitic brains and potential precursors to perivascular macrophages in blood. Am J Pathol 168: 822-34.
Klein R, Nanduri V, Jing SA, Lamballe F, Tapley P, Bryant S, Cordon-Cardo C, Jones KR, Reichardt LF, Barbacid M (1991) The trkB tyrosine protein kinase is a receptor for brain-derived neurotrophic factor and neurotrophin-3. Cell 66: 395-403.
Klineova S, Lublin FD (2018) Clinical Course of Multiple Sclerosis. Cold Spring Harbor Perspectives in Medicine 8.
Klinger A, Gebert A, Bieber K, Kalies K, Ager A, Bell EB, Westermann J (2009) Cyclical expression of L-selectin (CD62L) by recirculating T cells. Int Immunol 21: 443-55.
Kojima T, Hirota Y, Ema M, Takahashi S, Miyoshi I, Okano H, Sawamoto K (2010) Subventricular zone-derived neural progenitor cells migrate along a blood vessel scaffold toward the post-stroke striatum. Stem Cells 28: 545-54.
Kokaia Z, Martino G, Schwartz M, Lindvall O (2012) Cross-talk between neural stem cells and immune cells: the key to better brain repair? Nat Neurosci 15: 1078-87.
Kraeuter AK, Guest PC, Sarnyai Z (2019) Object Burying Test for Assessment of Obsessive Compulsive Behaviors in Mice. Methods Mol Biol 1916: 81-85.
Kumar M, Csaba Z, Peineau S, Srivastava R, Rasika S, Mani S, Gressens P, El Ghouzzi V (2014) Endogenous cerebellar neurogenesis in adult mice with progressive ataxia. Ann Clin Transl Neurol 1: 968-81.
Kurschus FC (2015) T cell mediated pathogenesis in EAE: Molecular mechanisms. Biomed J 38: 183-93.
La Rosa C, Ghibaudi M, Bonfanti L (2019) Newly Generated and Non-Newly Generated "Immature" Neurons in the Mammalian Brain: A Possible Reservoir of Young Cells to Prevent Brain Aging and Disease? J Clin Med 8.
Lehtinen MK, Zappaterra MW, Chen X, Yang YJ, Hill AD, Lun M, Maynard T, Gonzalez D, Kim S, Ye P, D'Ercole AJ, Wong ET, LaMantia AS, Walsh CA (2011) The cerebrospinal fluid provides a proliferative niche for neural progenitor cells. Neuron 69: 893-905.
Lemus HN, Warrington AE, Rodriguez M (2018) Multiple Sclerosis: Mechanisms of Disease and Strategies for Myelin and Axonal Repair. Neurol Clin 36: 1-11.
Lendahl U, Zimmerman LB, McKay RD (1990) CNS stem cells express a new class of intermediate filament protein. Cell 60: 585-95.
Lin R, Cai J, Nathan C, Wei X, Schleidt S, Rosenwasser R, Iacovitti L (2015) Neurogenesis is enhanced by stroke in multiple new stem cell niches along the ventricular system at sites of high BBB permeability. Neurobiol Dis 74: 229-39.
Lin W, Xu D, Austin CD, Caplazi P, Senger K, Sun Y, Jeet S, Young J, Delarosa D, Suto E, Huang Z, Zhang J, Yan D, Corzo C, Barck K, Rajan S, Looney C, Gandham V, Lesch J, Liang WC, Mai E, Ngu H, Ratti N, Chen Y, Misner D, Lin T, Danilenko D, Katavolos P, Doudemont E, Uppal H, Eastham J, Mak J, de Almeida PE, Bao K, Hadadianpour A, Keir M, Carano RAD, Diehl L, Xu M, Wu Y, Weimer RM, DeVoss J, Lee WP,

Balazs M, Walsh K, Alatsis KR, Martin F, Zarrin AA (2019) Function of CSF1 and IL34 in Macrophage Homeostasis, Inflammation, and Cancer. Front Immunol 10: 2019.
Livak KJ, Schmittgen TD (2001) Analysis of relative gene expression data using real-time quantitative PCR and the 2(-Delta Delta C(T)) Method. Methods 25: 402-8.
Lopez MF, Laber K (2015) Impact of social isolation and enriched environment during adolescence on voluntary ethanol intake and anxiety in C57BL/6J mice. Physiol Behav 148: 151-6.
Louveau A, Herz J, Alme MN, Salvador AF, Dong MQ, Viar KE, Herod SG, Knopp J, Setliff JC, Lupi AL, Da Mesquita S, Frost EL, Gaultier A, Harris TH, Cao R, Hu S, Lukens JR, Smirnov I, Overall CC, Oliver G, Kipnis J (2018) CNS lymphatic drainage and neuroinflammation are regulated by meningeal lymphatic vasculature. Nat Neurosci 21: 1380-1391.
Louveau A, Plog BA, Antila S, Alitalo K, Nedergaard M, Kipnis J (2017) Understanding the functions and relationships of the glymphatic system and meningeal lymphatics. J Clin Invest 127: 3210-3219.
Lublin FD, Reingold SC, Cohen JA, Cutter GR, Sorensen PS, Thompson AJ, Wolinsky JS, Balcer LJ, Banwell B, Barkhof F, Bebo B, Jr., Calabresi PA, Clanet M, Comi G, Fox RJ, Freedman MS, Goodman AD, Inglese M, Kappos L, Kieseier BC, Lincoln JA, Lubetzki C, Miller AE, Montalban X, O'Connor PW, Petkau J, Pozzilli C, Rudick RA, Sormani MP, Stuve O, Waubant E, Polman CH (2014) Defining the clinical course of multiple sclerosis: the 2013 revisions. Neurology 83: 278-86.
Luzzati F, Nato G, Oboti L, Vigna E, Rolando C, Armentano M, Bonfanti L, Fasolo A, Peretto P (2014) Quiescent neuronal progenitors are activated in the juvenile guinea pig lateral striatum and give rise to transient neurons. Development 141: 4065-75.
Madara JC, Levine ES (2008) Presynaptic and postsynaptic NMDA receptors mediate distinct effects of brain-derived neurotrophic factor on synaptic transmission. J Neurophysiol 100: 3175-84.
Magliozzi R, Howell O, Vora A, Serafini B, Nicholas R, Puopolo M, Reynolds R, Aloisi F (2007) Meningeal B-cell follicles in secondary progressive multiple sclerosis associate with early onset of disease and severe cortical pathology. Brain 130: 1089-104.
Malberg JE, Eisch AJ, Nestler EJ, Duman RS (2000) Chronic antidepressant treatment increases neurogenesis in adult rat hippocampus. J Neurosci 20: 9104-10.
Mauffrey P, Tchitchek N, Barroca V, Bemelmans AP, Firlej V, Allory Y, Romeo PH, Magnon C (2019) Progenitors from the central nervous system drive neurogenesis in cancer. Nature 569: 672-678.
Meeker RB, Williams KS (2015) The p75 neurotrophin receptor: at the crossroad of neural repair and death. Neural Regen Res 10: 721-5.
Mercier F (2016) Fractones: extracellular matrix niche controlling stem cell fate and growth factor activity in the brain in health and disease. Cell Mol Life Sci 73: 4661-4674.
Mercier F, Arikawa-Hirasawa E (2012) Heparan sulfate niche for cell proliferation in the adult brain. Neurosci Lett 510: 67-72.
Mercier F, Hatton GI (2003) Meninges and perivasculature as mediators of CNS plasticity. Advances in Molecular and Cell Biology 31: 215-253.
Micheli L, Ceccarelli M, D'Andrea G, Tirone F (2018) Depression and adult neurogenesis: Positive effects of the antidepressant fluoxetine and of physical exercise. Brain Res Bull 143: 181-193.
Miljkovic D, Spasojevic I (2013) Multiple sclerosis: molecular mechanisms and therapeutic opportunities. Antioxid Redox Signal 19: 2286-334.
Ming GL, Song H (2011) Adult neurogenesis in the mammalian brain: significant answers and significant questions. Neuron 70: 687-702.
Mori T, Tanaka K, Buffo A, Wurst W, Kuhn R, Gotz M (2006) Inducible gene deletion in astroglia and radial glia--a valuable tool for functional and lineage analysis. Glia 54: 21-34.
Moy JK, Szabo-Pardi T, Tillu DV, Megat S, Pradhan G, Kume M, Asiedu MN, Burton MD, Dussor G, Price TJ (2019) Temporal and sex differences in the role of BDNF/TrkB signaling in hyperalgesic priming in mice and rats. Neurobiol Pain 5: 100024.
Munoz JJ, Bernard CC, Mackay IR (1984) Elicitation of experimental allergic encephalomyelitis (EAE) in mice with the aid of pertussigen. Cell Immunol 83: 92-100.
Nafee T., Watanabe R., F. F (2018) Multiple Sclerosis Clinical Trials in Neurology. Humana Press, New York, NY.
Nagl S, Haas M, Lahmer G, Buttner-Herold M, Grabenbauer GG, Fietkau R, Distel LV (2016) Cell-to-cell distances between tumor-infiltrating inflammatory cells have the potential to distinguish functionally active from suppressed inflammatory cells. Oncoimmunology 5: e1127494.
Nait-Oumesmar B, Picard-Riera N, Kerninon C, Decker L, Seilhean D, Hoglinger GU, Hirsch EC, Reynolds R, Baron-Van Evercooren A (2007) Activation of the subventricular zone in multiple sclerosis: evidence for early glial progenitors. Proc Natl Acad Sci U S A 104: 4694-9.

Nakagomi T, Molnar Z, Nakano-Doi A, Taguchi A, Saino O, Kubo S, Clausen M, Yoshikawa H, Nakagomi N, Matsuyama T (2011) Ischemia-induced neural stem/progenitor cells in the pia mater following cortical infarction. Stem Cells Dev 20: 2037-51.
Nakagomi T, Molnar Z, Taguchi A, Nakano-Doi A, Lu S, Kasahara Y, Nakagomi N, Matsuyama T (2012) Leptomeningeal-derived doublecortin-expressing cells in poststroke brain. Stem Cells Dev 21: 2350-4.
Nakagomi T, Nakano-Doi A, Matsuyama T (2015) Leptomeninges: a novel stem cell niche harboring ischemia-induced neural progenitors. Histology and Histopathology 30: 391-399.
Nakahara J, Maeda M, Aiso S, Suzuki N (2012) Current concepts in multiple sclerosis: autoimmunity versus oligodendrogliopathy. Clin Rev Allergy Immunol 42: 26-34.
Nakamura T, Colbert MC, Robbins J (2006) Neural crest cells retain multipotential characteristics in the developing valves and label the cardiac conduction system. Circ Res 98: 1547-54.
Nam Y, Kim JH, Seo M, Kim JH, Jin M, Jeon S, Seo JW, Lee WH, Bing SJ, Jee Y, Lee WK, Park DH, Kook H, Suk K (2014) Lipocalin-2 protein deficiency ameliorates experimental autoimmune encephalomyelitis: the pathogenic role of lipocalin-2 in the central nervous system and peripheral lymphoid tissues. J Biol Chem 289: 16773-89.
Ninomiya S, Esumi S, Ohta K, Fukuda T, Ito T, Imayoshi I, Kageyama R, Ikeda T, Itohara S, Tamamaki N (2013) Amygdala kindling induces nestin expression in the leptomeninges of the neocortex. Neurosci Res 75: 121-9.
Ottone C, Krusche B, Whitby A, Clements M, Quadrato G, Pitulescu ME, Adams RH, Parrinello S (2014) Direct cell-cell contact with the vascular niche maintains quiescent neural stem cells. Nat Cell Biol 16: 1045-56.
Palace J, Duddy M, Bregenzer T, Lawton M, Zhu F, Boggild M, Piske B, Robertson NP, Oger J, Tremlett H, Tilling K, Ben-Shlomo Y, Dobson C (2015) Effectiveness and cost-effectiveness of interferon beta and glatiramer acetate in the UK Multiple Sclerosis Risk Sharing Scheme at 6 years: a clinical cohort study with natural history comparator. Lancet Neurol 14: 497-505.
Park H, Poo MM (2013) Neurotrophin regulation of neural circuit development and function. Nat Rev Neurosci 14: 7-23.
Parr AM, Tator CH, Keating A (2007) Bone marrow-derived mesenchymal stromal cells for the repair of central nervous system injury. Bone Marrow Transplant 40: 609-19.
Pikor NB, Cupovic J, Onder L, Gommerman JL, Ludewig B (2017) Stromal Cell Niches in the Inflamed Central Nervous System. J Immunol 198: 1775-1781.
Pikor NB, Prat A, Bar-Or A, Gommerman JL (2015) Meningeal Tertiary Lymphoid Tissues and Multiple Sclerosis: A Gathering Place for Diverse Types of Immune Cells during CNS Autoimmunity. Front Immunol 6: 657.
Pino A, Fumagalli G, Bifari F, Decimo I (2017) New neurons in adult brain: distribution, molecular mechanisms and therapies. Biochem Pharmacol 141: 4-22.
Pol S, Schweser F, Bertolino N, Preda M, Sveinsson M, Sudyn M, Babek N, Zivadinov R (2019) Characterization of leptomeningeal inflammation in rodent experimental autoimmune encephalomyelitis (EAE) model of multiple sclerosis. Exp Neurol 314: 82-90.
Prineas JW, Lee S (2019) Multiple Sclerosis: Destruction and Regeneration of Astrocytes in Acute Lesions. J Neuropathol Exp Neurol 78: 140-156.
Procaccini C, De Rosa V, Pucino V, Formisano L, Matarese G (2015) Animal models of Multiple Sclerosis. Eur J Pharmacol 759: 182-91.
Qin D, Gan Y, Shao K, Wang H, Li W, Wang T, He W, Xu J, Zhang Y, Kou Z, Zeng L, Sheng G, Esteban MA, Gao S, Pei D (2008) Mouse meningiocytes express Sox2 and yield high efficiency of chimeras after nuclear reprogramming with exogenous factors. J Biol Chem 283: 33730-5.
Radakovits R, Barros CS, Belvindrah R, Patton B, Müller U (2009) Regulation of radial glial survival by signals from the meninges. J Neurosci 29: 7694-705.
Rahmanzadeh R, Brück W, Minagar A, Sahraian MA (2018) Multiple sclerosis pathogenesis: missing pieces of an old puzzle. Rev Neurosci 30: 67-83.
Rangachari M, Kerfoot SM, Arbour N, Alvarez JI (2017) Editorial: Lymphocytes in MS and EAE: More Than Just a CD4(+) World. Front Immunol 8: 133.
Reich DS, Lucchinetti CF, Calabresi PA (2018) Multiple Sclerosis. N Engl J Med 378: 169-180.
Reiss K, Mentlein R, Sievers J, Hartmann D (2002) Stromal cell-derived factor 1 is secreted by meningeal cells and acts as chemotactic factor on neuronal stem cells of the cerebellar external granular layer. Neuroscience 115: 295-305.

Rostami A, Ciric B (2013) Role of Th17 cells in the pathogenesis of CNS inflammatory demyelination. J Neurol Sci 333: 76-87.
Russi AE, Brown MA (2015) The meninges: new therapeutic targets for multiple sclerosis. Transl Res 165: 255-69.
Russi AE, Walker-Caulfield ME, Brown MA (2018) Mast cell inflammasome activity in the meninges regulates EAE disease severity. Clin Immunol 189: 14-22.
Saino O, Taguchi A, Nakagomi T, Nakano-Doi A, Kashiwamura S, Doe N, Nakagomi N, Soma T, Yoshikawa H, Stern DM, Okamura H, Matsuyama T (2010) Immunodeficiency reduces neural stem/progenitor cell apoptosis and enhances neurogenesis in the cerebral cortex after stroke. J Neurosci Res 88: 2385-97.
Samuels BA, Hen R (2011) Neurogenesis and affective disorders. Eur J Neurosci 33: 1152-9.
Sarrazin S, Lamanna WC, Esko JD (2011) Heparan sulfate proteoglycans. Cold Spring Harb Perspect Biol 3.
Savage MA, McQuade R, Thiele A (2017) Segregated fronto-cortical and midbrain connections in the mouse and their relation to approach and avoidance orienting behaviors. J Comp Neurol 525: 1980-1999.
Scadden DT (2006) The stem-cell niche as an entity of action. Nature 441: 1075-9.
Schindelin J, Arganda-Carreras I, Frise E, Kaynig V, Longair M, Pietzsch T, Preibisch S, Rueden C, Saalfeld S, Schmid B, Tinevez JY, White DJ, Hartenstein V, Eliceiri K, Tomancak P, Cardona A (2012) Fiji: an open-source platform for biological-image analysis. Nat Methods 9: 676-82.
Schläger C, Körner H, Krueger M, Vidoli S, Haberl M, Mielke D, Brylla E, Issekutz T, Cabañas C, Nelson PJ, Ziemssen T, Rohde V, Bechmann I, Lodygin D, Odoardi F, Flügel A (2016) Effector T-cell trafficking between the leptomeninges and the cerebrospinal fluid. Nature 530: 349-353.
Schlager C, Korner H, Krueger M, Vidoli S, Haberl M, Mielke D, Brylla E, Issekutz T, Cabanas C, Nelsons PJ, Ziemssen T, Rohde V, Bechmann I, Lodygin D, Odoardi F, Flugel A (2016) Effector T-cell trafficking between the leptomeninges and the cerebrospinal fluid. Nature 530: 349-+.
Shrestha B, Jiang X, Ge SJ, Paul D, Chianchiano P, Pachter JS (2017) Spatiotemporal resolution of spinal meningeal and parenchymal inflammation during experimental autoimmune encephalomyelitis. Neurobiology of Disease 108: 159-172.
Siegenthaler JA, Ashique AM, Zarbalis K, Patterson KP, Hecht JH, Kane MA, Folias AE, Choe Y, May SR, Kume T, Napoli JL, Peterson AS, Pleasure SJ (2009) Retinoic acid from the meninges regulates cortical neuron generation. Cell 139: 597-609.
Sievers J, von Knebel Doeberitz C, Pehlemann FW, Berry M (1986) Meningeal cells influence cerebellar development over a critical period. Anat Embryol (Berl) 175: 91-100.
Slaker M, Barnes J, Sorg BA, Grimm JW (2016) Impact of Environmental Enrichment on Perineuronal Nets in the Prefrontal Cortex following Early and Late Abstinence from Sucrose Self-Administration in Rats. PLoS One 11: e0168256.
Sohur US, Emsley JG, Mitchell BD, Macklis JD (2006) Adult neurogenesis and cellular brain repair with neural progenitors, precursors and stem cells. Philos Trans R Soc Lond B Biol Sci 361: 1477-97.
Song E, Mao T, Dong H, Boisserand LSB, Antila S, Bosenberg M, Alitalo K, Thomas JL, Iwasaki A (2020) VEGF-C-driven lymphatic drainage enables immunosurveillance of brain tumours. Nature 577: 689-694.
Stromnes IM, Goverman JM (2006) Active induction of experimental allergic encephalomyelitis. Nat Protoc 1: 1810-9.
Stumm R, Höllt V (2007) CXC chemokine receptor 4 regulates neuronal migration and axonal pathfinding in the developing nervous system: implications for neuronal regeneration in the adult brain. J Mol Endocrinol 38: 377-82.
Suter T, DeLoughery ZJ, Jaworski A (2017) Meninges-derived cues control axon guidance. Dev Biol 430: 1-10.
Tomassoni-Ardori F, Fulgenzi G, Becker J, Barrick C, Palko ME, Kuhn S, Koparde V, Cam M, Yanpallewar S, Oberdoerffer S, Tessarollo L (2019) Rbfox1 up-regulation impairs BDNF-dependent hippocampal LTP by dysregulating TrkB isoform expression levels. Elife 8.
Unger MS, Marschallinger J, Kaindl J, Klein B, Johnson M, Khundakar AA, Roßner S, Heneka MT, Couillard-Despres S, Rockenstein E, Masliah E, Attems J, Aigner L (2018) Doublecortin expression in CD8+ T-cells and microglia at sites of amyloid-β plaques: A potential role in shaping plaque pathology? Alzheimer's & Dementia 14: 1022-1037.
Van Kaer L, Postoak JL, Wang C, Yang G, Wu L (2019) Innate, innate-like and adaptive lymphocytes in the pathogenesis of MS and EAE. Cell Mol Immunol 16: 531-539.
van Olst L, Rodriguez-Mogeda C, Picon C, Kiljan S, James RE, Kamermans A, van der Pol SMA, Knoop L, Michailidou I, Drost E, Franssen M, Schenk GJ, Geurts JJG, Amor S, Mazarakis ND, van Horssen J, de Vries HE, Reynolds R, Witte ME (2021) Meningeal inflammation in multiple sclerosis induces

phenotypic changes in cortical microglia that differentially associate with neurodegeneration. Acta Neuropathol 141: 881-899.
Vandenabeele F, Creemers J, Lambrichts I (1996) Ultrastructure of the human spinal arachnoid mater and dura mater. J Anat 189 (Pt 2): 417-30.
Venna VR, Xu Y, Doran SJ, Patrizz A, McCullough LD (2014) Social interaction plays a critical role in neurogenesis and recovery after stroke. Transl Psychiatry 4: e351.
Wagner CA, Roqué PJ, Mileur TR, Liggitt D, Goverman JM (2020) Myelin-specific CD8+ T cells exacerbate brain inflammation in CNS autoimmunity. J Clin Invest 130: 203-213.
Waiczies H, Millward JM, Lepore S, Infante-Duarte C, Pohlmann A, Niendorf T, Waiczies S (2012) Identification of cellular infiltrates during early stages of brain inflammation with magnetic resonance microscopy. PLoS One 7: e32796.
Wang JW, David DJ, Monckton JE, Battaglia F, Hen R (2008) Chronic fluoxetine stimulates maturation and synaptic plasticity of adult-born hippocampal granule cells. J Neurosci 28: 1374-84.
Wei B, Liu Z, Fan Y, Wang S, Dong C, Rao W, Yang F, Cheng G, Zhang J (2021) Analysis of Cellular Heterogeneity in Immune Microenvironment of Primary Central Nervous System Lymphoma by Single-Cell Sequencing. Front Oncol 11: 683007.
Weiss H, Millward J, Holst P, Sorensen MR, Owens T (2008) CD8+T-cells in inflammatory demyelinating disease. Journal of Neuroimmunology 203: 229-229.
Wiese C, Rolletschek A, Kania G, Blyszczuk P, Tarasov KV, Tarasova Y, Wersto RP, Boheler KR, Wobus AM (2004) Nestin expression--a property of multi-lineage progenitor cells? Cell Mol Life Sci 61: 2510-22.
Wu F, Cao W, Yang Y, Liu A (2010) Extensive infiltration of neutrophils in the acute phase of experimental autoimmune encephalomyelitis in C57BL/6 mice. Histochem Cell Biol 133: 313-22.
Xie X, Shi Q, Wu P, Zhang X, Kambara H, Su J, Yu H, Park SY, Guo R, Ren Q, Zhang S, Xu Y, Silberstein LE, Cheng T, Ma F, Li C, Luo HR (2020) Single-cell transcriptome profiling reveals neutrophil heterogeneity in homeostasis and infection. Nat Immunol 21: 1119-1133.
Yasuda K, Takeuchi Y, Hirota K (2019) The pathogenicity of Th17 cells in autoimmune diseases. Semin Immunopathol 41: 283-297.
Young D, Lawlor PA, Leone P, J. DMDM (1999) Environmental enrichment inhibits spontaneous apoptosis, prevents seizures and is neuroprotective. Nature Medicine 5: 448-453.
Zappone MV, Galli R, Catena R, Meani N, De Biasi S, Mattei E, Tiveron C, Vescovi AL, Lovell-Badge R, Ottolenghi S, Nicolis SK (2000) Sox2 regulatory sequences direct expression of a (beta)-geo transgene to telencephalic neural stem cells and precursors of the mouse embryo, revealing regionalization of gene expression in CNS stem cells. Development 127: 2367-82.
Zeisel A, Muñoz-Manchado AB, Codeluppi S, Lönnerberg P, La Manno G, Juréus A, Marques S, Munguba H, He L, Betsholtz C, Rolny C, Castelo-Branco G, Hjerling-Leffler J, Linnarsson S (2015) Brain structure. Cell types in the mouse cortex and hippocampus revealed by single-cell RNA-seq. Science 347: 1138-42.
Zhou QG, Lee D, Ro EJ, Suh H (2016) Regional-specific effect of fluoxetine on rapidly dividing progenitors along the dorsoventral axis of the hippocampus. Sci Rep 6: 35572.
Zhou Z, Liu T, Sun X, Mu X, Zhu G, Xiao T, Zhao M, Zhao C (2017) CXCR4 antagonist AMD3100 reverses the neurogenesis promoted by enriched environment and suppresses long-term seizure activity in adult rats of temporal lobe epilepsy. Behav Brain Res 322: 83-91.
Ziv Y, Ron N, Butovsky O, Landa G, Sudai E, Greenberg N, Cohen H, Kipnis J, Schwartz M (2006) Immune cells contribute to the maintenance of neurogenesis and spatial learning abilities in adulthood. Nat Neurosci 9: 268-75.

PRODUCT OF RESEARCH

Posters presented at International congresses:

- "Enriched environment increases immature neurons in meninges by TrkB signaling". Neuroscience 2021 - Society for Neuroscience. 8-16 November 2021.
  Authors: **Zorzin S**, Corsi A, Ciarpella F, Bottani E, Dolci S, Malpeli G, Pino A, Amenta A, Fumagalli G F, Chiamulera C, Bifari F, Decimo I.

- "An ever-changing niche: unraveling the meningeal response to neurogenic stimuli". FENS 2020 Virtual Forum, 11-15 July 2020.
  Authors: **Zorzin S**, Corsi A, Giulia G, Fumagalli G F, Bifari F & Decimo I.

- "The role of meningeal neural progenitor cells in brain auto-reactive immune cell regulation". 52nd Congress of the Italian Society of Multiple Sclerosis (FISM), 26 -27 November 2020.
  Authors: **Zorzin S**, Dusi S, Lopez N, Lucianer G, Corsi A, Poli A, Constantin G, Fumagalli G F, Bifari F & Decimo I.

- "The role of meningeal neural progenitor cells in brain auto-reactive immune cell regulation". 51st Congress of the Italian Society of Multiple Sclerosis (FISM), Roma (Italy), 28 -30 May 2019.
  Authors: **Zorzin S**, Bifari F & Decimo I.

- "Meningeal neural precursors contribute to cortical neurons of aged mice."; 38th Congress of the Italian Society of Pharmacology (SIF), Rimini (Italy), 25 -28 October 2017.
  Authors: Pino A, Dolci S, **Zorzin S**, Llorens-Bobadilla E, Zhao S, Lange C, Panuccio G, Vinckier S, Wyns S, Bouché A, Giugliano M, Dewerchin M, Martin-Villalba A, Carmeliet P, Bifari F & Decimo I.

- "Transplantation of meningeal-derived oligodendrocytes remyelinate lysophosphatidylcoline (LPC) spinal cord lesion". 38th Congress of the Italian Society of Pharmacology (SIF), Rimini (Italy), 25 -28 October 2017.
  Authors: Dolci S, Pino A, Berton V, Rodriguez F J, **Zorzin S**, Amoroso C, Fumagalli G F, Bifari F & Decimo I.

- "Meningeal neural precursors contribute to cortical neurons of aging mice". Society for Neuroscience (SfN) 2017 Meeting, Washington DC (US), 11-15 November 2017
  Authors: Pino A, Dolci S, **Zorzin S**, Llorens-Bobadilla E, Zhao S, Lange C, Panuccio G, Vinckier S, Wyns S, Bouché A, Giugliano M, Dewerchin M, Martin-Villalba A, Carmeliet P, Bifari F & Decimo I.

- "Meningeal neural precursors contribute to cortical neurons in aging mice". FENS-SfN Summer school 2018, Bertinoro (Italy), 3-9 June 2018.
  Authors: Pino A, **Zorzin S**, Dolci S, Panuccio G, Giugliano M, Carmeliet P, Bifari F & Decimo I.

Publications in the pipeline

The content of aim 1 led to the publication of a paper entitled "Environmental enrichment induces meningeal niche remodeling through trkb-mediated signaling" in the International Journal of Molecular Sciences.
The content of aim 2 will be the object for future publication on meninges and meningeal neural precursors during multiple sclerosis.

Other Publications:

During these 3 years I had the opportunity to publish 3 papers of previous completed experiments as a coauthor, and a paper as the first author:

- Dolci S, Mannino L, Bottani E, Campanelli A, Di Chio M, **Zorzin S**, D'arrigo G, Amenta A, Segala A, Paglia G, Denti V, Fumagalli G F, Nisoli E, Valerio A, Verderio C, Martano G, Bifari F, Decimo I; "Therapeutic induction of energy metabolism reduces neural tissue damage and increases microglia activation in severe spinal cord injury"; PNAS, under revision

- **Zorzin S**, Corsi A, Ciarpella F, Bottani E, Dolci S, Malpeli G, Pino A, Amenta A, Fumagalli G F, Chiamulera C, Bifari F, Decimo I; "Environmental enrichment induces meningeal niche remodeling through trkb-mediated signaling"; International Journal of Molecular Sciences, October 2021. DOI: https://doi.org/10.3390/ijms221910657

- Bifari F, Dolci S, Bottani E, Pino A, Di Chio M, **Zorzin S**, Ragni M, Zamfir R G, Brunetti D, Bardelli D, Delfino P, Cattaneo MG, Bordo R, Tedesco L, Rossi F, Bossolasco P, Corbo V, Fumagalli G F, Nisoli E, Valerio A, Decimo I; "Complete neural stem cell (NSC) neuronal differentiation requires a branched chain amino acids-induced persistent metabolic shift towards energy metabolism"; Pharmacological Research, May 2020. DOI: https://doi.org/10.1016/j.phrs.2020.104863

- Dolci S, Pino A, Berton V, Malpeli G, Braga A, Pari F, **Zorzin S**, Amoroso C, Moscon D, Rodriguez FJ, Fumagalli GF, Bifari F, Decimo I; "High yields of adult oligodendrocyte lineage cells obtained from meningeal biopsy"; Frontiers in Pharmacology, October 2017. DOI: 10.3389/fphar.2017.00703